Summer 2011

Characterization of carbon fiber polymer matrix composites subjected to simultaneous application of electric current pulse and low velocity impact

Robert James Hart
University of Iowa

CHARACTERIZATION OF CARBON FIBER POLYMER MATRIX COMPOSITES

SUBJECTED TO SIMULTANEOUS APPLICATION OF ELECTRIC CURRENT

PULSE AND LOW VELOCITY IMPACT

by

Robert James Hart

A thesis submitted in partial fulfillment
of the requirements for the Master of
Science degree in Mechanical Engineering
in the Graduate College of
The University of Iowa

July 2011

Thesis Supervisor: Assistant Professor Olesya I. Zhupanska

Graduate College
The University of Iowa
Iowa City, Iowa

CERTIFICATE OF APPROVAL

_____

MASTER'S THESIS

_____

This is to certify that the Master's thesis of

Robert James Hart

has been approved by the Examining Committee
for the thesis requirement for the Master of Science
degree in Mechanical Engineering at the July 2011 graduation.

Thesis Committee: _____
　　　　　　　　　　Olesya I. Zhupanska, Thesis Supervisor

　　　　　　　　　　_____
　　　　　　　　　　Jia Lu

　　　　　　　　　　_____
　　　　　　　　　　Albert Ratner

To My Family

ACKNOWLEDGMENTS

I would like to express my sincere appreciation to Professor Oleysa I. Zhupanska for her support and guidance throughout this research process and throughout my education at The University of Iowa. The research skills that I have developed will benefit me greatly in my career in research and development. In addition I would like to thank Professor Albert Ratner and Professor Jia Lu for serving on the thesis defense committee. My appreciation also goes to Phillip Deierling and Christopher Hill for their assistance with experimentation. Finally, I would like to thank my family and friends for their support during my education at The University of Iowa.

TABLE OF CONTENTS

LIST OF TABLES

LIST OF FIGURES

CHAPTER 1

INTRODUCTION

1.1 Background Information

The importance of composite materials plays an increasing role in everyday life from energy conservation, to national security, to recreational activities. Their superior combination of stiffness, strength, and low density has given composite materials a competitive advantage in aerospace, automotive, civil infrastructure, and wind energy industries. Current applications include the US Air Force's F-22 Raptor and Joint Strike Fighter which consist of approximately 25% composites by weight. The Committee on Materials Research for Defense After Next (2003) claimed that fiber-reinforced polymer composites have the potential to achieve a 20-25% increase in performance over the next 15-25 years. In addition, the United States National Committee on Theoretical and Applied Mechanics (2007) named composite mechanics as a field of engineering that has a profound impact on American competitiveness.

Composite materials are made of a combination of two or more constituents to make one heterogeneous material. The advantage of the resultant material is that it is designed to take advantage of the beneficial properties of each constituent without being limited as much by the detrimental properties of the original constituents. Composite materials consist of a matrix and filler. The matrix usually consists of an epoxy type polymer, and the filler is usually particles or fibers. Thin layers can then be stacked into a resultant called a laminate (Jones, 1999). Figure 1.1 shows an example of a fiber-epoxy matrix composite laminate.
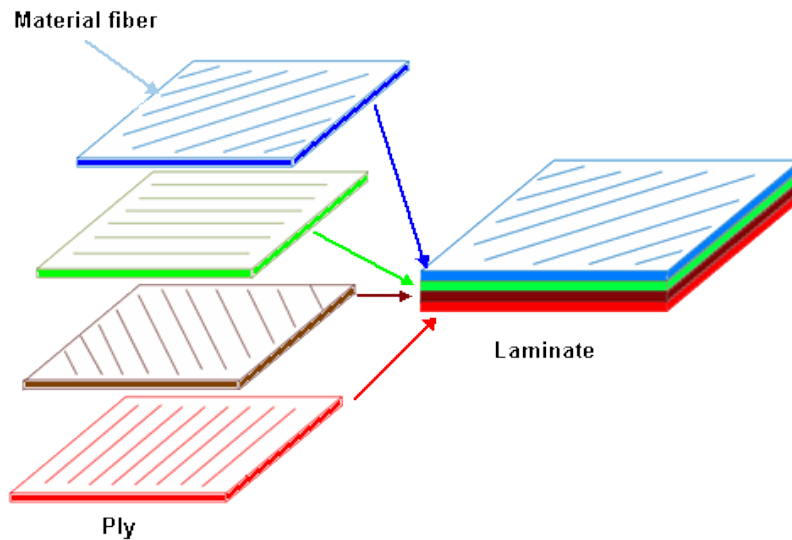
Figure 1.1: Fiber-Epoxy Matrix Composite Laminate (SolidWorks, 2011)

A composite laminate, as shown in Figure 1.1, has high stiffness, high strength, and low density and is used extensively in structural applications. Although composite laminates have obvious advantages to traditional metals, the composites are much more susceptible to damage induced by impact from foreign objects. In addition, impact induced damage in composite materials is often internal with no visible indications on the surface. Even without visible damage, the structure's strength and stiffness could be severely compromised. Often, the composite structure must withstand an impact event and continue to serve its mechanical purpose. Hence, there is strong research interest into the impact resistance and damage tolerance of fiber-reinforced composites.

Moreover, current engineering trends demand materials perform well when subjected to many different types of loads. Composite materials are often sought to meet

these demands, because composites can be tailored to the exact mechanical and other functional specifications required for a particular use. The use of composite materials in aerospace, electronics, and wind industries has become increasingly common, and the composite components are required to carry mechanical, electrical, and thermal loads simultaneously. For instance, carbon fiber epoxy matrix composites are expected to disperse high electric currents during lightning strike events, which has sparked research interest into the electrical properties of composites. Lightning strike is a very serious concern for aircraft.

For commercial aircraft, lightning strike occurs between the first 1,000 and 10,000 hours of flight, which is equivalent to once every year (Gou, 2009). Most lightning strike occurrences do not result in catastrophe, however, there were a total of 40 lightning related aircraft accidents between 1963 and 1989 (Cherington, 1995). In addition, 8% of wind turbines are struck by lightning every year, but 80% of wind turbine insurance claims are lightning strike related (Parrish, 2010). This threat is of serious concern, because although carbon fibers carry electricity very well, the polymer matrix is dielectric, so the carbon fiber components are much more likely to incur damage from lightning strike when compared to previous metal components that were better at dispersing energy. The high electrical currents due to lightning strike can cause vaporization of the polymer matrix at the strike area and can cause large increases in temperature due to Joule heating. In addition to these nature-induced applications of electrified composites, research has been performed that investigated the effects of electrification on composite materials, however, very little research has focused on the application of large current magnitudes.

In the present work, the behavior of carbon fiber polymer matrix composites subjected to electric current pulse and impact loads. The literature review in the following section focuses on studies on the impact and electrical properties of carbon fiber polymer matrix composite materials.

1.2 Literature Review

Throughout the life of a composite structure, impact induced damage is inevitable. In the aerospace industry, maintenance workers often drop tools on the composite structure during the general maintenance process. In addition, both the aerospace and wind turbine industries face the threat of impact from flying birds and debris during operation. In each of the cases, low velocity impact can cause catastrophic damage even without leaving visible damage. Great attention must be given to the potentially severe repercussions of preventable impact events during maintenance, and design consideration must be given to inevitable impact events during operation. Impact induced damage presents a much more serious design concern for fiber-reinforced composite materials as compared to similar metallic structures (Abrate, 1998, Sierakowski and Newaz, 1995). Therefore, a great deal of attention has been given to the behavior of composites under various types of impact loads.

Research into the impact properties of carbon fiber composites dates back decades to works such as that of Bader et al. (1973), which considered the effect of the fiber-matrix interface on the fracture properties of carbon fiber composites subjected to impact. Since then experimental, analytical, and computational studies have been extensively pursued. These studies are categorized into those concerned with local compression, deformation, and failure due to low velocity impact and those concerned with wave propagation and failure in composites due to high velocity impact.

Several sources of structural failure must be considered when assessing the damage caused by low velocity impact of foreign objects in thin composite laminates. Sources of failure include fiber breakage, delamination between adjacent plies, polymer matrix cracking, and plastic damage due to contact and large deformation (Tita, 2008).

Delamination is the separation of two adjacent layers, or plies, of the composite laminate. For laminated composite plates subjected to low velocity impact, extensive damage in the form of delamination often occurs with no visible damage. Although the composite structure may not necessarily show visible damage, the structural integrity could be undermined. Compressive strength reduction can be as high as 60% with no visible indication (de Moura, 2002). When examining a cross section of the specimen, it can be seen that most of the damage occurs in the bottom plies of the laminate (Bernard, 1989). Delamination due to impact in a cross-ply composite laminate is shown in Figure 1.2.
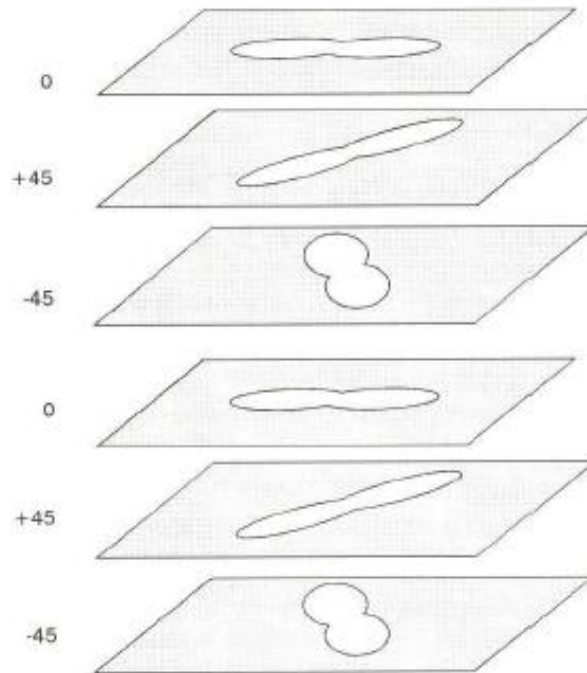
Figure 1.2: Delamination in Cross-Ply Composite (Abrate, 1998)

The peanut shaped delamination is in the fiber direction and is characteristic of fiber-reinforced composite laminates. If visible damage occurs, the failure is usually on the back side of the composite relative to the side in contact with the impact device (Bernard, 1989). The failure in fiber-reinforced composite laminates subjected to an impact load at the center has been modeled successfully using a spring, gap, and dashpot system. By numerical approximation it was determined that damage induced by the impact softens the laminate resulting in a loss in stiffness (Oguibe, 1999). It has also been shown that delamination causes a change in the bending behavior of the composite laminate structure and must be considered in the original design of the structure (Amaro, 2008). The tradition of research into impact on fiber-reinforced polymer matrix composite laminates is rich, however, in recent years research has begun to trend towards investigating the more obscure capabilities of these structures. In particular, a research niche has been found in the area of electrified fiber-reinforced composite materials.

Some of the earliest use of carbon fiber composite laminates in electrical applications was in the development of an electromechanical battery (EMB). The EMB consisted of a carbon fiber rotor connected to magnetic bearings surrounded by a permanent magnet array. Applications included electric hybrid vehicles and other solid-state electronics on the order of 1 kW-hr (Post et al., 1993). In addition to EMB's, researchers have investigated the use of fiber-reinforced polymer matrix composites for the purpose of actually carrying an electric current. A common application of current carrying composite materials is in the area of damage sensing.

Carbon fibers are very good electrical conductors and are able to carry electrical current well, however, the polymer matrix is dielectric. For the application of damage sensing, 2-probe resistance measurement technique is used. An electric current is applied to the composite using 2 electrodes, and the resistance is measured across the electrodes. The idea in this method is that if a composite structure endures damage by impact, electrical conductivity will decrease due to fiber breakage and delamination and thus the

resistance of the overall specimen will increase (Prasse et al., 2007, Chung et al., 2007). As damage increases, the resistance of the specimen increases (Schulte et al., 1989, Angelidis et al., 2005, Wang et al., 2006). This resistance measurement, however, does not perfectly represent the composite sample but also accounts for the contact resistance between the electrode and specimen (Shen, 2007). The contact resistance is caused by both the contact between materials of different electrical conductivity as well as surface roughness. The current is therefore constricted through the contact area, as shown in Figure 1.3.

SURFACE A

INTERFACE

SURFACE B   CURRENT FLOW
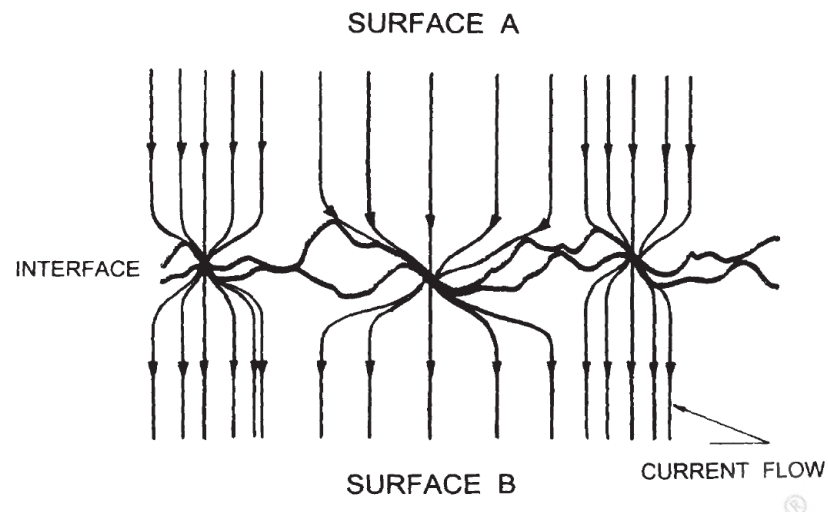
Figure 1.3: Current Constricted Through Contact of Rough Surfaces (Braunovic, 2007)

By applying a conductive filler into the discontinuities in the interface, contact resistance has been successfully decreased. A conductive silver epoxy called Duralco 120 has been determined to be the superior option for minimizing contact resistance for composite laminate plates (Tudela, 2004). These recent advances in the electromagnetic capabilities of carbon fiber polymer matrix composite and their innate structural advantages have motivated researchers to seek out the potential for utilizing these structures for multifunctional applications.

In recent years, multifunctional materials have been attracting significant attention in the research community due to demands for materials to perform more than one function. Multifunctional materials are capable of carrying multiple types of loads and serve more than one purpose. Examples would include materials that can carry a combination of mechanical, thermal, magnetic, and electrical loads. Composite materials naturally lend themselves to the concept of multifunctionality, which includes the coupling of structural, magnetic, electric, thermal, and other fields. Fiber-reinforced polymer matrix composites have been investigated for use in so called structural capacitors that are able to carry a load while acting as a battery (Stefanescu et al., 2011). Multifunctional polymer nanocomposites have applications in data storage, magnetic sensors, and biomedical and pharmaceutical applications (Zhu, 2011). In addition, it has been found that the application of an electromagnetic field can improve the impact properties of carbon fiber polymer matrix composites.

The present work was motivated by experimental research performed by Snyder et al. (2001), Sierakowski et al. (2007 & 2008), Telitchev et al. (2008). Each of these works suggested that exposure of composite materials to an electromagnetic field leads to an increase in the material's strength and impact resistance to delamination. The works of Sierakowski et al. (2007 & 2008) and Telitchev et al. (2008) were concerned with the low velocity impact response of electrified unidirectional and cross-ply carbon fiber polymer matrix composite plates. The results showed that the impact resistance of the composite

plates was highly dependent on the intensity of the applied electric field. In the experimental work of Sierakowski et al. (2007 and 2008) and Telitchev et al. (2008), the specimens were inserted into a wooden test fixture, as shown in Figure 1.4.
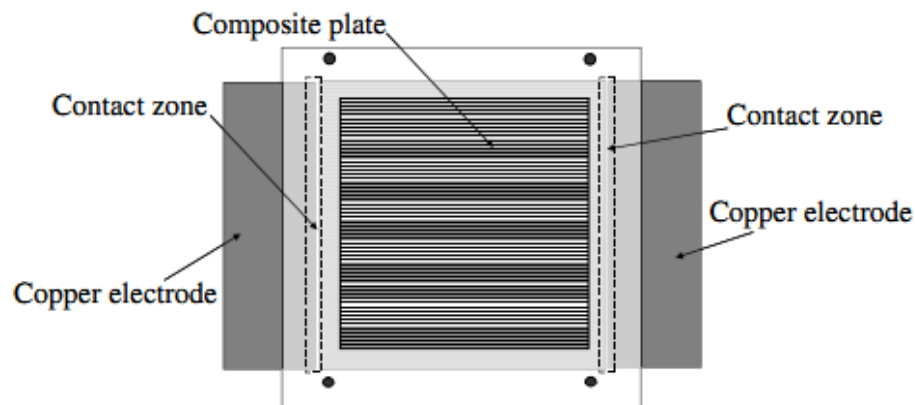
Figure 1.4: Composite Plate Clamped in Test Fixture (Sierakowski et al., 2008)

The unidirectional composite specimens were clamped into the test fixture such that the fibers were aligned with the direction of the current flow. Next, the test fixture was placed inside of an impact tower. A GRC 8120 Drop Weight Impact Test Machine was used for low velocity tests and was capable of impact energies of up to 2105 J, impact velocities up to 6.9 m/s, and a minimum drop mass of 102.1 kg. For testing at higher velocities, a second mini tower was designed which had a minimum drop mass of 5 kg and a maximum velocity of 5.7 m/s. Impact tests were performed without electrification,

with a 25 A DC current, and with a 50 A DC current. The results of the coordinated

impact tests are shown in Figures 1.5 and 1.6.
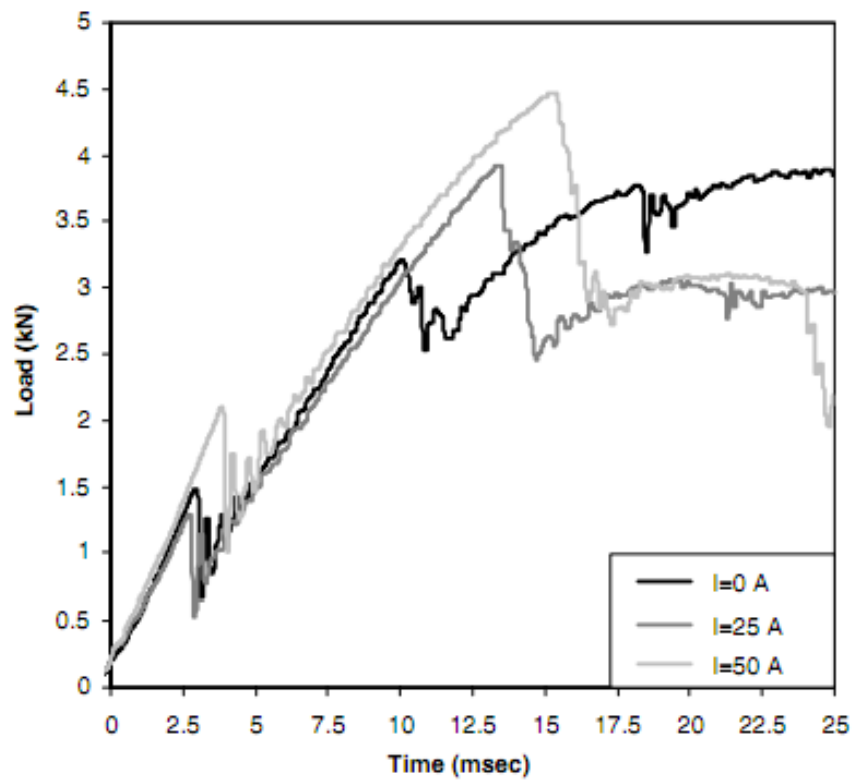
Figure 1.5: Load versus Time for 32 Ply Unidirectional Impact Tests (Sierakowski et al., 2008)
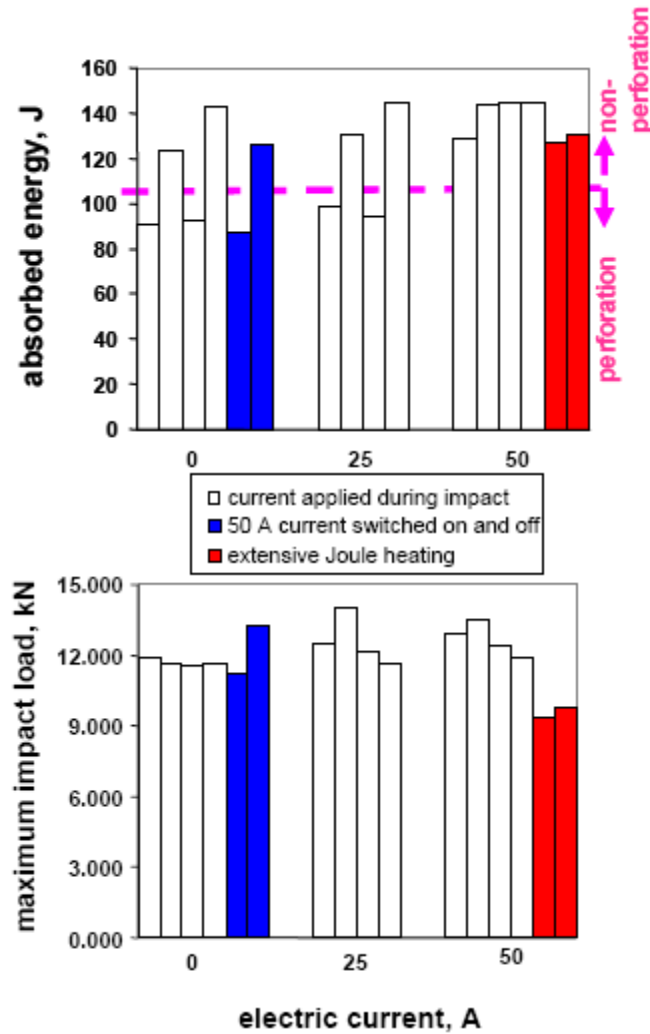
Figure 1.6: Impact Load and Absorbed Energy for Cross-Ply Plates (Sierakowski et al., 2007)

Figure 1.5 shows that in 32 ply unidirectional specimens, the peak load increased with the current application. It was also noted that the higher the current, the greater the increase in peak load. Although the peak load increased with current application, the visible damage on the specimens did not change noticeably (Sierakowski et al., 2008).

Figure 1.6 shows the influence of coordinated application of DC current with an impact event on 32 ply cross-ply composite plates. In cross-ply plates, it was determined that the peak load was not increased by the presence of electrical current. There was, however, a significant influence on damage by the applied current. As the current increased, the visible damage decreased to the point that the 50 A tests resulted in no visible damage. The absorbed energy in the cross-ply specimens increased as the magnitude of the applied current increased. The findings also reported that removing the electric field just prior to impact removed any of the positive effects of the electric current. In addition, prolonged current application decreased the peak load and absorbed energy. This phenomenon was caused by the detrimental effects of Joule heating (Sierakowski et al., 2007). The deformation of the composites due to the coupling of mechanical and electromagnetic fields (Zhupanska and Sierakowski, 2007) and/or changes in materials properties contribute to this phenomenon. This work focuses on multi-field interaction.

The Lorentz force is the force on charged particle caused by an electromagnetic field. In the case of an electrically anisotropic solid body without magnetization the Lorentz ponderomotive force takes the form

$$\boldsymbol{F}^L = \rho_e \left(\boldsymbol{E} + \frac{\partial \boldsymbol{u}}{\partial t} \times \boldsymbol{B} \right) + \left(\boldsymbol{\sigma} \cdot \left(\boldsymbol{E} + \frac{\partial \boldsymbol{u}}{\partial t} \times \boldsymbol{B} \right) \right) \times \boldsymbol{B}$$
$$+ (((\boldsymbol{\varepsilon} - \varepsilon_o \cdot \boldsymbol{1}) \cdot \boldsymbol{E}) \times \boldsymbol{B})_\alpha \nabla \left(\frac{\partial \boldsymbol{u}}{\partial t} \right)_\alpha + (\boldsymbol{J}^* \times \boldsymbol{B}) \tag{1.1}$$

where $\boldsymbol{F}^L$ is the Lorentz force, ρ_e is the charge density, $\boldsymbol{E}$ is the electric field vector, $\boldsymbol{u}$ is the displacement, $\boldsymbol{t}$ is time, $\boldsymbol{B}$ is the magnetic induction vector, $\boldsymbol{\sigma}$ is the electrical conductivity tensor, $\boldsymbol{\varepsilon}$ is the electrical permittivity, ε_o is the electrical permittivity in vacuum, and $\boldsymbol{J}^*$ is the density of the external electric current (Zhupanska and Sierakowski, 2007). For electrically conductive composite plates, the Lorentz force depends on the external magnetic field, magnitude and orientation of the electric current,

and the speed of the plate's deformation. In this case, the Lorentz force has a significant influence on the deformation of the impacted composite specimen. The deflection of the plate was determined to decrease with increasing electric current magnitude, and it was concluded that the impact event could be counterbalanced by the application of the electromagnetic field (Zhupanska and Sierakowski, 2007). The works of the previously mentioned authors motivated the thesis work of Zantout (2009) on the electrical and impact characterization of IM7/977-2 and AS4/3501-6 carbon fiber composites.

Zantout (2009) developed a test fixture based on Figure 1.4 and performed electrified impact tests. From these tests, it was determined that the peak load and absorbed energy increased with increasing electrical current in AS4/3501-6 carbon fiber composites. This indicated that the impact resistance of the composite material increased with application of electric current. IM7/977-2 carbon fiber plates experienced adverse effects due to the electrification. The peak load and absorbed energy both decreased in IM7/977-2 composite plates. The work of Deierling (2010) utilized the accomplishments of Zantout (2009) and expanded the experimental setup to include a semi-automated impact testing system. The modified setup allowed for the application of time-varying electric current and real-time data acquisition. The setup also included infrared thermocouples that measured the temperature of the composite along the centerline. Deierling (2010) performed extensive work on the effects of electric current magnitude and duration, electrical resistance, and thermal effects in IM7/977-3 32 ply unidirectional and symmetric cross-ply specimens.

The experimental methods of Zantout (2009) and Deierling (2010) are discussed in detail in section 2.2, as they are the foundation of the current work. In order to build upon the accomplishments of the former authors, an outline of objectives was planned.

1.3 Thesis Objectives

There were four objectives of this thesis. The first objective was to design an experimental setup that is capable of performing fully automated electrical and impact tests on carbon fiber polymer matrix composite materials at pulsed electric currents. The experimental setup was required to be used for pure electrical tests with no impact, pure impact tests with no electrification, and coordinated impact tests with electrification. The coordinated impact tests include the simultaneous application of a current pulse with an impact load (i.e. to coordinate the peak of the maximum current and maximum impact load). A custom current pulse generator was designed and built by the Iowa Institute of Hydraulic Research (IIHR) for the present research project. The integration of the current pulse generator into the experimental setup along with the programming required to coordinate the electric current pulse application with an impact event were completed as parts of the present thesis.

The setup design consisted of four parts. The first part was development of a data acquisition system for measuring voltage signals during the application of a current pulse to the composite specimen. The second goal was to improve on a trigger for automatic initiation of a current pulse for electrified test. The third goal was to develop a trigger for automatic drop of a drop weight for an impact test. Finally, the two triggering systems needed to be combined in order to coordinate the application of a current pulse with an impact event. Upon successful development of the experimental setup, the experimental research objectives were determined.

The second objective of this thesis was to determine the response of carbon fiber polymer matrix composite plates to the application of an electric current pulse. A series of electrical characterization tests with current pulse magnitudes of up to 1700 A were performed on 16 and 32 ply unidirectional and cross-ply carbon fiber polymer matrix composite specimens.

The third objective was to determine the response of the non-electrified composite plates during a low velocity impact event. The impact energy was selected such that some visible damage was induced without complete failure.

The final objective was to determine the effect of application of a current pulse coordinated with an impact event and the resulting mechanical response and failure of electrified carbon fiber polymer matrix composites. The results of the tests were then compared in order to determine the differences between the impact characterization tests on non-electrified composites and the coordinated tests on electrified samples so that the effect of current application could be determined.

CHAPTER 2

EXPERIMENTAL SET-UP AND EXPERIMENTAL

PROCEDURES

2.1 Experimental Considerations

There were three considerations in electrical and impact characterization that were addressed: (i) effective current pulse application by a custom current pulse generator, (ii) reliable and repeatable triggering of current pulse and impact drop, (iii) and appropriate timing sequence between the current pulse and impact.

This work builds upon the accomplishments of Telitchev et al. (2008), Sierakowski et al. (2008), Zantout (2009), and Deierling (2010) who investigated carbon fiber polymer matrix composites subjected to electric currents. This experimental setup utilizes the previous work of Deierling (2010) and expands the experimental setup to include the implementation of a coordinated impact of carbon fiber polymer matrix composites with the application of a large current pulse of up to 2000 Amps (A). Deierling (2010) developed an automated system to coordinate the occurrence of an impact with application of direct current (DC), alternating current (AC), and pulse waves of up to 100 A.

In order to utilize the previous experimental setup to accommodate the coordination of an impact event with the application of a current pulse, the previous triggering system was reconfigured in order to provide a triggering system with much better time repeatability. Since the current pulse generated by the current pulse generator has a duration of approximately 20 milliseconds the triggering system required a repeatability of ±1 millisecond in order to effectively time an impact event with the current pulse. It was determined that the triggering system from Deierling (2010) was not accurate enough to accommodate this. The PIC microcontroller from the previous trigger

used 2 sequential signals to trigger the drop mass and current pulse. The PIC was unable to send the 2nd of the 2 signals quick enough. Also, the PIC would sometimes get jammed and would not send the trigger signals, so a new system was required. The necessary modifications were made and are outlined later in this paper.

Once the set-up was completed, impact and electrical characterization experiments were conducted in order to determine the effect of the application of a current pulse on the impact resistance of carbon fiber polymer matrix composite plates. Experiments were performed on electrified specimens without impact, impacted specimens without electrification, and specimens subjected to coordinated impact and electrification.

2.2 Previous Experimental Setup

The works of Deierling (2010) and Zantout (2009) studied the effects of application of DC current on carbon fiber polymer matrix composite materials quite extensively. The experimental setup developed by the abovementioned authors was utilized for DC current tests in this work, as outlined below. The experimental setup for DC current application to the carbon fiber polymer matrix specimens involved a power supply, a shunt resistor, the specimen test fixture, a data acquisition unit, Agilent Measurement Manager software, and an Agilent VEE Pro 8.5 program.

2.2.1 Experimental Setup for D.C. Electric Current Tests

The Agilent 6692A 6600 Watt System Power Supply was chosen to provide electrical current to the composite specimens. The Agilent 6692A has a current rating of 110 A and a voltage rating of 60 V DC. The 6692A also has a precision programming

accuracy of 0.04% +60 mV and 0.1% + 65 mA on the voltage and current, respectively, when operated at 25°C ±5°C (Agilent, 2011). The greatest advantage of the Agilent 6692A is that it is controllable either manually on the unit or automatically through an Agilent VEE Pro 8.5 program. In the Agilent VEE Pro 8.5 program, the magnitude and duration of electric current outputted by the 6692A power supply was specified via commands which were sent to the power supply via USB connection.

A shunt resistor was placed in series with the current application to the composite specimens. The shunt resistor selected was the Deltec MKB-100-200. This shunt resistor has a rating of 100 millivolts (mV) and 200 A, which equates to a resistance of 0.5 milliohms (mΩ). When voltage measurements were sampled across the shunt resistor, the current was calculated at any given point in time by dividing the voltage by the shunt resistance of 0.5 mΩ, using Ohm's Law.

The data acquisition unit used was the Agilent U2531A simultaneous sampling DAQ. The U2531A has 4 high precision measurement channels and can sample at a rate of up to 2 mega-samples per second per channel. The U2531A has a 14-bit resolution and can measure voltage ranges from -10 V to +10 V (Agilent, 2011). In order to tabulate data collected by the data acquisition unit, Agilent Measurement Manager Software was utilized. This software uses a graphical user interface in which the user can specify the sampling rate, measurement range, and trigger conditions. The data collected from each channel is then tabulated and saved in a comma-separated value file. The complete experimental setup is shown in Figure 2.1.
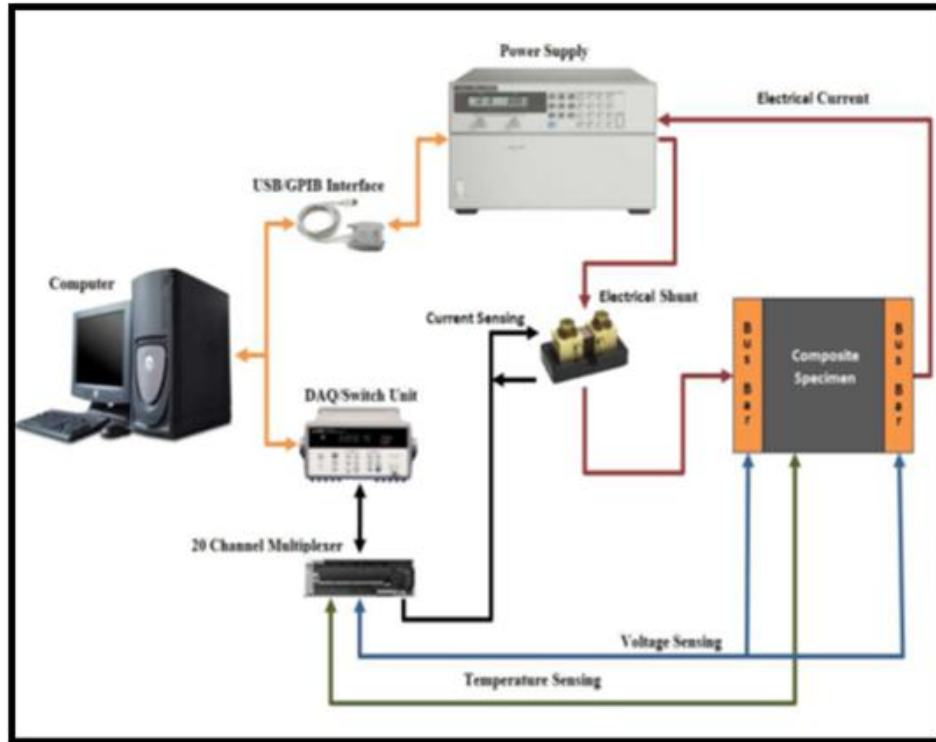
Figure 2.1: DC Electrical Characterization Test Setup (Zantout, 2009)

2.2.2 Specimen Test Fixture

Zantout (2009) designed and fabricated a custom test fixture to hold the composite specimens during testing. The test fixture needed to: (i) be usable as a stand-alone bench top unit and mounted within the impact tower, (ii) accommodate 6 inch x 6 inch specimens of varying thickness, (iii) provide a foundation for mounting thermocouples for temperature measurements, and (iv) meet ASTM standard D5728-07, ASTM standard D3763-06, and NASA's Standard Tests for Toughened Resin

Composites (Zantout, 2009). The solid model design and completed test fixture are

shown in Figure 2.2.

(a)   (b)
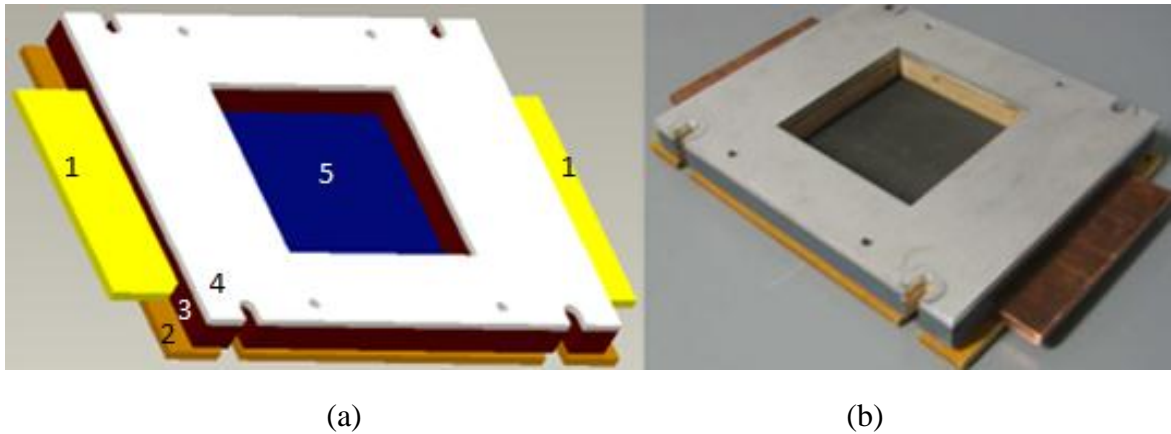
Figure 2.2: Test Fixture (a) Solid Model (b) Fabricated Assembly (Zantout, 2009)

        The parts labeled (1) in Figure 2.2 (a) are the copper electrodes, which are

clamped into contact with the edges of the plate. The component labeled (2) is the

foundation, made of wood, which can sit on a bench or mount into an Instron 8200

impact tower. The part labeled (3) fits over the top of the electrodes and composite

specimen and was fabricated from wood. The component labeled (4) is a top plate

machined from aluminum and provides a stable surface for mounting clamps. Finally, the

component labeled (5) is the composite specimen.

2.2.3 Contact Resistance and Sample Preparation

Contact heating occurs at the interface between the copper electrodes and the surface of the composite specimen. The danger of contact heating is burning of the epoxy matrix at the composite/electrode interface. This heating occurs due to constriction of current at the composite/electrode interface and can result in a large temperature gradient at the edge of the composite plate. Since the amount of heating depends on the current running through the sample, the effects of contact heating were of particular concern in the large current conditions of the experiments detailed in this report. Composite specimens were prepared in such a way to decrease the contact resistance, as performed in Zantout (2009) and Deierling (2010).

Surface roughness, surface corrosion, small contact area, and dissimilar electrical properties all contribute to contact resistance (Braunovic, 2007). In the case of contact between a copper electrode and a carbon fiber polymer matrix composite, the main contributor to contact resistance is the surface roughness of the carbon fiber specimens (Deierling, 2010). In these experiments, the surface roughness was developed during the process in which the 6 x 6 inch specimens were cut from a larger plate. Both frayed fiber edges and the inherit discontinuity between the carbon fibers and the polymer matrix contributed to the surface roughness of the specimens. If contact heating caused the temperature at the boundary to elevate high enough, degradation of the polymer matrix could occur. Therefore, it was most desirable to create a smooth contact surface. A smooth contact surface was developed through the application of a conductive silver epoxy.

The works of Zantout (2009) and Deierling (2010) utilized the application of a thin layer of Duralco 120 silver-filled epoxy to the edges of the composite specimens that contacted the electrodes. The rationale in applying a layer of electrically conductive epoxy to the composite specimen is to smooth the surface of the composite so that a

greater area of the composite comes in flush contact with the electrode, and thus contact resistance would decrease. This method has also been supported by other works investigating electrified composites (Tudela, 2004, Sierakowski et al. 2008, and others).

In order to insure that composite specimens had consistent electrical results, all samples were prepared using the same procedure. First, the composite edges were sanded lightly by hand using fine grit sandpaper. This was performed in order to remove any small imperfections on the contact surface such as rough edges created when the specimen was cut or stray fibers that protruded from the contact surface. Secondly, Duralco 120 silver-filled epoxy was prepared according to manufacturer's specifications. This process involved the combination the appropriate amounts of the silver-filled epoxy resin with hardener. While wearing protective gloves, the epoxy was applied so that all discontinuities in the contact surface were filled and smoothed over with epoxy. Excess epoxy was removed while still wet, since clumps of epoxy would make it difficult to ensure a completely flat contact surface. The specimens were then left to cure for 24 hours at room temperature. After the epoxy was dry, the specimens were sanded lightly on the contact edges in the following four stage sanding procedure.

First, rough sandpaper with 220 grit was used to remove excess epoxy. Then progressively, 320 grit, 400 grit, and 600 grit sandpaper was used create a smooth and flat contact surface. After the sample preparation was complete, a thin layer of wet epoxy without hardener was applied to both the composite specimen and electrode. The wet layer of Duralco 120 was intended to fill in any imperfections remaining in the contact surface. As a quality control check, the resistance of each composite specimen was checked. The resistance was monitored using a 2-probe method for each composite specimen at a current of 1 A. This check was to ensure that the resistance of each specimen was reasonable, because if the resistance of a given specimen was abnormally high compared to similar specimens, dangerous situations could arise from arcing of electrical current and burning of the epoxy matrix.

2.3 New Experimental Setup

In order to investigate the influence of large current application on the impact response of carbon fiber composite plates, a custom current pulse generator was designed and built for the present research project by the Iowa Institute of Hydraulic Research (IIHR). This current pulse generator was integrated into the previous experimental setup as a replacement for the 6692A DC power supply, and algorithms were added to the Agilent VEE Pro 8.5 programs to coordinate the current pulse with an impact event.

2.3.1 Current Pulse Generator

The current pulse generator, as shown in Figure 2.3, combines a bank of five modules each capable of producing up to 500 A for a total of 2500 A of current into a short circuit. Each module consists of two parallel 6800 uF capacitors (Hitachi AIC, HCGF6A2W682Y), an inductor, an insulated gate bipolar transistor (IGBT) (Powerex, CM600HA-24H), triggers, and protection circuitry. When the IGBTs are fired, the capacitors discharge through an inductor and to an emitter bus bar where all modules connect. The IGBTs are a solid state switch capable of handling large currents, such as those produced by the current pulse generator. The inductors oppose the capacitors' sudden discharge in order to smooth the current pulse curve. The total amount of current available to be delivered to the composite sample is determined by Ohm's law given the charge voltage and system resistance. Charge voltage, displayed by the analog voltmeter, is manually set via the front panel mounted variable transformer (charge controller knob). The pushbutton switch labeled N/A is to aide development and troubleshooting and should never be pushed if charge remains in the system. The charge controller knob,

analog voltmeter, and N/A pushbutton are labeled in Figures 2.3 (a) and 2.3 (b). Finally, control of the system is based on a microcontroller circuit which allows for flexibility in future modification.
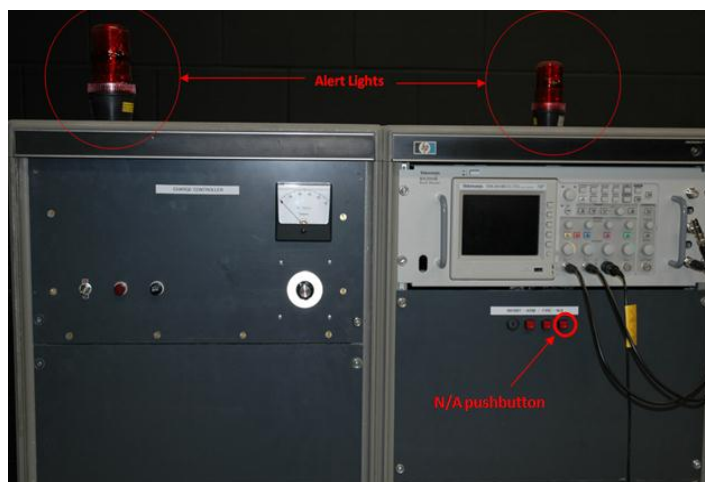
(a)

(b)

Figure 2.3: Current Pulse Generator (a) Exterior View (b) Zoomed in View

The current pulse generator operates on a 5 step process. The first step is to turn the system power toggle switch to the "ON" position, as shown in Figure 2.3 (b). Next, the inhibit key is inserted, and the switch is turned to the horizontal position. Third, the arm pushbutton is pushed, and the alert lights begin to flash. Forth, the charge controller knob is adjusted until the desired voltage is displayed on the analog voltmeter, as shown in Figure 2.3 (b). It is important to note that the voltage displayed on the analog voltmeter is the variable that the user controls in the electrical pulse test. A larger analog voltage generates a larger current pulse for a given plate. Finally, the current pulse is delivered by either pushing the "FIRE" pushbutton or by remotely applying a 5 to 0 V falling edge signal to the BNC cable input that is connected to channel 2 of the oscilloscope. In order to develop a semi-automated test setup, it was necessary to develop a remote trigger for the current pulse generator as well as an Agilent VEE Pro 8.5 program to coordinate the test.

2.3.2 Current Pulse Generator Trigger

A semi-automated trigger had previously been developed through the work of Deierling (2010). The previously developed trigger provided a 5 to 0 V falling edge signal to the current pulse generator through a PIC microcontroller. This previous setup satisfied the trigger conditions but did not operate consistently, thus a new trigger needed to be developed. The primary design consideration in the new current pulse generator trigger was coordination with the existing Agilent brand products in the laboratory. The Agilent U2356A 64-channel data acquisition unit was used in the works of Deierling (2010) and Zantout (2009) for data collection from K-type thermocouples. The U2356A is also capable of providing voltage signals of arbitrary waveform from 0 to ± 10 V. These specifications satisfy the requirement to provide a 5 to 0 V falling edge signal, so the

U2356A was chosen as the trigger source to the current pulse generator. In order to remotely control the trigger source, an Agilent VEE Pro 8.5 program was developed.

2.3.3 Agilent VEE Pro 8.5 Program for Current Pulse Tests

An Agilent VEE Pro 8.5 program was written in order to control the voltage output from the U2356A. The Agilent VEE Pro 8.5 interface was chosen, since it provides a polished user interface that is fully compatible with all of the Agilent brand products in the laboratory. The program logic is outlined in Figure 2.4.
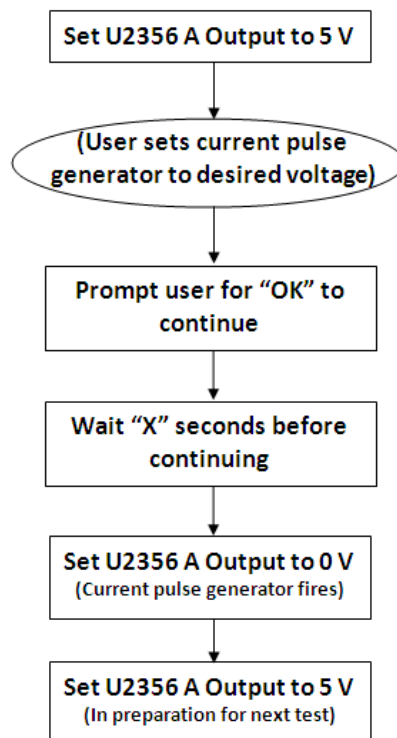
Figure 2.4: Program logic for current pulse generator trigger

The first step in the Agilent VEE Pro 8.5 program was to set the voltage output of the

Agilent U2356A to 5 V. Next, the user follows the 5 step process outline in section 2.3.1

in order to set the current pulse generator to the desired settings. After the current pulse

generator is set, the user must press "OK" button in Agilent VEE Pro 8.5 program to alert

the program that the system is ready to fire. The program waits "X" seconds, as specified

by the user, before continuing with the program. Next, the program sets the output of the

Agilent U2356A to 0 V. This steps the output signal from 5 to 0 V, as shown in Figure

2.5. This change in voltage triggers the current pulse generator to fire. Finally, the

Agilent VEE Pro 8.5 program sets the voltage output back to 5 V to prepare the system

for the next test.
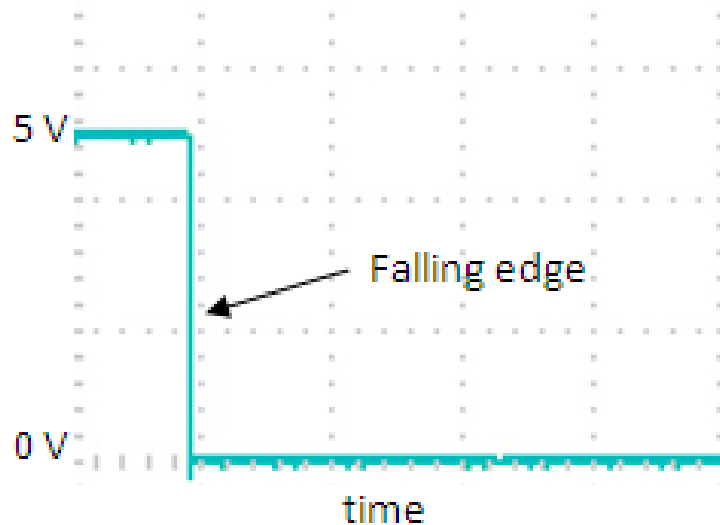
Figure 2.5: Trigger signal for current pulse generator

Next, the data acquisition setup was developed for measuring voltage across the shunt resistor and voltage across the composite sample.

2.3.4 Data Acquisition for Current Pulse Tests

The developer of the current pulse generator installed a Tektronix TDS 2014B oscilloscope directly into the generator housing so that a data acquisition system was readily available. The TDS 2014B is capable of sampling up to 100 MHz over 4 channels (Tektronix, 2011). The electrical characterization tests of section 3.2 were carried out using the TDS 2014B oscilloscope as the data acquisition system, however, there was a significant amount of noise in the data due to the fact that the oscilloscope was mounted within the current pulse generator. For this reason, a new data acquisition system was desired.

The Agilent U2531A data acquisition unit was selected to acquire voltage signals during the current pulse event. The coordinated impact tests of section 3.4 were performed using the Agilent U2531A. Since the duration of the current pulse is 30 milliseconds, the data acquisition duration was selected to be 30 milliseconds. The 30 millisecond period of data collection was defined by a single-shot data acquisition event of 300 sampling points at a rate of 10,000 samples per second. The data acquisition was triggered by the same 5 to 0 V falling edge signal used to fire the current pulse generator. This trigger was selected so that the data acquisition was guaranteed to begin data collection at the same point in time relative to the initiation of the current pulse for every test.

The most concerning issue with the data acquisition was that the voltage drop across the shunt located in the current pulse generator was much less than 1 volt, where as the voltage drop across the composite sample was measured up to 100 V. The Agilent

U2531A is capable of measuring a minimum voltage range of 0 to ±1.25 V and a

maximum voltage range of 0 to ±10 V, thus the voltage signal from the shunt need to be

amplified and that of the composite sample needed to be divided in order to better match

the resolution of the data acquisition unit (Agilent, 2011). The voltage across the shunt

resistor needed to be measured so that the current in the system could be determined by

dividing voltage across the shunt resistor by resistance of the shunt resistor. It was

decided to measure the shunt resistor voltage by measuring across an amplifier that was

already integrated into the current pulse generator. This amplifier amplifies the voltage

across the shunt resistor 11 times. The voltage across the composite sample was divided

by 21 using a simple voltage divider circuit with an accuracy of ±1%. The voltage

measured by the data acquisition system on channel 1 was divided by 11 to get the actual

voltage across the shunt resistor, and voltage measured by channel 3 was multiplied by

21 to get the actual voltage across the composite specimen. Finally, the voltage across the

shunt resistor was divided by the shunt resistance of 0.0001 Ohms to get the current in

the system. Once the data acquisition system was developed, it was desired to determine

the relationship between the analog voltage of the current pulse generator and the

magnitude of the current pulse.

2.3.5 Calibration of Current Pulse Generator

The goal of the calibration of the current pulse generator was to determine the

relationship between the amplitude of the current pulse and the analog voltmeter for any

given composite specimen. The developer of the current pulse generator from IIHR

indicated that there should be a linear relationship between the analog voltage and the

magnitude of the current pulse. In order to determine this linear relationship, a series of

electrical characterization tests were performed according the procedures in 2.3.1 to

2.3.4. The magnitude of the current pulse was found for analog voltages of 20 V, 50 V, 70 V, 100V, etc. for each specimen. Once the electrical tests were performed, the magnitude of the current pulse was plotted against the analog voltage of the voltmeter for each specimen. Next, a linear regression was fit to the data for each specimen using Microsoft Excel. Next, the equation of the linear fit was used in order to determine the required analog voltage for a given desired current value. This process of calibration was determined to be successful, and the results for the electrical characterization calibration are shown in section 3.2.5.

2.3.6 Impact Testing Machine

The Instron 8200 Dynatup impact test machine was used to conduct all impact tests. The Instron 8200, as shown in Figure 2.6, is a low velocity impact tester suited primarily for plastic and composite materials. This impact machine is capable of a maximum drop height of 1 meter, a maximum impact velocity of 4.4 m/s, and a maximum impact energy of 132.8 Joules. The drop height was measured as the distance between the top surface of the clamped specimen and the bottom of the tup, with the drop weight carriage at the set position. The dimensions of the impact tower are 406 mm wide, 457 mm deep, and 2305 mm tall. (Dynatup, 2011). The Instron 8200 was used in the works of Zantout (2009) and Deierling (2010) as a design consideration when developing the test fixture that holds the composite sample during electrification, thus the Instron 8200 was compatible with the test fixture described in section 2.2.2. This made the Instron 8200 ideal for use in coordinated electrical and impact tests.

Figure 2.6: Instron 8200 Dynatup Impact Tester (Dynatup, 2010)

A pneumatic rebound brake was added to the Instron 8200 impact machine so that after an impact event occurs, the mass is automatically raised back above the composite specimen. The rebound brake lessens the occurrence of bouncing of the drop weight and thus decreases the chance of subsequent impacts after the initial impact. Additionally, the rebound brake can lift the drop weight out of the composite sample if the load cell is stuck in the specimen in the case of complete perforation. An important experimental consideration in the impact testing process was alignment of the composite specimens in the test fixture.

The test fixture described in 2.2.2 fits securely within the Instron 8200 drop weight tester, however, the composite specimen is adjustable within the test fixture. It was desired to impact the center of the composite specimens, so alignment marks were made in the center of the plate. A crosshair was created in the center of the plate, as shown in Figure 2.7, by intersecting the diagonals of the square plates. The crosshair was then aligned with the tup so that the center of the tup was positioned directly over the crosshair. In addition to drawing alignment marks on the top of the composite specimens, the bottom of each specimen was covered with a thin application of white spray paint so that impact induced damage was more easily visible.
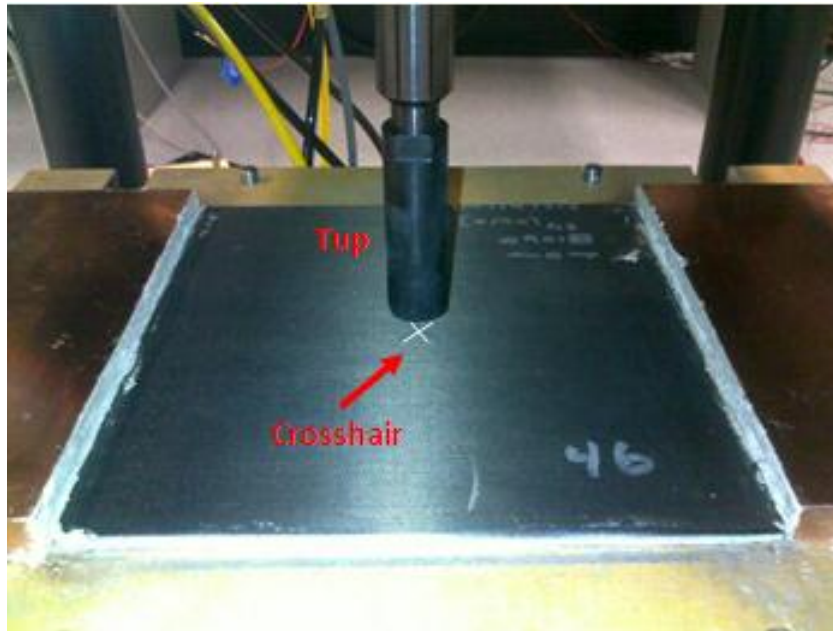
Figure 2.7: Composite specimen showing alignment crosshair with tup

Once the composite specimen was aligned with the tup, the top plates were clamped onto the specimen and the copper electrodes were clamped onto the specimen. Figure 2.8 (a) shows the top plate clamped onto the specimen, and Figure 2.8 (b) shows the clamps used to secure the copper electrodes to the specimen. All clamps were tightened by hand to the minimum torque such that the specimen and electrodes were secure, but were not tightened unnecessarily. This was to ensure that the stresses induced by the clamps would have as little effect on the experimental results as possible.
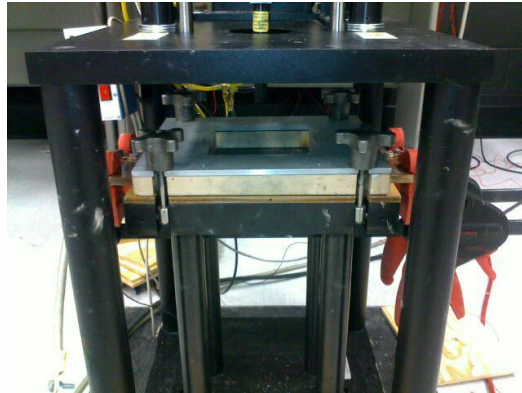
(a)

(b)

Figure 2.8: Test fixture showing top clamps (a) and electrode clamps (b)

2.3.6 Impact Data Acquisition and Signal Conditioner

The Instron 8200 utilizes a load cell, or tup, to measure load data and infrared velocity detectors to measure the velocity of the drop weight. The tup consists of two parts: a load cell, which is referred to as the tup, and a tup insert, which is a sheath covering the outside of the load cell. The tup insert is the component that actually impacts the specimen. The tup was calibrated to a maximum load of 15.569 kN at 24 °C (Dynatup, 2011). The tup and corresponding carriage assembly are shown in Figure 2.9.
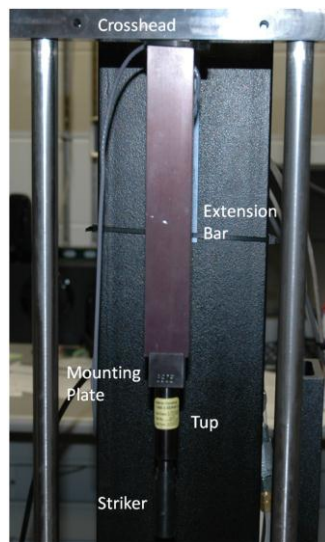
Figure 2.9: Complete Instrumented Load Cell Assembly

The standard tup insert is fabricated from tool steel, which is electrically conductive. This component was not compatible with the experimental setup, since an electrically

conductive tup could create potentially dangerous conditions during an electrified test for both the equipment as well as the user. Zantout (2009) designed a tup insert machined from DELRIN®. This material was chosen, since DELRIN® is dielectric and has excellent impact properties. The standard tool steel and DELRIN® tup inserts are shown side by side in Figure 2.10.

Figure 2.10: Tool steel (left) and DELRIN® (right) tup inserts (Zantout, 2009)

The second source of data measurement is an infrared velocity detector.

A double pronged stainless steel velocity flag is mounted on the drop weight. As the drop weight moves down the drop tower, the velocity flag passes through and interrupts an infrared beam emitted from a fixed velocity detector mounted near the base of the tower. The interruption of the infrared light beam initiates the data acquisition

process. Figure 2.11 shows the velocity flag just before it passes through the infrared velocity sensor.
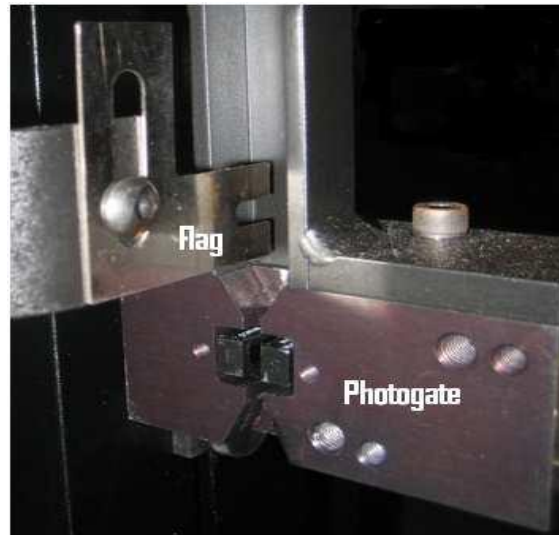
Figure 2.11: Velocity flag and infrared velocity photogate (Zantout, 2009)

 The velocity flag was adjusted such that when the tup rested on the sample, the velocity flag was 6 mm below the bottom of the velocity detector. The velocity detector measures the instantaneous velocity of the drop weight just before the onset of the impact (Dynatup, 2011). The signals from the tup and velocity detector are received by the Instron Dynatup data acquisition unit.

The Inston Dynatup data acquisition unit was designed specifically to be used with the Instron 8200 impact machine. The data acquisition unit, as shown in Figure 2.12,

has a maximum sampling rate of 5 MHz and has built in filters and signal conditioning

(Dyntaup, 2011).

Figure 2.12: Impact Data Acquisition Unit

The signals from the velocity detector and tup are conditioned and filtered by the data

acquisition unit and are then interpreted by the Instron Dynatup Impulse software.

      The force is determined directly from the output of the load cell. Acceleration of

the drop weight is then calculated by dividing force by mass at every data point. Velocity

is then determined by integrating the acceleration with respect to time. Next, the software

calculates the deflection through integration of the velocity with respect to time. Finally,

the energy is determined by integrating the load versus deflection curve. The integrations

to determine velocity, deflection, and energy performed are approximated numerically

through simple trapezoidal approximations by the Instron Dynatup Impulse software

(Dynatup, 2011).

2.3.7 Previous Coordinated Impact Contributions

In order to time an impact event with the application of a current pulse, a semi-automated system was developed based on previous experimental setups. A remotely triggered release system for the Instron 8200 was successfully developed in previous work (Deierling, 2011). The previously developed release trigger system consisted of an electric air solenoid, an air actuated cylinder, a compressed air supply, and a 12 V DC power supply. The air actuated cylinder was implemented by fixing it just above the release trigger on the Instron8200 so that when compressed air fills the cylinder, the piston expands and presses the release trigger, as shown in Figure 2.13.
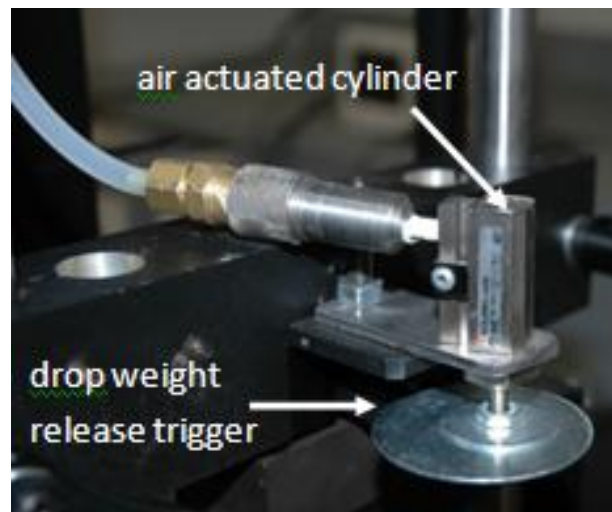
Figure 2.13: Air Actuated Cylinder Mounted on Instron 8200 (Deierling, 2010)

In order to control the release of compressed air into the air actuated cylinder, an electric

air solenoid was placed in line between the compressed air supply and the air actuated

cylinder. The electric air solenoid implemented in the system requires a 12 V DC power

supply and draws 0.67 Watts of power (McMaster-Carr, 2011). The solenoid purchased

from McMaster-Carr is shown in Figure 2.14.
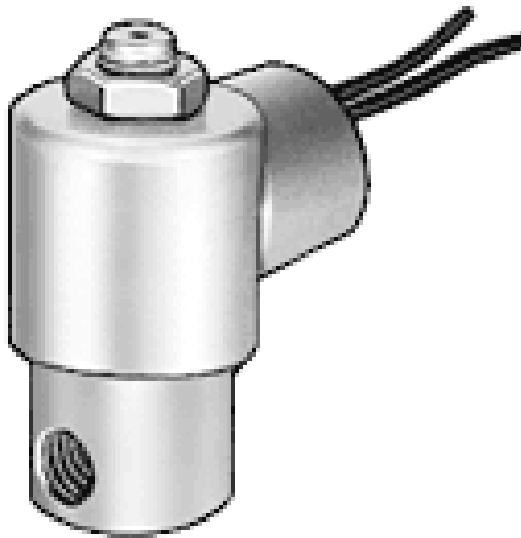
Figure 2.14: Electric Air Solenoid Valve (McMaster-Carr, 2011)

Since the remote drop trigger had already been developed, the next goal was to

implement an Agilent VEE Pro 8.5 program that would control the timing of the drop

weight trigger.

2.3.8 New Coordinated Impact Setup & Experimental

Method

The primary considerations in the development of the new coordinated impact setup were compatibility with the previous drop weight trigger and repeatability. The previous setup utilized the PIC microcontroller discussed in 2.3.2 to control the supply of a 12 V DC power supply. The microcontroller did not operate reliably, so a new control system was necessary. It was decided to use an Agilent 6612C DC power supply, since its specifications met the power requirements, and it is compatible with Agilent VEE Pro 8.5 programming. The Agilent 6612C, as shown in Figure 2.15, has a maximum voltage output of 20 V and a maximum current output of 2 A (Agilent, 2011).

Figure 2.15: Infrared Thermocouple Power Supply (Agilent, 2011)

The implementation of the Agilent 6612C power supply as the power supply for the drop weight trigger into the current pulse test was accomplished by modifying the Agilent VEE Pro 8.5 program logic detailed in Figure 2.4. The new coordinated impact program logic is displayed in Figure 2.16.
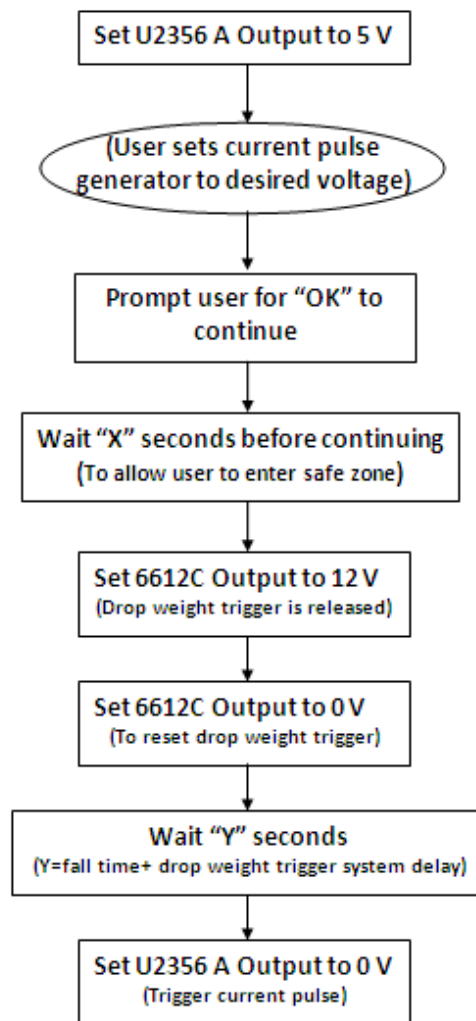
Figure 2.16: Coordinated Impact Program Logic

The first step in the Agilent VEE Pro 8.5 program was to set the voltage output of the Agilent U2356A to 5 V. Next, the user follows the 5 step process outline in section 2.3.1 in order to set the current pulse generator to the desired settings. After the current pulse generator is set, the user must press "OK" button in Agilent VEE Pro 8.5 program to alert the program that the system is ready to fire. The program waits "X" seconds, as specified by the user, before continuing with the program. This delay time is intended so that the user has time to travel a safe distance away from the Instron 8200 impact machine before the impact occurs. The program then sets the output of the Agilent 6612C power supply to 12 V. The 12 V supply opens the electric air solenoid. This allows compressed air to flow into the air actuated cylinder, which expands the piston and triggers the release of the drop weight. After the drop weight trigger is released, the Agilent 6612C is set to 0 V so that electric air solenoid is closed. At this point, the programs waits an amount of time, labeled "Y" in Figure 2.16, which corresponds to the fall time of the drop weight assembly plus the delay time of the drop weight trigger. The fall time is calculated as

$$t = \frac{\sqrt{2gh}}{g} \qquad (2.1)$$

where t is the fall time (s), g is the acceleration due to gravity (m/s), and h is the drop height (m). The delay time of the drop weight trigger is determined empirically and was found to depend on the mass of the drop weight. Next, the program sets the output of the Agilent U2356A to 0 V. This steps the output signal from 5 to 0 V, which triggers the current pulse generator to fire. By changing the delay time between the trigger for the drop weight and the trigger for the current pulse, it was possible to coordinate the peak of the current pulse with the peak of the impact load within ± 1 milliseconds, as determined empirically. For impact tests without current application, the same experimental method

was performed, except the current pulse generator was not charged. Though this experimental setup was verified to work successfully, a few experimental limitations should be addressed before further experimentation is performed.

2.3.9 Limitations on the Coordinated Impact Setup

The greatest limitation on the new coordinated impact setup was the influence of the mass of the drop weight on the delay time of the drop weight trigger. As the mass of the drop weight increased, the delay time in the drop weight trigger also increased. It was determined that for larger masses, it takes longer for the air actuated cylinder to expand and activate the release trigger on the Instron 8200. This occurs because larger masses increase frictional forces in the drop weight trigger. This limitation is significant, since the system requires recalibration if the mass of the drop weight carriage is changed. The second limitation in the experimental setup is the difficulty in clamping the copper electrodes to the edges of the composite specimen. During the impact event, a large amount of vibration and deflection occurs within the electrified plate. This causes the resistance between the copper electrode and composite specimen to increase significantly. This drastic rise in resistance can cause arcing of the current pulse at the composite/electrode interface which leads to burning. Burning of the electrified composite specimen occurs in near 1 out of 3 coordinated impact tests. Future experimental setups must work at reducing this phenomenon so that specimens are not wasted and also so that the effect of higher current magnitude can be studied.

2.4 Summary of Experimental Setup and Procedures

The goal of the current research project was to perform electrical characterization experiments to observe the response of carbon fiber composite specimens to the application of a current pulse. The electrical characterization tests were performed using the experimental methods in sections 2.3.1 to 2.3.4. Next, impact characterization tests were performed according to section 2.3.7 in order to the critical energy at which each specimen would incur visible damage without complete failure. Once the impact characterization tests were completed, coordinated impact tests were performed at this critical energy. In these tests, the application of a current pulse was coordinated with an impact event. Experimental results were tabulated and compared between tests.

CHAPTER 3

EXPERIMENTAL RESULTS

3.1 Material Characterization

The four carbon fiber specimen types tested in this report varied in thickness, layup, and epoxy matrix composition. The carbon fiber composite specimens included IM7/977-3 $[0]_{32T}$ called 32 ply unidirectional, IM7/977-3 $[0/90]_{8S}$ called 32 ply cross-ply, IM7/977-2 $[0]_{16T}$ called 16 ply unidirectional, and IM7/977-3 $[0/90]_{4S}$ called 16 ply cross-ply. In the standard notation for carbon fiber composite laminates, the identifier IM7 distinguishes the carbon fiber type. IM7 carbon fibers are high performance aerospace grade carbon fibers with high stiffness and strength (Hexcel, 2011). The numbers 977-2 and 977-3 after the slash identifies the type of matrix. 977-2 and 977-3 are toughened epoxy resins with exceptional impact properties. The materials properties of the two epoxy types are very similar; however, the 977-2 epoxy resin has a slightly higher tensile strength of 2690 MPa at room temperature compared to 2510 MPa for 977-3 (Cycom, 2011). The term in the square bracket identifies the lamina orientation. Unidirectional, or $[0]_{\#T}$, signifies that all plies are oriented in the same direction. Cross-ply, or $[0/90]_{\#S}$, indicates that the fiber orientation in each layer alternates at 0° and 90° and the "S" indicates that the layers are symmetric with respect to the middle plane of the plate. Time varying and direct current electrical characterization experiments were performed on these composite materials specimens by Zantout (2009) and Deierling (2010). Table 3.1 shows a summary of all of the specimens tested in the current work.

Table 3.1: Summary of Materials Tested

Specimen Type	# of Specimens	Specimen ID #'s	Length/Width [mm]	Thickness [mm]
IM7/977-3 [0]$_{32T}$	12	23, 24, 25, 52, 53, 54, 55, 56, 57, 58, 59, 60	152.4	4.953
IM7/977-3 [0/90]$_{8S}$	3	33, 34, 35	152.4	5.004
IM7/977-2 [0]$_{16T}$	7	26, 28, 32, 61, 62, 63, 64	152.4	2.477
IM7/977-2 [0/90]$_{4S}$	9	29, 30, 31, 46, 47,48, 49, 50, 51	152.4	2.502

Table 3.1 displays the number of each specimen type tested in the current work along

with the specimen id numbers and the dimensions of the specimens. In order to

characterize the electrical response of these composite specimens to the application of

high amplitude current pulse, a series of electrical characterization tests were performed

on 3 specimens of each type for a total of 12 specimens.

3.2 Electrical Characterization

The goals of the electrical characterization were to determine the influence of

changing the analog voltage of the current pulse generator on the electrical response of

each specimen and to determine the variations in electrical response between specimen

types. The specimens were all prepared using silver epoxy, as outlined in 2.2.3. The

resistance of each sample was tested at a DC current of 1 A prior to pulse tests. The

resistance check was to insure that none of the samples had abnormally high resistances

compared to the other samples. The resistances of each of the samples used for the

electrical testing are tabulated in Table 3.2.

Table 3.2: Resistance at 1 A DC for Electrical and Coordinated Impact Test Specimens

Specimen ID #	Specimen Type	Resistance [Ohms]
Electrical Characterization Specimens		
23	IM7/977-3 $[0]_{32T}$	0.0190
24	IM7/977-3 $[0]_{32T}$	0.0205
25	IM7/977-3 $[0]_{32T}$	0.0197
26	IM7/977-2 $[0]_{16T}$	0.0590
27*	IM7/977-2 $[0]_{16T}$	0.1386
28	IM7/977-2 $[0]_{16T}$	0.0448
32	IM7/977-2 $[0]_{16T}$	0.0555
29	IM7/977-2 $[0/90]_{4S}$	0.0816
30	IM7/977-2 $[0/90]_{4S}$	0.1118
31	IM7/977-2 $[0/90]_{4S}$	0.1240
33	IM7/977-3 $[0/90]_{8S}$	0.0513
34	IM7/977-3 $[0/90]_{8S}$	0.0384
35	IM7/977-3 $[0/90]_{8S}$	0.0641
Coordinated Impact Specimens		
55	IM7/977-3 $[0]_{32T}$	0.0370
56	IM7/977-3 $[0]_{32T}$	0.0585
57	IM7/977-3 $[0]_{32T}$	0.0322
58	IM7/977-3 $[0]_{32T}$	0.0273
59	IM7/977-3 $[0]_{32T}$	0.0394
60	IM7/977-3 $[0]_{32T}$	0.0503
64	IM7/977-2 $[0]_{16T}$	0.0816
46	IM7/977-2 $[0/90]_{4S}$	0.0925
47	IM7/977-2 $[0/90]_{4S}$	0.1274
51	IM7/977-2 $[0/90]_{4S}$	0.1064

All of the specimens had reasonable resistance values, except for specimen 27. Sample 27 had a resistance that was 2 or 3 times higher than the rest of the 16 ply unidirectional specimens. Since the goal of the electrical characterization tests was to determine the general response of each specimen type to the application of a current pulse, it was determined to discard sample 27, since the resistance was abnormally high. Sample 27 was replaced with sample 32, which had a reasonable resistance. Once the resistance values were verified, the electrical characterization tests were performed according to the procedures laid out in 2.3.1 to 2.3.5. The current versus time curves for the electrical characterization tests are displayed in sections 3.2.1 to 3.2.4. There was a significant amount of noise present in the voltage versus time and resistance versus time curves, so those curves are shown in Appendix A and Appendix C, respectively.

3.2.1 IM7/977-3 $[0]_{32T}$ Electrical Characterization

Three 32 ply unidirectional IM7/977-3 composite specimens were available for testing. The 32 ply unidirectional specimens were chosen for first testing, since they have the lowest resistance of any of the specimens available. The low resistance was desired, because the operation of the current pulse generator was new and a lower resistance would decrease the chance of burning or arcing. The specimens labeled 23, 24, and 25 were prepared for electrical testing and clamped into the test fixture. The response of the composite specimens to the application of a current pulse was unknown, so electrical characterization tests were initiated at a low voltage, and the voltage was increased successively. Specimens 23, 24, and 25 were tested using the current pulse generator at analog voltage levels of 50 V, 100 V, 150 V, 200 V, and 250 V. Figures 3.1, 3.2, and 3.3 show the current plotted versus time for each of the three specimens.
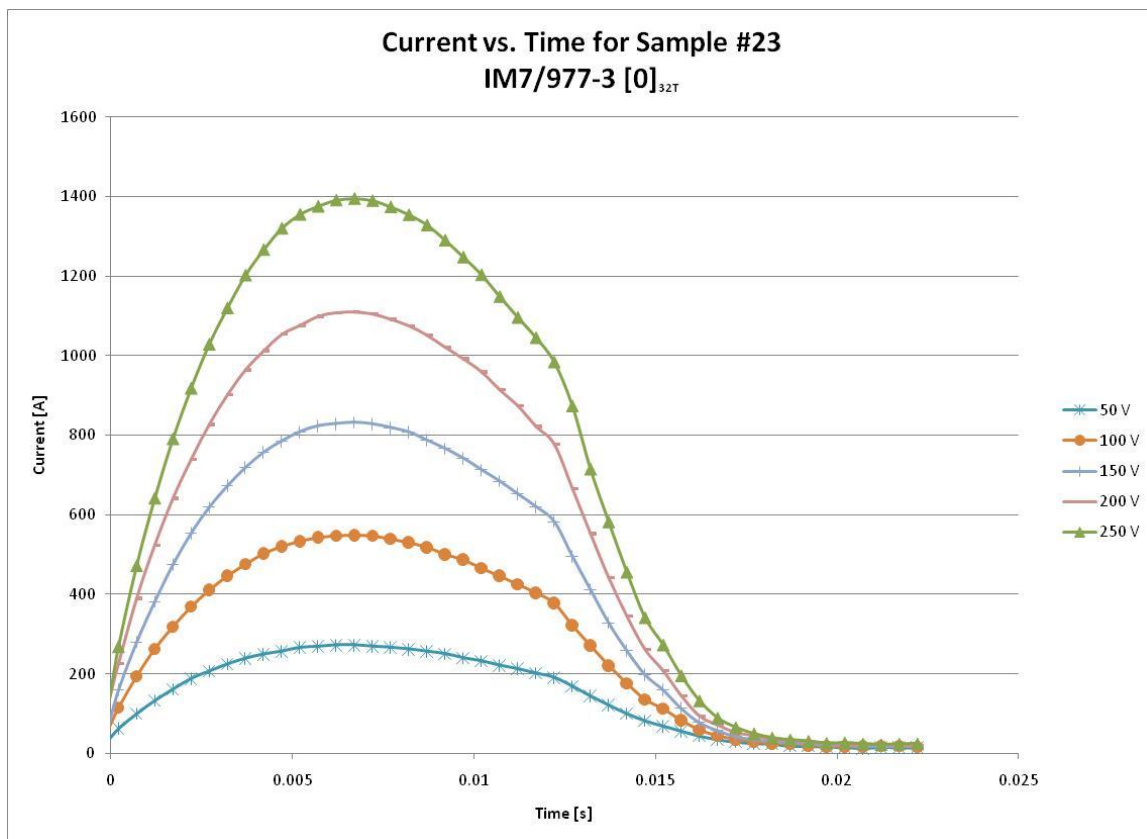
Figure 3.1: Current versus Time for Electrical Characterization of Sample 23
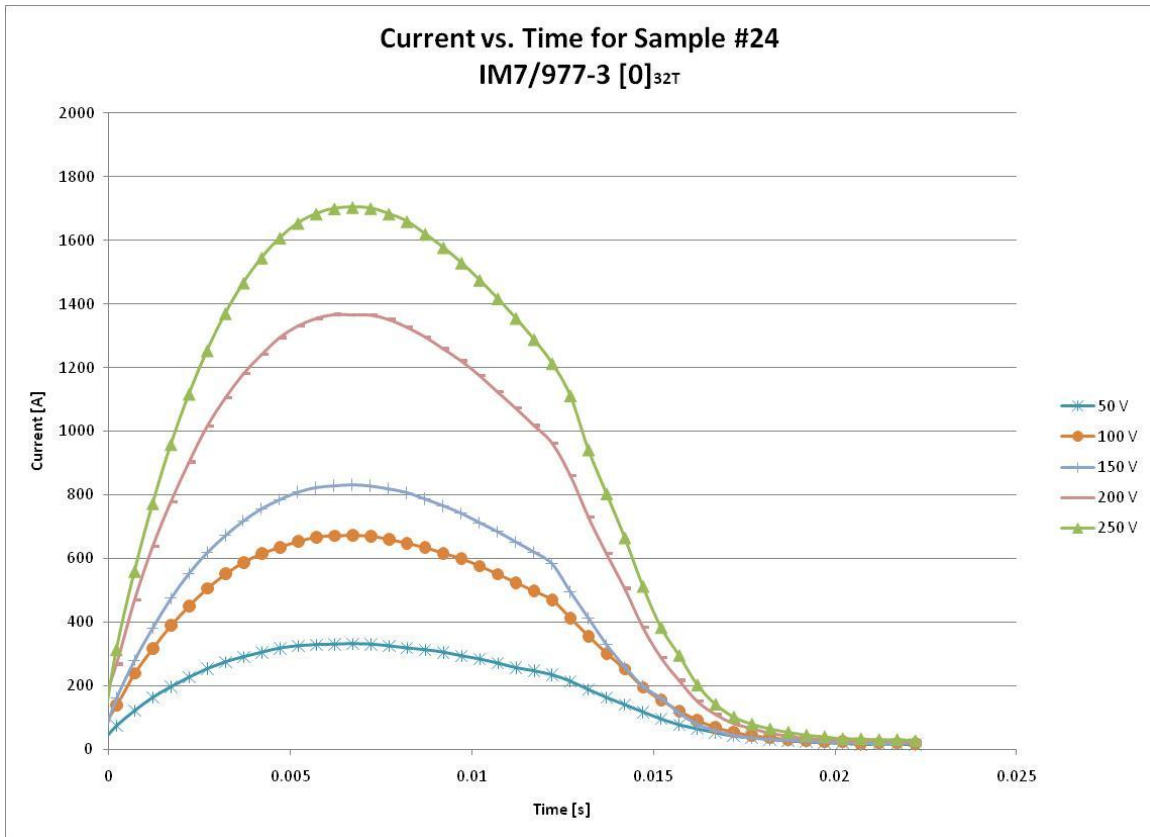
Figure 3.2: Current versus Time for Electrical Characterization of Sample 24
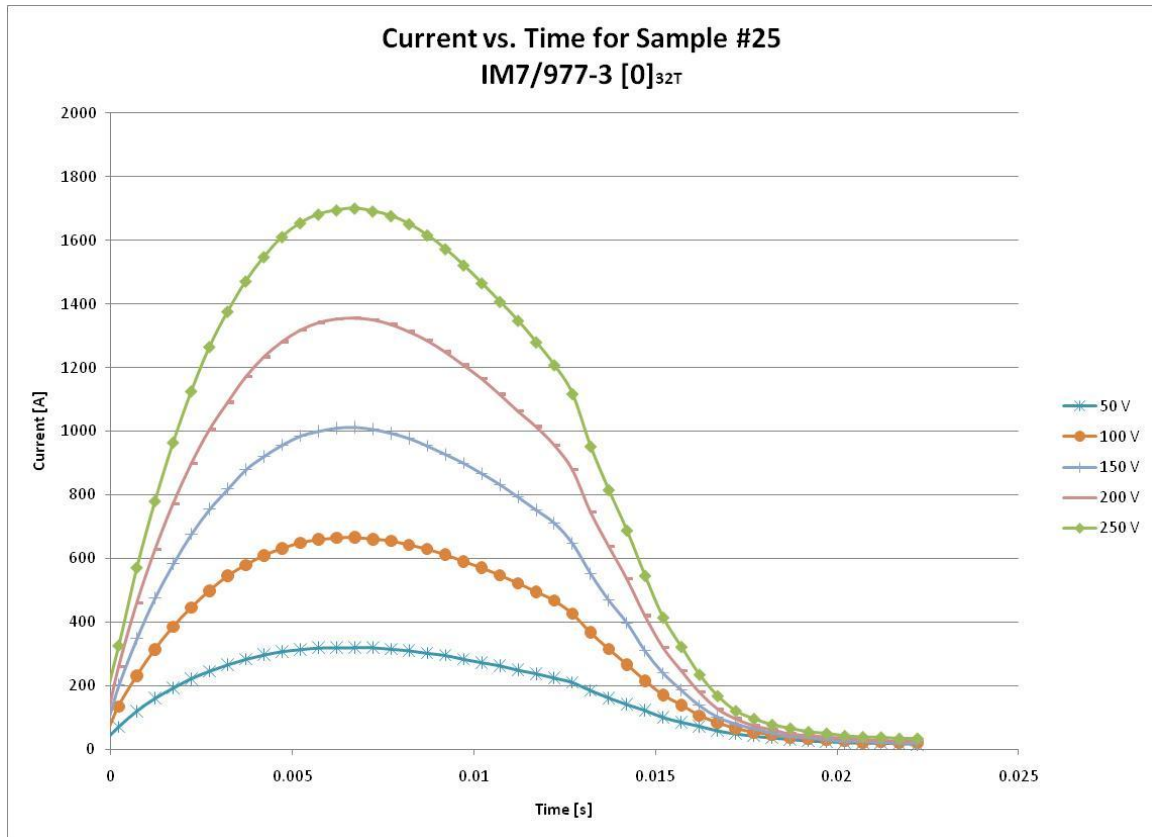
Figure 3.3: Current versus Time for Electrical Characterization of Sample 25

For all three specimens, as the analog voltage increased, the magnitude of the current

pulse increased as well. The duration of the current pulse was the same for every test in

Figures 3.1 to 3.3, which was expected, because the duration of the current pulse is an

inherent property of the capacitor modules in the current pulse generator. In order to

more easily compare each of the tests, the analog voltage of the current pulse generator,

the maximum current, and the resistance of the sample were tabulated in Table 3.3. The

resistance of the sample varied with time, so the resistance values shown in Table 3.3 were selected as the resistance of the sample at the instant of maximum current.

Table 3.3: Analog Voltage, Maximum Current, and Resistance of 32 ply Unidirectional Specimens

	Analog Voltage [V]	Max Current [A]	Resistance [Ohms]
Sample 23	50	271.6	0.020
	100	548.2	0.021
	150	830.1	0.016
	200	1107.7	0.018
	250	1393.7	0.018
Sample 24	50	330.0	0.021
	100	670.0	0.016
	150	1012.0	0.015
	200	1365.0	0.017
	250	1708.0	0.017
Sample 25	50	320.3	0.022
	100	664.3	0.027
	150	1009.6	0.019
	200	1352.9	0.018
	250	1694.9	0.015

As evident from Figures 3.1 to 3.3 and Table 3.3, the results from samples 24 and 25 were very similar for each analog voltage, where as the results from sample 23 were not. The largest difference between the maximum current in samples 24 and 25 was 3% at an analog voltage of 50 V. This discrepancy was miniscule and could be attributed to the poor resolution of the analog voltmeter on the current pulse generator. In comparison,

the largest difference between the maximum current in samples 23 and 24 was 19% at an analog voltage of 200 V. This inconsistency was quite large and could not be attributed to the resolution of the analog voltmeter. At an analog voltage of 200 V, the resistance values of samples 23 and 24 differed by only 6%. Although the difference in resistance between the composite specimens could slightly affect the results, this difference in resistance could not be completely at fault for the large difference in current pulse magnitude. At an analog voltage of 100 V, the resistance of samples 24 and 25 differed by 41%, however, the maximum current differed by only 1%. It was concluded that further electrical characterization was required before any generalizations could be made about the response of the plates to the application of a current pulse.

3.2.2 IM7/977-3 $[0/90]_{8S}$ Electrical Characterization

Three 32 ply cross-ply IM7/977-3 specimens were available for electrical characterization tests. In general, the resistance of a cross-ply plate is twice the resistance of a unidirectional plate for a given thickness. This phenomenon occurs, because current only flows through the plies in which the fibers align with the direction of the current. For unidirectional plates, there are twice as many conducting plies as compared to a cross-ply plate of the same thickness. Since resistance is inversely related to conductivity, the resistance of a 32 ply cross-ply plates is approximately twice as high as the resistance of a 32 ply unidirectional plate. The increase in resistance is an increase in the contact resistance between the composite specimen and the copper electrode. Since the resistance of the 32 ply cross-ply specimen was higher than the resistance of the 32-ply unidirectional specimen, electrical characterization tests were started at a lower analog voltage of 20 V and were increased successively. Figure 3.4 shows the current versus time for specimen 33 at four voltage levels.

Figure 3.4: Current versus Time for Electrical Characterization of Sample 33

The first electrical characterization test on sample 33 was performed at an analog voltage of 20 V. The 20 V test was successful, so tests were also completed at 50 V and 100 V. Once these tests were completed, it was desired to see if a specific current could be attained by applying the appropriate analog voltage. The maximum current was plotted versus analog voltage for the 20 V, 50 V, and 100 V tests, and the linear fit equation was determined according to the method in section 2.3.5. Using the linear fit line, the analog voltage required to produce a current pulse of 1200 A was determined to

be 182.1 V. The analog voltage was set to approximately 182 V, and a final pulse test was performed successfully. More detailed results on the linear fit developed for sample 33 are discussed in section 3.2.5. Next, electrical characterization tests were performed on sample 34, as shown in Figure 3.5.
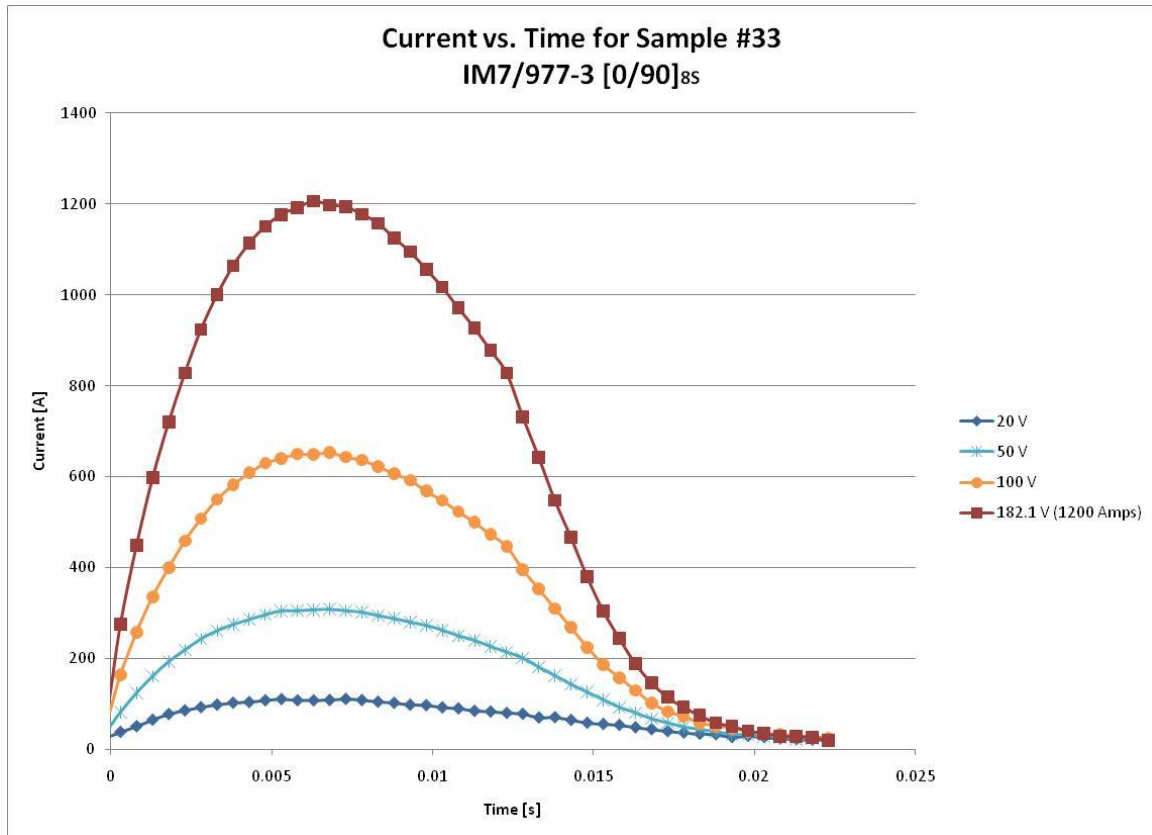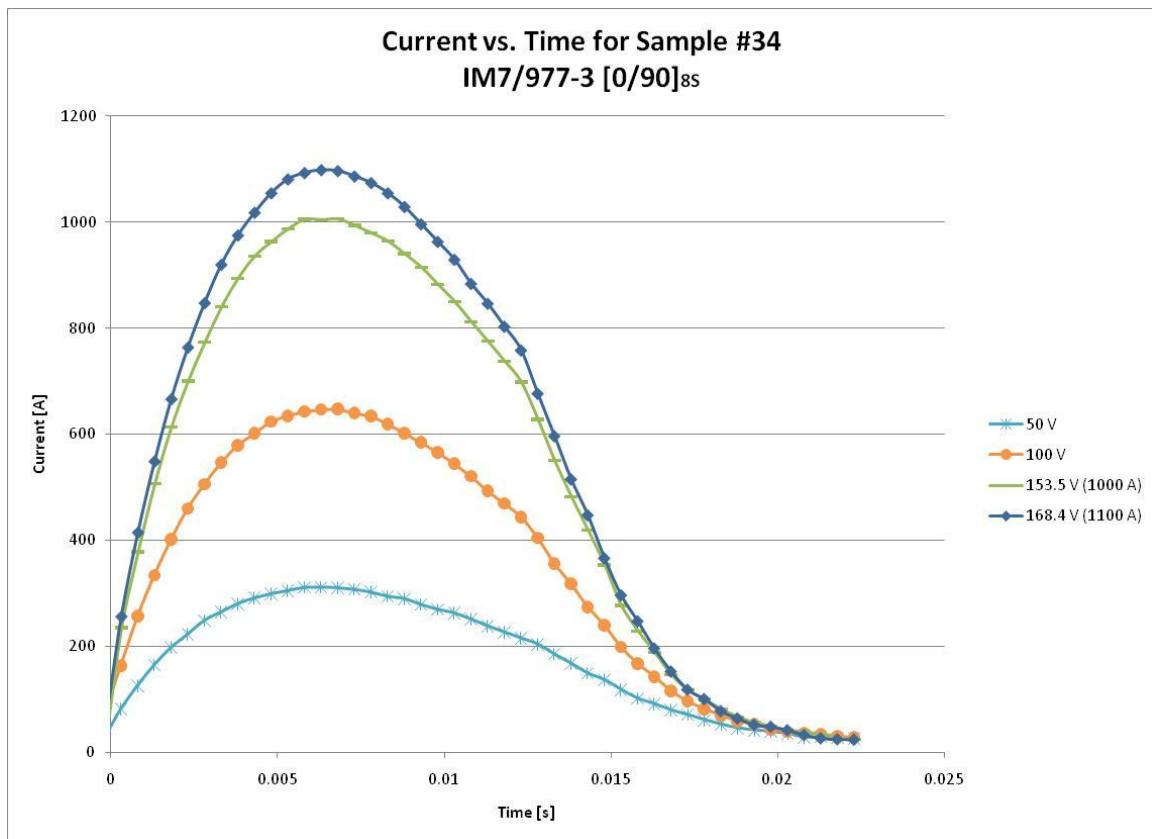

Figure 3.5: Current versus Time for Electrical Characterization of Sample 34

Initial electrical characterization tests were performed at analog voltage levels of 50 V and 100 V. Next, it was desired to determine if it was possible to accurately predict the required analog voltage to produce a given current using an interpolation of only two points. The linear approximation of the maximum current versus analog voltage was determined using the method of 2.3.5, and the analog voltages were determined for desired current values of 1000 A and 1100 A as 152.5 V and 168.4 V, respectively. Similar to specimen 34, the electrical characterization of sample 35 testing began at 50 V and 100 V and was increased successively thereafter. Electrical characterization results are shown in Figure 3.6.
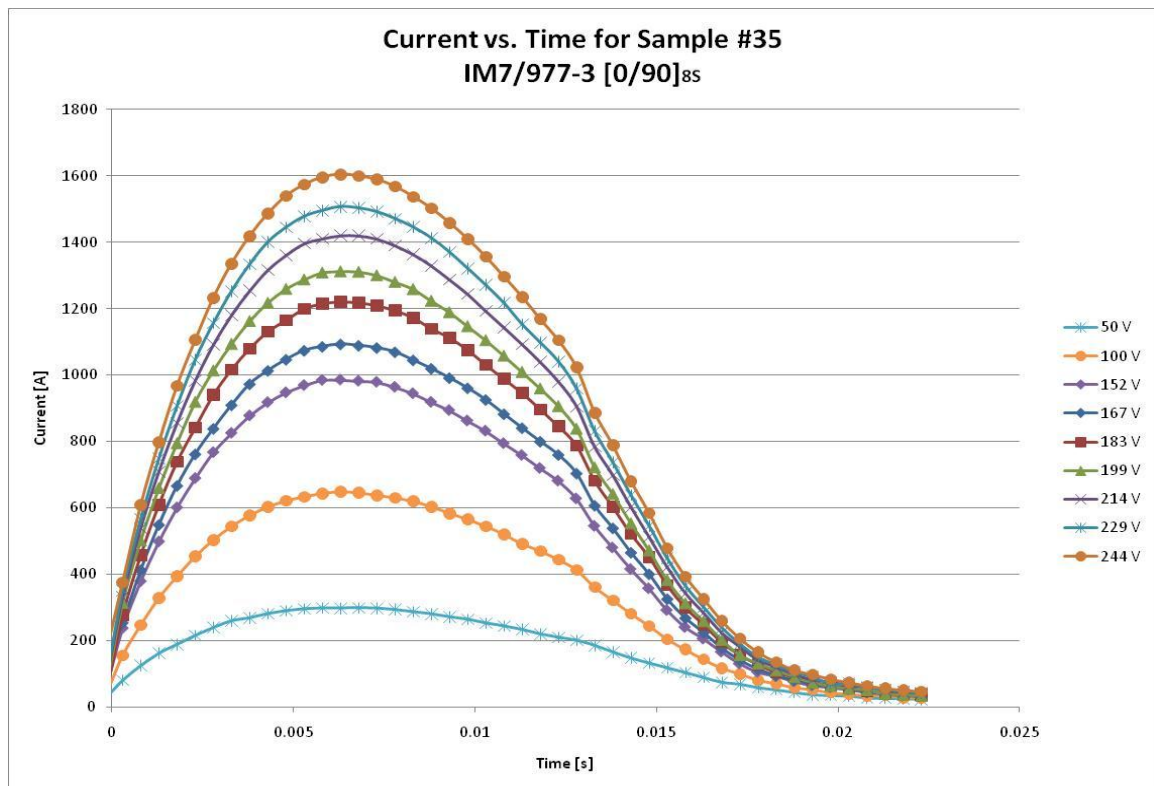
Figure 3.6: Current versus Time for Electrical Characterization of Sample 35

Once the tests were completed at analog voltage levels of 50 V and 100 V, the linear approximation of current versus analog voltage was determined. Using the linear approximation, the required analog voltages to produce current pulses of 1000 A, 1100 A, 1200 A, 1300 A, 1400 A, 1500 A, and 1600 A were determined. Electrical characterization tests were also performed at these analog voltages. A complete summary of analog voltage, maximum current, and resistance for samples 33, 34, and 35 is tabulated in Table 3.4.

Table 3.4: Analog Voltage, Maximum Current, and Resistance of 32 ply Cross-ply Specimens

	Analog Voltage [V]	Max Current [A]	Resistance [Ohms]
Sample 33	20	108.2	0.047
	50	305.8	0.034
	100	647.3	0.024
	182	1194.3	0.029
Sample 34	50	309.0	0.033
	100	642.9	0.027
	154	999.1	0.026
	168	1091.0	0.027
Sample 35	50	297.4	0.032
	100	641.7	0.028
	152	980	0.024
	167	1084.6	0.026
	183	1212.3	0.023
	199	1303.8	0.022
	214	1412.1	0.022
	229	1495.3	0.021
	244	1592.6	0.023

In comparing the maximum current values at 50 V for samples 33, 34, and 35, the maximum currents ranged from 297.4 A to 309.0 A, with a mean value of 304.1 A. Compare to the mean value, sample 35 had the largest error of 2%, which was acceptable. Similarly, the mean value for maximum current was 644.0 A. The maximum relative error compared to the mean current at 100 V was 0.5% for sample 33. Additionally, it was desired to evaluate the accuracy of predicting current output using the current versus analog voltage curves.

For sample 33, the desired current at 182 V was 1200 A, where as the actual current obtained was 1193.4 A. The error in this test was 0.6%, which was acceptable. For sample 34, the tests aiming to achieve 1000 A and 1100 A were also successful and had errors of 0.01% and 0.1%, respectively. For sample 35, the test aiming to achieve a current of 1000 A resulted in a maximum current of 980 A, which was an error of 2%. The 1100 A, 1200 A, 1300 A, 1400 A, 1500 A, and 1600 A tests all had errors of 1% or less. For 32 ply cross-ply specimens, it was determined that consistent current output could be expected for a given analog voltage for different specimens. In addition, it was determined that current output could be accurately predicted using a linear interpolation with only two points, as evidenced from specimens 34 and 35.

3.2.3 IM7/977-2 $[0]_{16T}$ Electrical Characterization

Three 16 ply unidirectional IM7/977-2 specimens were available for electrical characterization tests. In general, the resistance of a unidirectional plate is about equal to the resistance of a cross-ply plate with twice the thickness. In this case, the 16 ply unidirectional has a resistance that is similar to a 32 ply cross-ply plate. This occurs, because there are the same number of conducting plies in each of the two specimens. Due to this similarity, it was decided to start the electrical characterization tests at 20 V. Once

the 20 V test was determined to be successful, additional tests were run at higher voltage

levels. Figure 3.7 shows the current versus time for specimen 26 at four voltage levels.

Figure 3.7: Current versus Time for Electrical Characterization of Sample 26

Current pulse tests were carried out successfully at analog voltage level of 20 V, 50 V, and 100 V. For the 150 V test, there was significant burning on the edge of the specimen at the composite/electrode interface, as shown in Figure 3.8.
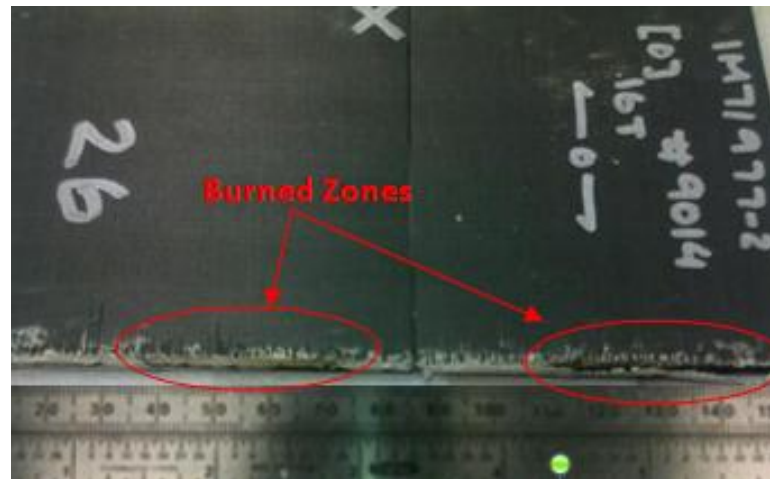
Figure 3.8: Burned Edges of Sample 26

The electrical arc was so strong that it blew a hole through the silver epoxy, as evident on the right side of the specimen in Figure 3.8. The electrical results of the 150 V test were also very strange. As evident in Figure 3.7, the current versus time curve for the 150 V test had an abnormal shape and did not reach a maximum value at 6.5 milliseconds, which was the time at which all other tests reached a maximum current value. Due to this strange result, further testing was performed on sample 28 in order to supplement the

findings. The results for 20 V, 50 V, 100 V, 120 V, 150 V, and 170 V pulse tests are shown in Figure 3.9.

Figure 3.9: Current versus Time for Electrical Characterization of Sample 28

For sample 28, pulse tests were successful at analog voltage level of 20 V, 50 V, and 100 V. Since sample 26 failed at a voltage level of 150 V, it was decided to test

sample 28 at an intermediate voltage level before proceeding to 150 V. A pulse test was successfully carried out at 120 V, so an additional test was performed at 150 V to determine if failure would again occur at 150 V. The 150 V pulse test on specimen 28 was also successful, so one final test was performed at 170 V to see if a voltage above 150 V could be reached successfully. The 170 V pulse test was also successful, so it was determined that failure of specimen 26 could have been possibly been an anomaly. In order to confirm this conjecture, three more tests were performed on sample 32, as shown in Figure 3.10.
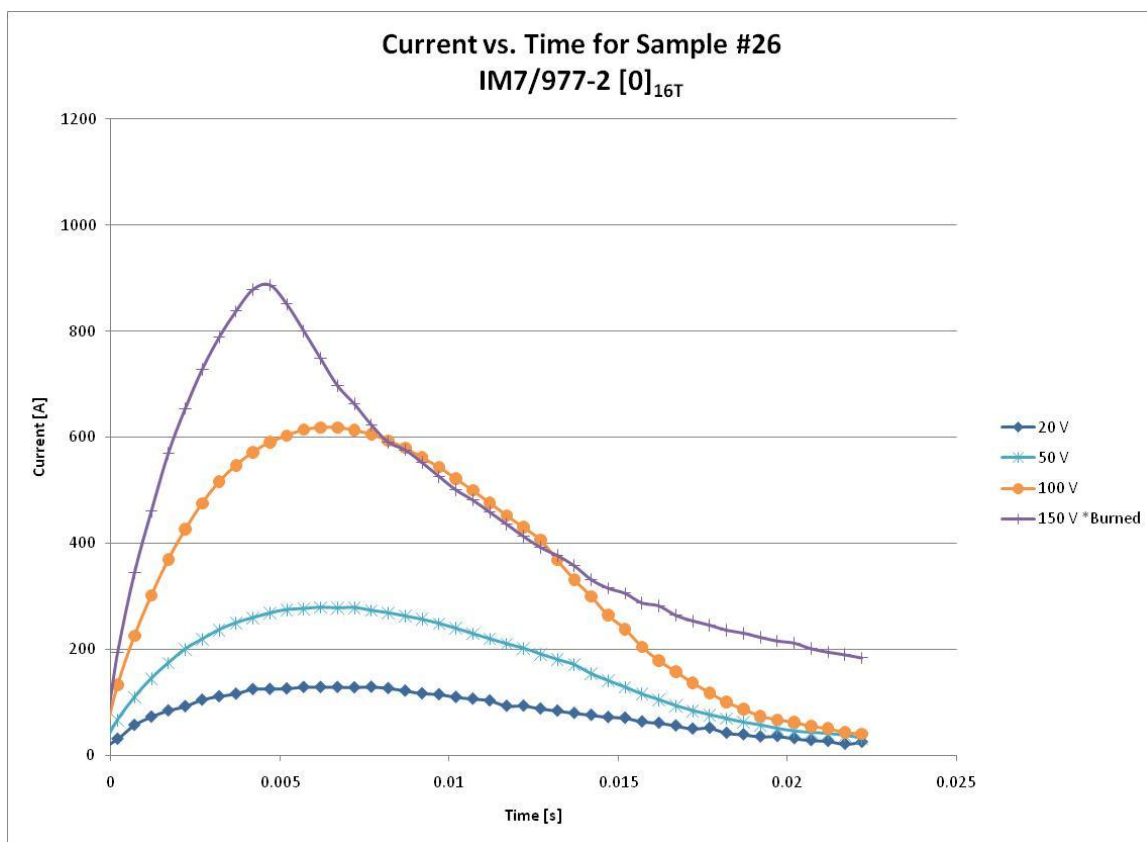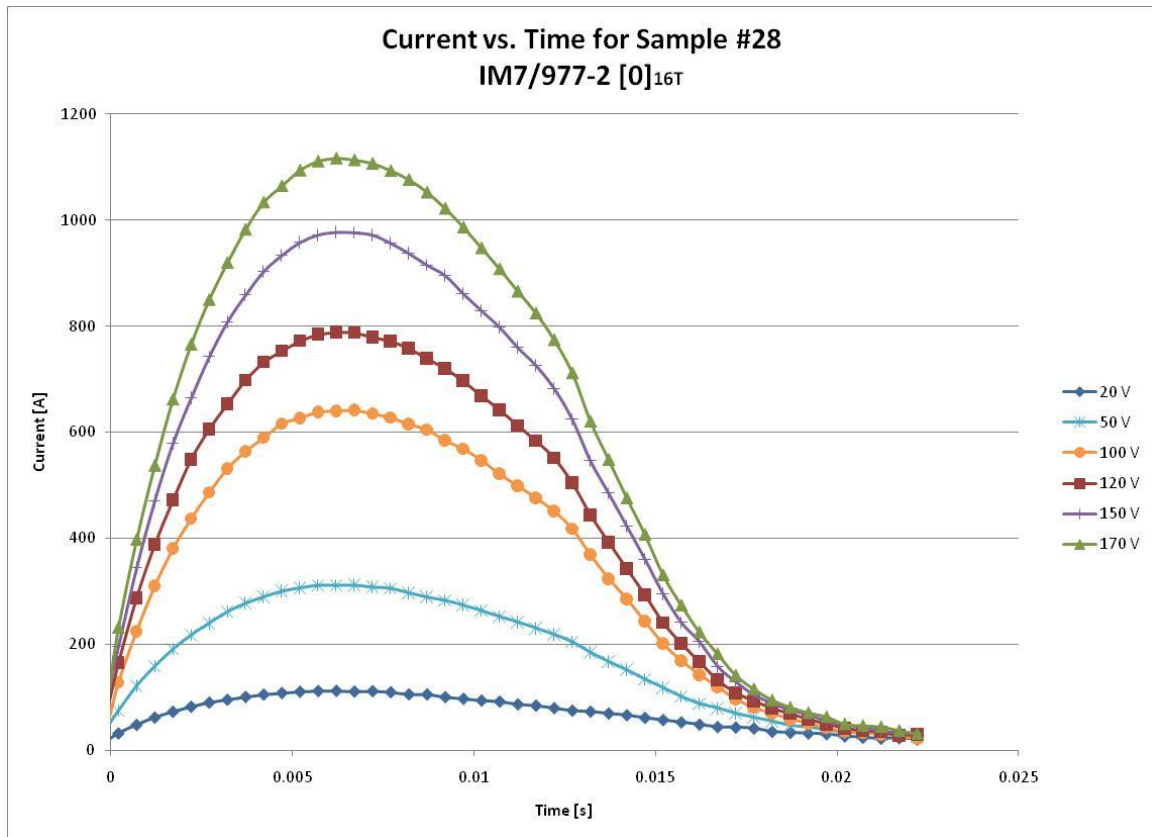

Figure 3.10: Current versus Time for Electrical Characterization of Sample 32

Normal current pulse tests were successful at analog voltages of 50 V, 100 V, and 150 V on sample 32. In order to compare tests for the 16 ply unidirectional specimens the results from the electrical characterization tests were tabulated in

Table 3.5: Analog Voltage, Maximum Current, and Resistance of 16 ply Unidirectional Specimens

	Analog Voltage [V]	Max Current [A]	Resistance [Ohms]
Sample 26	20	128.8	0.059
	50	278.0	0.047
	100	617.2	0.035
	150	734.5	0.111
Sample 28	20	111.6	0.045
	50	310.2	0.035
	100	637.4	0.028
	120	783.3	0.027
	150	972.5	0.027
	170	1108.9	0.025
Sample 32	50	280.4	0.039
	100	625.8	0.034
	150	949.5	0.036

The current reached at 150 V for sample 26 was 734 A and was much less than the current reached by samples 28 and 32 which were 972.5 A and 949.5 A, respectively. This significant difference in maximum current was attributed to arcing in the sample. The current pulse generator is driven by capacitors. If arcing occurred between the composite specimen and electrode, the energy discharged by the capacitor was wasted by

arcing, so less current was generated. Discrepancies between the resistances of the samples were also noteworthy. The resistance of sample 26 was 0.111 Ω for the 150 V test, where as the resistances of samples 28 and 32 were 0.027 Ω and 0.036 Ω, respectively. The high resistance of sample 26 followed intuition, since arcing occurs across highly resistive interfaces. Although sample 26 had abnormal results, samples 28 and 32 had more similar results. The largest difference between the current results for samples 28 and 32 was at 50 V. At this voltage level, sample 28 yielded a maximum current of 310.2 A, where as sample 32 was subjected to a current of 280.4 A. The two current values differed by 10 %. This difference between the two 16 ply unidirectional specimens was larger than error between 32 ply specimens. In order to determine whether the incongruity between specimens was due to the thickness, additional electrical characterization tests were performed on 16 ply cross-ply specimens.

3.2.4 IM7/977-2 $[0/90]_{4S}$ Electrical Characterization

Three 16 ply cross-ply IM7/977-2 specimens were available for electrical characterization tests. As in the case of 32 ply specimens, the resistances of the 16 ply cross-ply plates were assumed to be twice as high as the resistances of the 16 ply unidirectional specimens. Current pulse tests were begun at 20 V and were increased after successful tests. Figure 3.11 shows the current versus time results for specimen 29.
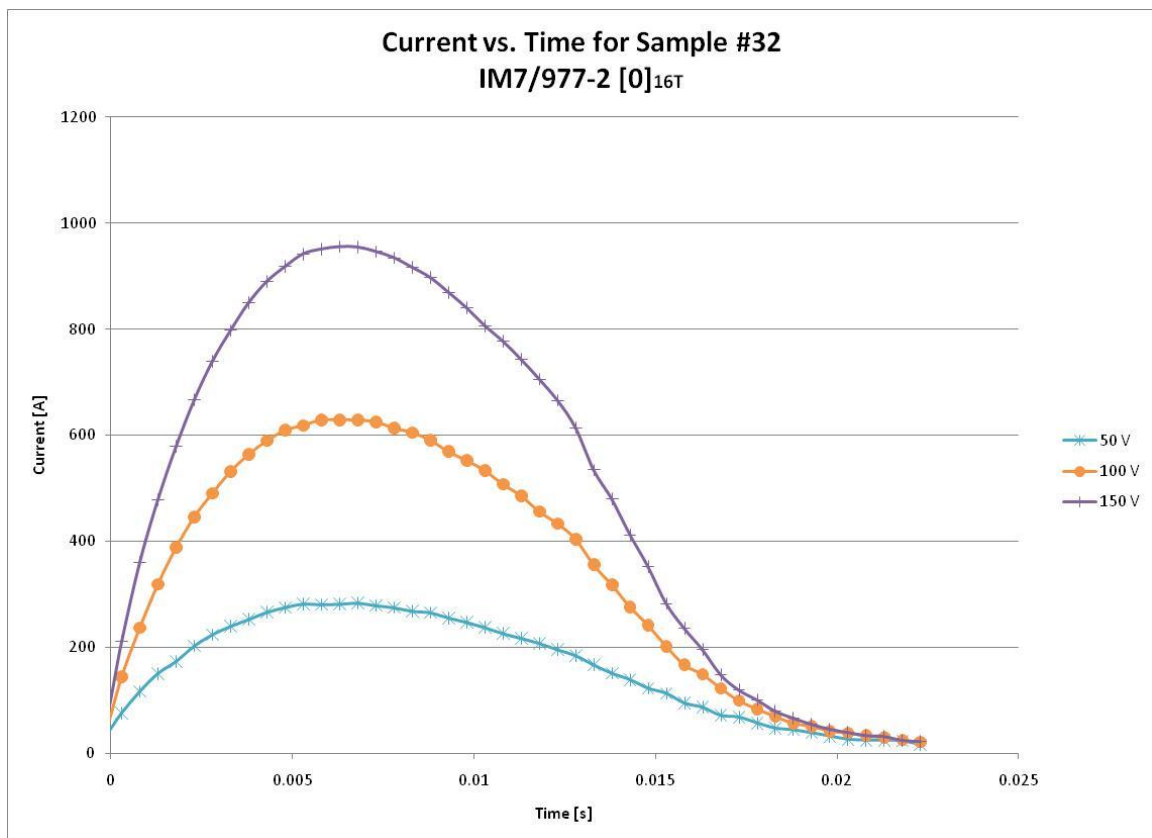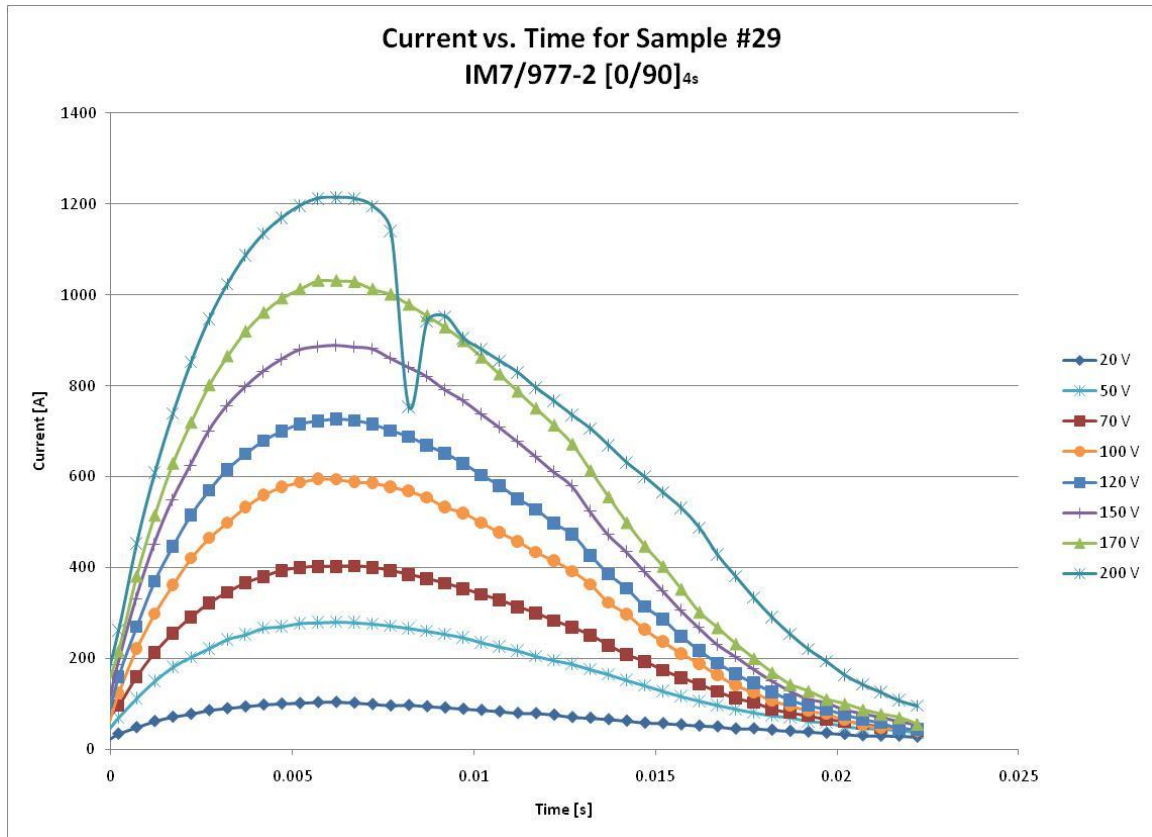
Figure 3.11: Current versus Time for Electrical Characterization of Sample 29

        Successful current pulse tests were carried out at analog voltage levels of 20 V, 50 V, 70 V, 100 V, 120 V, 150 V, and 170 V on sample 29. The results from the 200 V pulse test were strange in that a drop in current occurred at approximately 8 milliseconds. The cause of the drop in current was identified as arcing, since burn marks were left on the surface of the composite at the interface between the specimen and electrode, as shown in Figure 3.12.
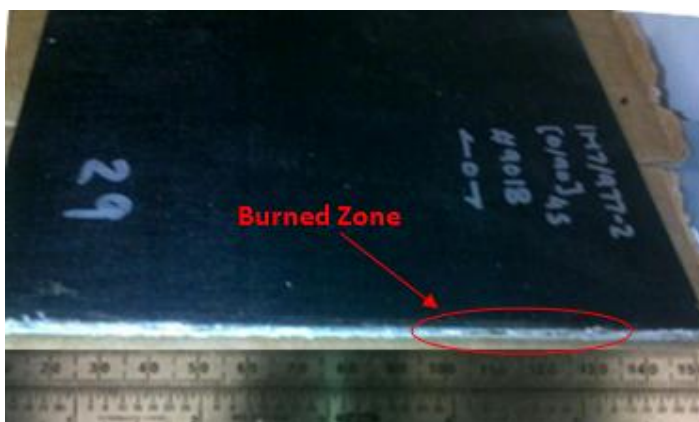
Figure 3.12: Burned Edges of Sample 29
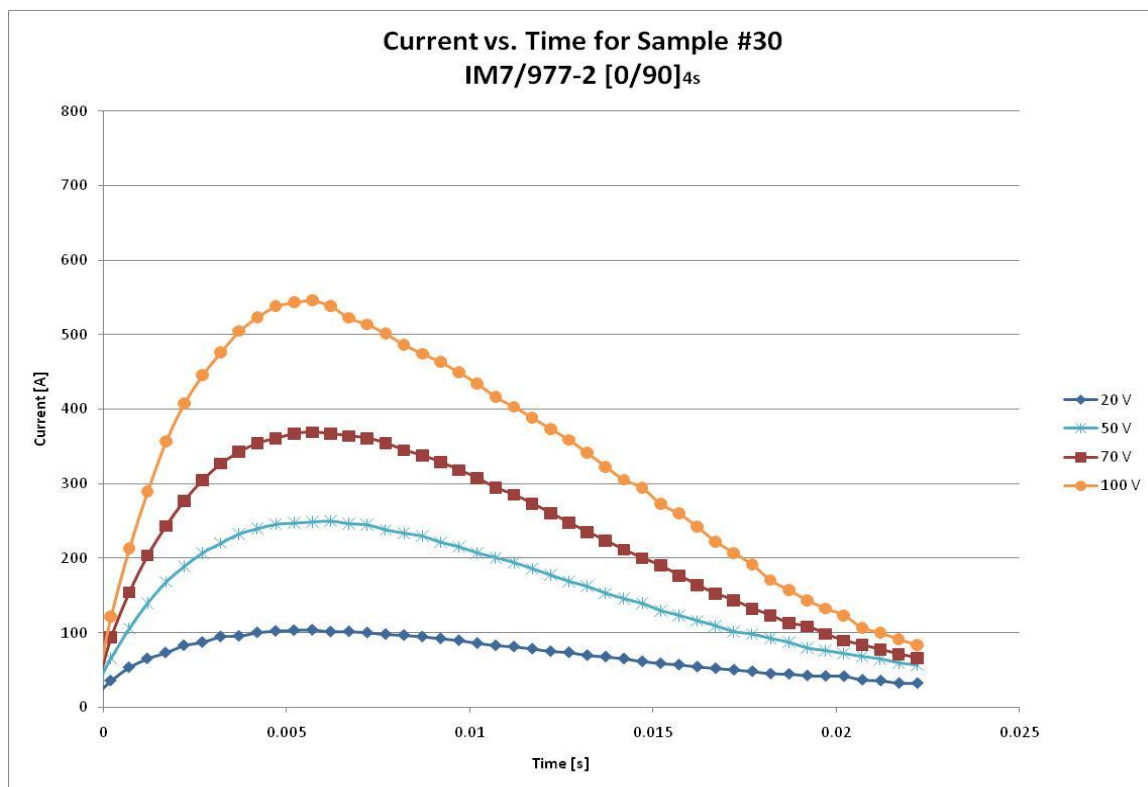
Figure 3.13: Current versus Time for Electrical Characterization of Sample 30

Further testing was performed in order to determine if arcing would occur again. Figure 3.13 shows the results of the electrical characterization tests on sample 30.

For sample 30, successful current pulse tests were performed at analog voltages of 20 V, 50 V, and 70 V. At 100 V, the current pulse curve had strange results. The falling edge of the current pulse was flattened more than usual. In normal pulse curves, the falling edge is rounded, however, in this test, this was not the case. Although there were no signs of burning, it was decided to forego further testing on sample 30 proceed to the next specimen. Figure 3.14 shows the electrical characterization results of sample 31.
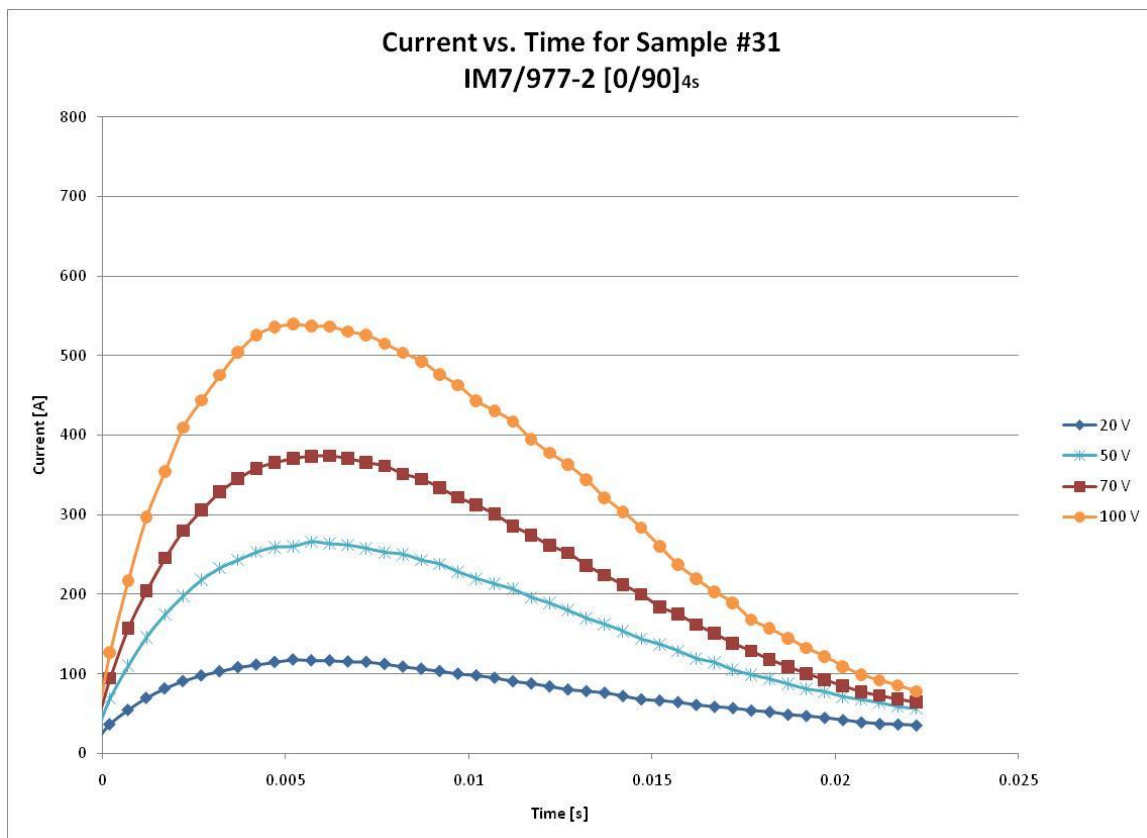
Figure 3.14: Current versus Time for Electrical Characterization of Sample 31

For specimen 31, current pulse tests were carried out successfully at analog voltage levels of 20 V, 50 V, 70 V, and 100 V. Testing was stopped at 100 V, since this was the voltage level at which sample 30 showed strange results. In order to compare the results between specimens 29, 30, and 31, results were tabulated in Table 3.6.

Table 3.6: Analog Voltage, Maximum Current, and Resistance of 16 ply Cross-ply
Specimen

	Analog Voltage [V]	Max Current [A]	Resistance [Ohms]
Sample 29	20	105.0	0.070
	50	280.9	0.054
	70	403.5	0.051
	100	595.3	0.047
	120	726.6	0.043
	150	889.1	0.041
	170	1031.3	0.039
	200	1213.8	0.039
Sample 30	20	104.0	0.099
	50	249.9	0.085
	70	369.2	0.073
	100	545.8	0.08
Sample 31	20	117.1	0.103
	50	266.2	0.076
	70	374.1	0.07
	100	537.1	0.072

An important observation can be made by examining the data in Table 3.6. As the analog voltage increased, the maximum current in sample 29 increased at a faster rate than it did in samples 30 and 31. For example, at an analog voltage level of 20 V,

samples 29, 30, and 31 had maximum currents of 105.0 A, 104.0 A, and 117.1 A, respectively. At 70 V, sample 29 was about 30 A higher than samples 30 and 31. Finally, at 100 V, the current in sample 29 was 50 A higher than samples 30 and 31. It was noteworthy that at 70 V and 100 V, the resistance of sample 29 was much lower than the resistances of samples 30 and 31. At 100 V, the resistance of sample 29 was 41% less than that of sample 30 and 35% less than sample 31. As mentioned in section 2.3.1, the total current in the system is determined by the analog voltage and total system resistance. The system resistance is the resistance of the composite specimen plus the resistance of the internal components of the current pulse generator. Therefore, since the resistance of sample 29 was much less than resistances of samples 30 and 31, the total system resistance was lower, and thus the current in the plate was higher. This finding was quite significant, since if the resistance of a given specimen is abnormally high or low, the current in the plate could be affected. In order to further examine the response of maximum current in the specimens to the analog voltage, the maximum current was plotted versus analog voltage.

3.2.5 Electrical Characterization Calibration

The maximum current and voltage values from Tables 3.3 to 3.6 were plotted in Figure 3.15. Next, linear approximations were fit to the data from each specimen so that a unique linear approximation equation was found for each specimen. The correlation coefficient for each approximation was either 1 or nearly 1, which indicates a nearly perfect linear approximation. A unique observation of Figure 3.15 is that all of the samples, regardless of thickness and layup, had very similar curves except for samples 23, 26, and 29. Samples 26 and 29 were both samples that arced. Sample 23 did not arc, however, the current in sample 23 was much less than the other 32 ply unidirectional

samples. From these findings, it can be assumed that if the maximum current versus analog voltage curve shows diverges from the norm, there is an increased likelihood of electrical failure. All 12 current versus voltage curves and the associated linear approximations are shown in Figure 3.15.
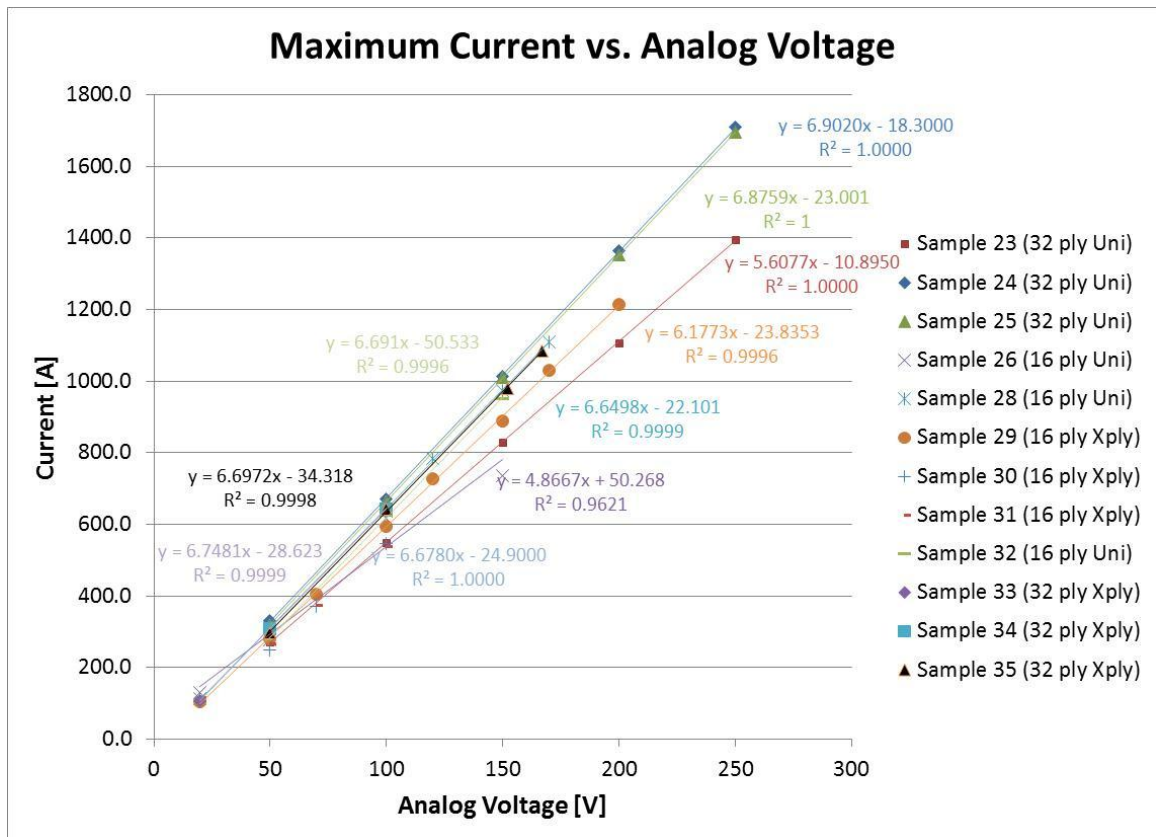

Figure 3.15: Maximum Current versus Analog Voltage for Electrical Characterization

3.2.6 Electrical Characterization Summary

A few significant trends were observed during the electrical characterization tests. First, it was determined that as the analog voltage increases on the current pulse generator, the maximum current in the test increases at a linear rate. Second, it was determined that the maximum current for a successful current pulse test will always occur at 6.5 milliseconds. Next, the safe analog voltage limits for each specimen type were determined by observing the maximum voltage before arcing or burning of the specimen occurred. Finally, it was determined that by using the unique current versus analog voltage curve for a given specimen, the applied current can be accurately predicted given an arbitrary voltage level. Before coordinate current pulse and impact tests could be performed, impact characterization tests were required in order to observe the response of carbon fiber composite specimens to an impact event.

3.3 Impact Characterization

The goal of the impact characterization was to use the Instron 8200 impact machine to determine the energy at which each type of carbon fiber composite specimen endures visible damage. For all specimens the tests were carried out by starting at a low drop height and mass and therefore a low energy. The drop height and mass were gradually increased until an energy level was determined at which the specimens showed visible damage, called the critical energy. This energy was found for 16 ply unidirectional and cross-ply and 32 ply unidirectional plates. Impact tests were not performed on 32 ply cross-ply specimens, because the DELRIN© tup insert was not strong enough to withstand the impact load required to cause visible damage to this specimen. Once the critical energy was determined for each of the three specimen types,

3 specimens of each type were impacted at those energies for a total of 9 non-electrified impact tests.

3.2.1 IM7/977-3 $[0]_{32T}$ Impact Characterization

Three 32 ply unidirectional IM7/977-3 samples were used for impact testing. The critical energy was found through trial and error. With a mass of 5.054 kg dropped from a height of 0.16 m, the theoretical critical energy was determined to be 7.9 J. The critical energy was determined by

$$U = mgh \qquad\qquad (3.1)$$

where U is the potential energy (J), m is the mass (kg), g is acceleration due to gravity (9.81 m/s), and h is height (m). Three composite specimens were clamped into the test fixture and impacted at the critical energy. The results from the impacts of the non-electrified specimens 52, 53, and 54 are shown in Figures 3.16 and 3.17.

All three specimens 52, 53, and 54 incurred visible damage in the form of a line crack due to the impact. Specimen 52 incurred the highest load before failing, specimen 54 endured the next highest load, and specimen 53 withstood the smallest load before failure, as shown in Figure 3.16. In contrast, Figure 3.17 shows that sample 53 had the largest deflection, sample 54 had the next largest deflection, and sample 52 had the smallest deflection. This result indicates if a specimen fails at a lower force, more damage is incurred, and the sample is less able to resist deformation.
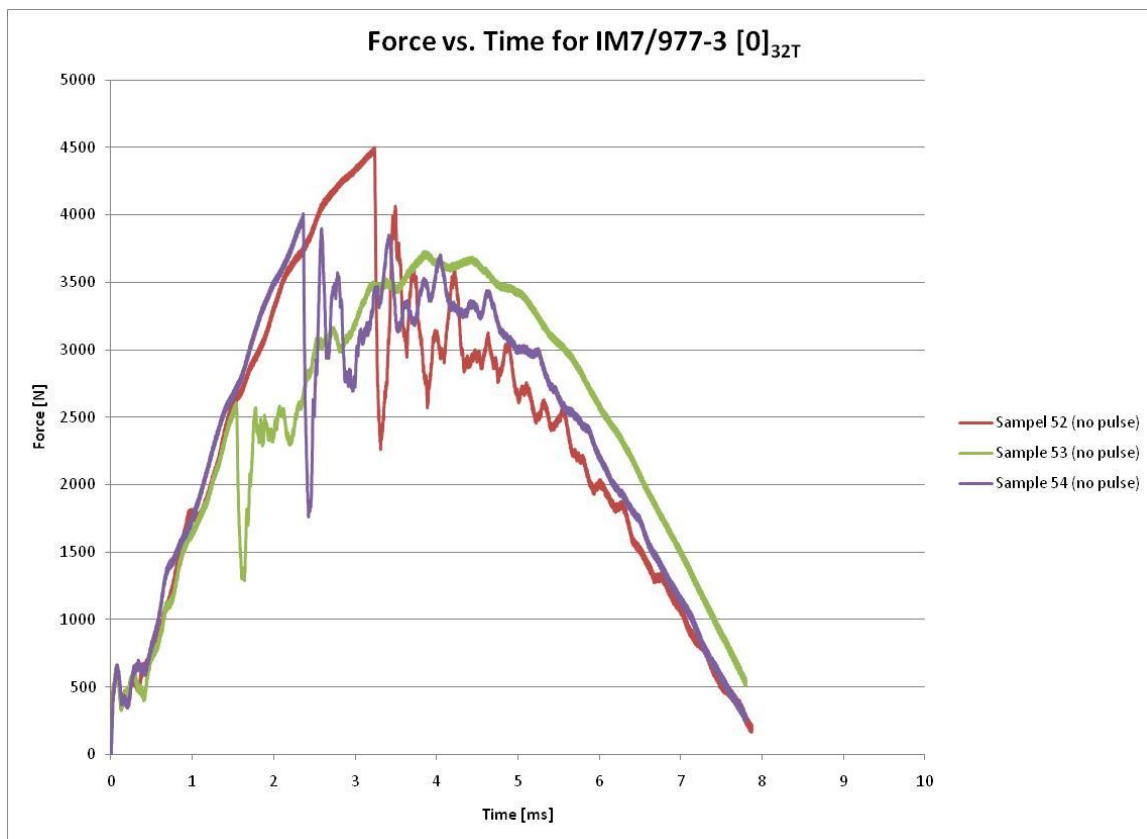
Figure 3.16: Force versus Time for Impact Characterization of Samples 52, 53, & 54
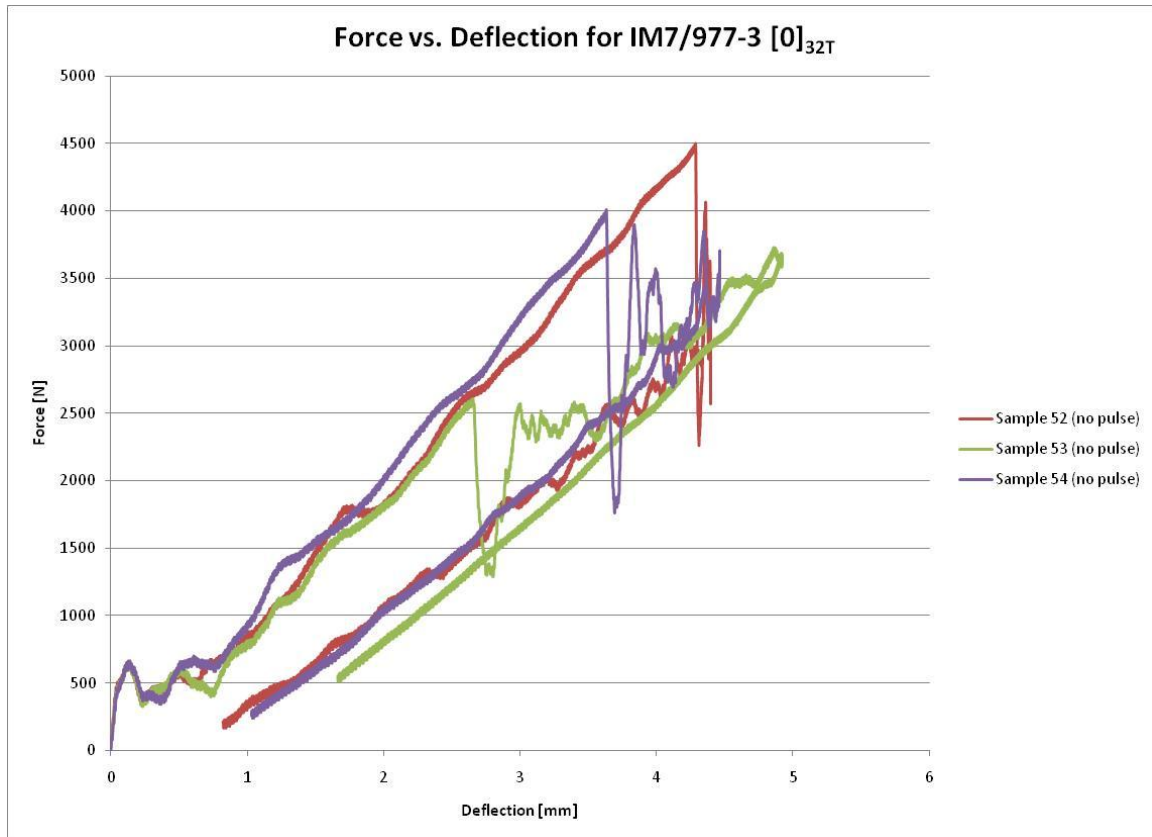
Figure 3.17: Force versus Deflection for Impact Characterization of Samples 52, 53, 54

Table 3.7: Impact Characterization Data for 32 ply Unidirectional Specimens

Specimen #	Electrical	Mass [kg]	Height [m]	Velocity [m/s]	Impact Energy [J]	Absorbed Energy [J]	Peak Load [N]	Peak Current [A]	Visible Damage
Sample 52	no pulse	5.054	0.160	1.769	8.6103	9.1890	4496.9	---	Line Crack
Sample 53	no pulse	5.054	0.160	1.767	8.5915	9.3200	3730.6	---	Line Crack
Sample 54	no pulse	5.054	0.160	1.768	8.5998	6.9678	4009.2	---	Line Crack
Average	no pulse	5.054	0.160	1.768	8.6005	8.4923	4078.9		

In order to better compare the results from the 32 ply unidirectional impact test, the relevant data was tabulated in Table 3.7.

The mean impact energy of the three 32 ply unidirectional samples was 8.6005 J. The impact energy was calculated by the Instron software using the given mass, the measured impact velocity, and the principle of kinetic energy. The peak load was measured by the instrumented load cell for each sample. The average peak load was 4078.9 N for the three 32 ply unidirectional samples. The absorbed energy was calculated by the Instron software by integrating the force versus deflection curve in Figure 3.17. The absorbed energy was taken as the amount of energy up to the peak load, as recommended by Instron (Instron, 2011). The average absorbed energy of the three specimens was 8.4923 J. Absorbed energy is greater in specimens that incur less damage, so the tests suggest that sample 54 incurred the greatest damage and sample 53 incurred the least. The damage visible on the specimens was not noticeably different, so the difference in damage must have been internal. The visible damage to the 32-ply unidirectional specimens is shown in Figure 3.18 for sample 52.
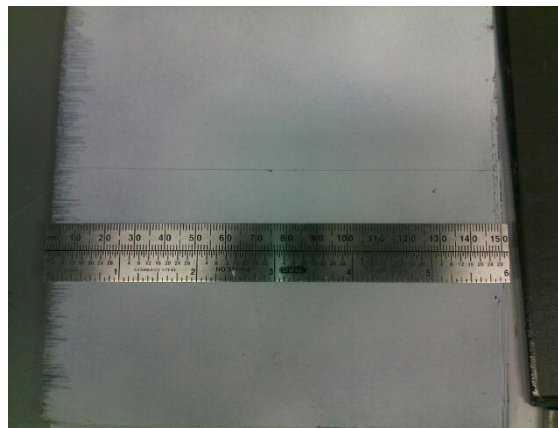

Figure 3.18: Visible Damage on the Back Side of Sample 52

3.2.2 IM7/977-3 $[0]_{16T}$ Impact Characterization

Three 16 ply unidirectional IM7/977-2 specimens were used for impact testing. The critical energy was found through trial and error. Through the trial and error method, as the energy approached the critical energy, some of the specimens were split in half by the falling tup. The damage to the test specimens that were split in half resembled Figure 3.18, however, the crack propagated through the thickness of the plate. If the plate was completely broken in half, dangerous conditions could arise in an electrified test, so it was decided to test below the critical energy. A mass of 5.054 kg was dropped from a height of 0.075 m, and the theoretical critical energy was determined to be 3.7 J by equation (3.1). At this energy, no visible damage was present in the specimens. Samples 61, 62, and 62 were clamped into the test fixture and impacted at the critical energy. The results from the impacts of the non-electrified specimens 61, 62, and 63 are shown in Figures 3.19 and 3.20.

The three 16 ply unidirectional specimens incurred no visible damage due to the impact. Specimens 61, 62, and 63 had nearly identical force versus time curves, as shown in Figure 3.19. Since no visible damage was present in the specimens, it follows that the force versus time curves should be very similar. In contrast, Figure 3.20 illustrates that there were slight differences between the deflections of the specimens. Sample 62 had the largest deflection, sample 63 had the next largest deflection, and sample 61 had the smallest deflection. Results were tabulated from the 16 ply unidirectional tests, as shown in Table 3.8.
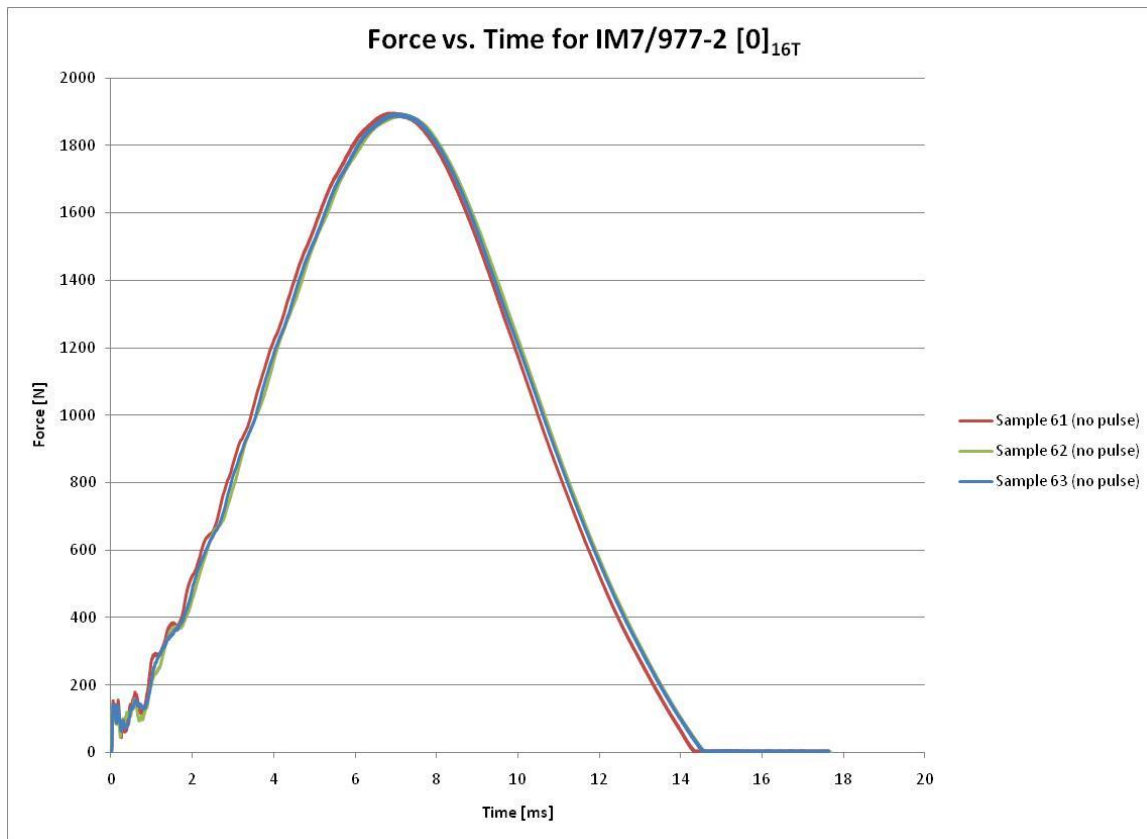
Figure 3.19: Force versus Time for Impact Characterization of Samples 61, 62, & 63
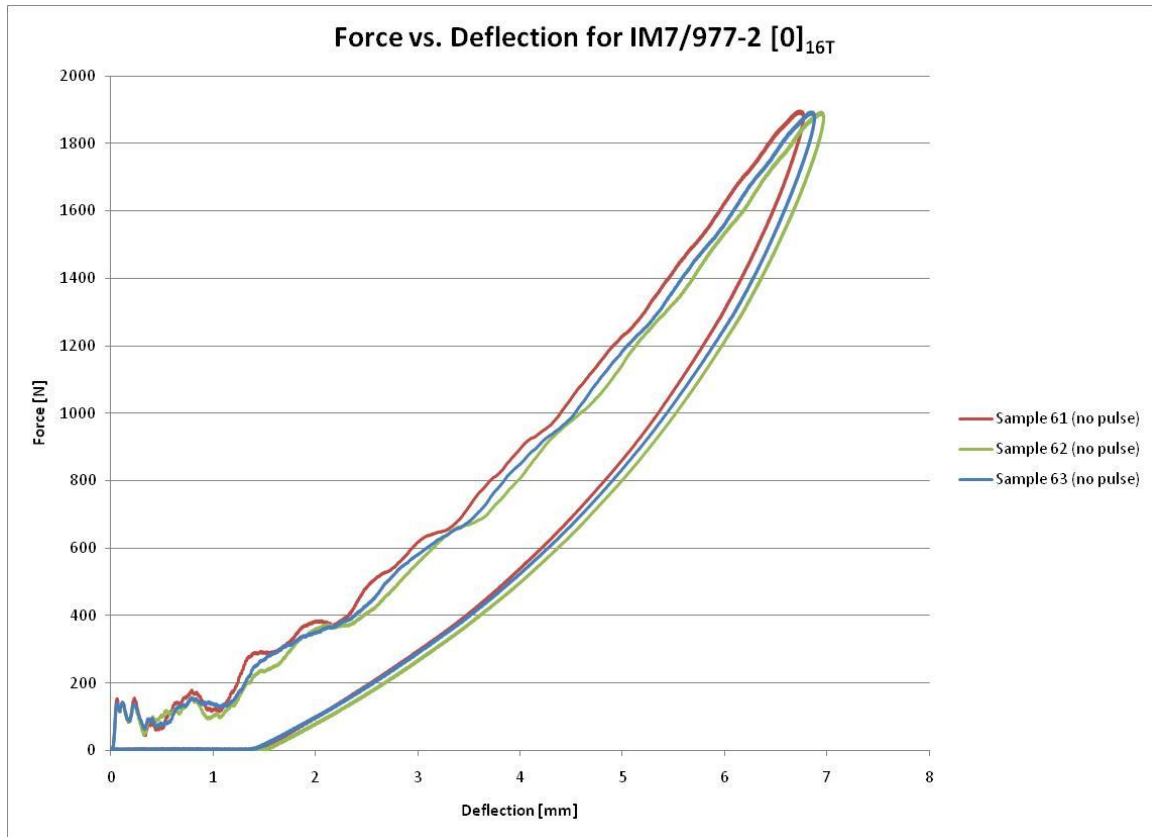
Figure 3.20: Force versus Deflection for Impact Characterization of Samples 61, 62, 63

Table 3.8: Impact Characterization Data for 16 ply Unidirectional Specimens

Specimen #	Electrical	Mass [kg]	Height [m]	Velocity [m/s]	Impact Energy [J]	Absorbed Energy [J]	Peak Load [N]	Peak Current [A]	Visible Damage
Sample 61	no pulse	5.054	0.075	1.235	4.1962	5.3388	1895.4	---	none
Sample 62	no pulse	5.054	0.075	1.235	4.1982	5.3867	1894.7	---	none
Sample 63	no pulse	5.054	0.075	1.232	4.1793	5.3350	1894.7	---	none
Average	no pulse	5.054	0.075	1.234	4.1912	5.3535	1894.9		

The mean impact energy of the three 16 ply unidirectional samples was 4.1912 J. The impact energy was calculated by the Instron software using the given mass, the measured impact velocity, and the principle of kinetic energy. The peak load was measured by the instrumented load cell for each sample. The average peak load was 1894.9 N for the three 32 ply unidirectional samples. Each sample was within 0.02% of the mean peak load. The absorbed energy was calculated by the Instron software by integrating the force versus deflection curve in Figure 3.20. The average absorbed energy of the three specimens was 5.3535 J. All samples were within 1% of the mean, which makes sense, since all three force versus deflection curves were similar except that the maximum deflections varied slightly. Finally, impact characterization tests were performed on 16 ply cross-ply specimens.

3.2.3 IM7/977-2 $[0/90]_{4S}$ Impact Characterization

Three 16 ply cross-ply IM7/977-2 samples were used for impact testing. The critical energy was found through trial and error. With a mass of 12.97 kg dropped from a height of 0.30 m, the theoretical critical energy was determined to be 38.2 J. Three composite specimens were clamped into the test fixture and impacted at the critical energy. Samples 48 and 49 incurred visible damage on the back side of the specimen due to the impact. Sample 50 showed no visible damage due to the impact. The results from the impacts of the non-electrified specimens 48, 49, and 50 are shown in Figures 3.21 and 3.22.

Figure 3.21: Force versus Time for Impact Characterization of Samples 48, 49, & 50

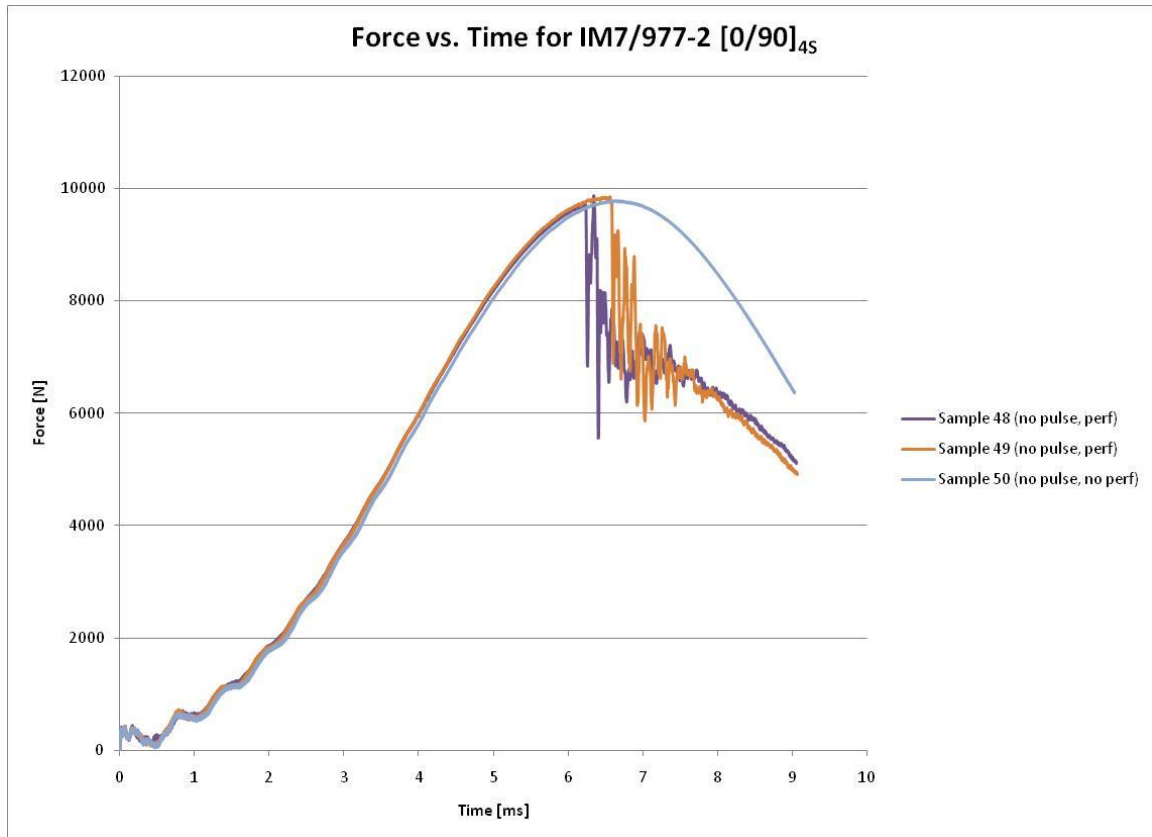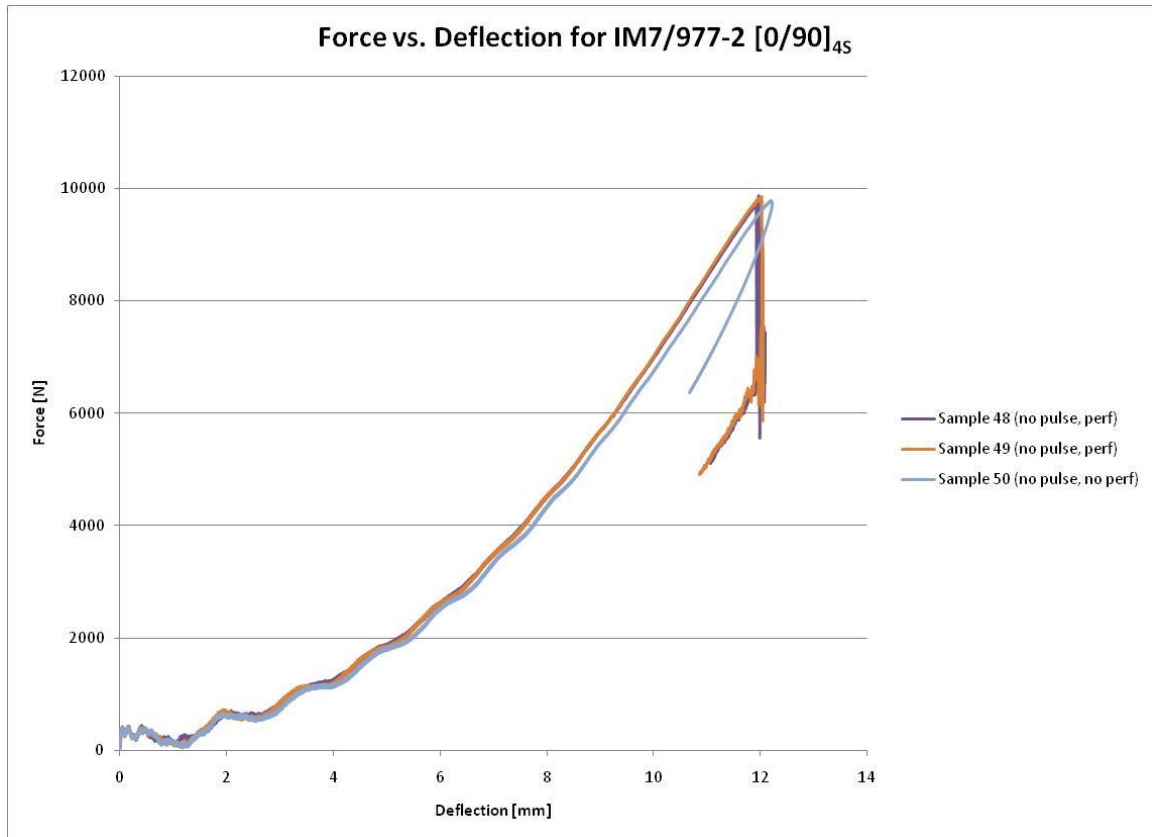Figure 3.22: Force versus Deflection for Impact Characterization of Samples 48, 49, 50

Specimen 48 incurred the highest load before failing, specimen 49 endured the next highest load, and specimen 50 withstood the smallest load, as shown in Figure 3.21. In contrast, Figure 3.22 shows that sample 50 had the largest deflection, sample 49 had the next largest deflection, and sample 48 had the smallest deflection. These results indicate an inverse correlation between maximum load and deflection. This result makes sense, since a stiffer specimen would withstand a higher force with less deflection. In

order to better compare the results from the 16 ply cross-ply impact tests, the relevant data was tabulated in Table 3.9.

Table 3.9: Impact Characterization Data for 16 ply Cross-Ply Specimens

Specimen #	Electrical	Mass [kg]	Height [m]	Velocity [m/s]	Impact Energy [J]	Absorbed Energy [J]	Peak Load [N]	Peak Current [A]	Visible Damage
Sample 48	no pulse	12.97	0.300	2.434	38.4266	40.9138	9863.3	---	yes
Sample 49	no pulse	12.97	0.300	2.432	38.3706	41.5141	9844.8	---	yes
Sample 50	no pulse	12.97	0.300	2.433	38.4042	41.4866	9785.8	---	none

The impact energy was calculated by the Instron software using the given mass, the measured impact velocity, and the principle of kinetic energy. The peak load was measured by the instrumented load cell for each sample, and the absorbed energy was calculated by the Instron software by integrating the force versus deflection curve in Figure 3.22. Absorbed energy is greater in specimens that incur less damage, so the results indicate that sample 50 incurred slightly more damage than sample 49 even though sample 50 showed no visible damage and sample 49 did not. This result suggests that the majority of the damage induced by the impact is internal, which is common in composite materials. The visible damage to the 16-ply unidirectional specimens is shown in Figure 3.23 for sample 48.

Figure 3.23: Visible Damage on the Back Side of Sample 48

3.2.4 Impact Characterization Summary

From the impact characterization tests, a couple noteworthy trends were found. It was determined from both the 32 ply unidirectional and 16 ply cross-ply specimens that there was an inverse correlation between the maximum load and maximum deflection of impacted specimens. It was also found from the 32 ply unidirectional and 16 ply cross-ply impact tests that the greater the absorbed energy of the specimen the less the damage

in the specimen. In addition, it was determined that the majority of the induced damage was internal damage. Upon completion of the non-electrified impact characterization tests, the testing was repeated with the addition of a coordinated current pulse. Since the application of the current pulse was the only variable changed in the test, any differences in the impact results could be attributed purely to electrification.

3.4 Coordinated Impact Characterization

The goal of the coordinated impact tests was to perform impact characterization tests with the addition of the application of a current pulse. The system was calibrated by adjusting the time delays in the program logic, as described in 2.3.8, such that the peak of the current pulse coincided with the peak of the impact load. The calibration was verified empirically by applying a 25 A DC current during an impact event.

3.4.1 Coordinated Impact Calibration

Before testing new specimens with a coordinated current pulse and impact, a 25 A DC current was applied to an arbitrary specimen and an impact event occurred. This test was to ensure that the impact occurred with the appropriate timing relative to the application of a current pulse. Figure 3.24 shows the voltage versus time for the test specimen.
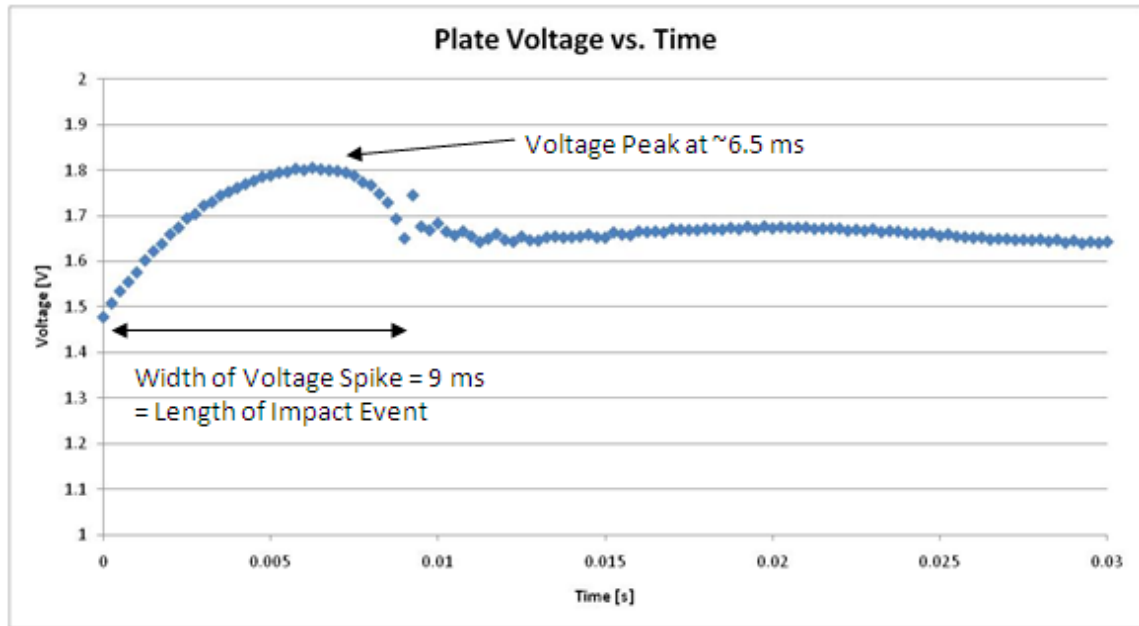
Figure 3.24: Voltage versus Time Plot Showing Peak Voltage at 6.5 milliseconds

The voltage spike in during the 25 A electrification shown in Figure 3.24 was caused by the impact event. As the impact occurred, the contact resistance between the copper electrodes and the composite specimen increased due to deflection of the specimen and induced vibration. This increase in resistance caused the sample voltage to increase, and the peak voltage was identified as the point at which the maximum impact load occurred. Since the maximum voltage during the calibration tests was at 6.5 milliseconds, it was determined that the maximum load was effectively coordinated with the peak of the current pulse, which was determined to occur at 6.5 milliseconds from the electrical characterization tests. In order to show the coordinated impact with the application of a current pulse, the current versus time and load versus time curves were

normalized and plotted simultaneously. Figure 3.25 shows the normalized impact load

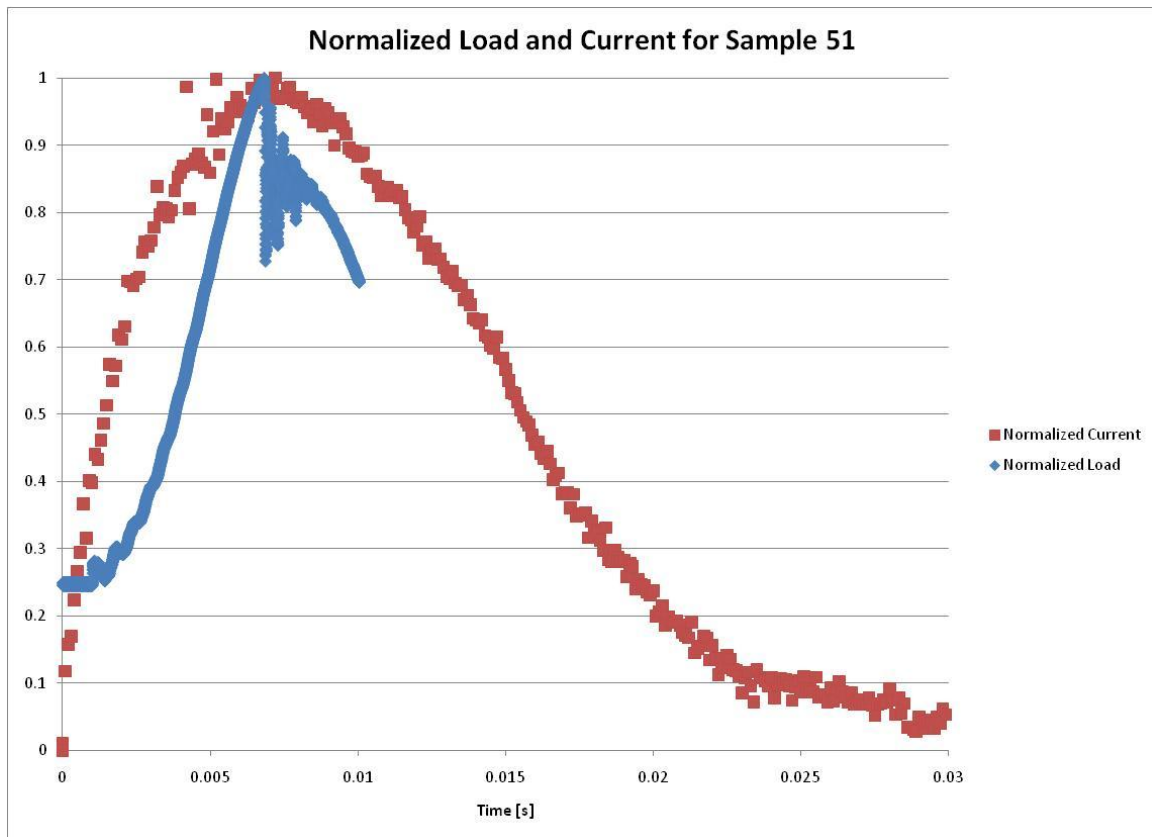coordinated with the normalized current pulse curve for a 16 ply cross-ply specimen.

Figure 3.25: Normalized Load and Current vs. Time for Coordinated Impact

For all specimens the impact tests were performed at the same drop height and mass as

the impact characterization tests of section 3.3 so that any variations in results between

impact characterization and coordinated impact results could be attributed only to the current pulse. The current and voltage versus time curves for all coordinated impact tests are found in Appendix B.

3.4.2 IM7/977-3 $[0]_{32T}$ Coordinated Impact

Six 32 ply unidirectional IM7/977-3 samples were used for coordinated impact testing. The specimens were impacted under the same conditions as samples 52, 53, and 54. The drop mass and height were 5.054 kg and 0.16 m, respectively. Three samples were impacted with the addition of a 150 V current pulse and three samples were impacted with the addition of a 250 V current pulse. The results from the impacts of both the non-electrified and electrified specimens 55, 56, 57, 58, 59, and 60 are shown in Figures 3.26 to 3.29. Figures 3.27 and 3.29 compare non-electrified and electrified specimens.
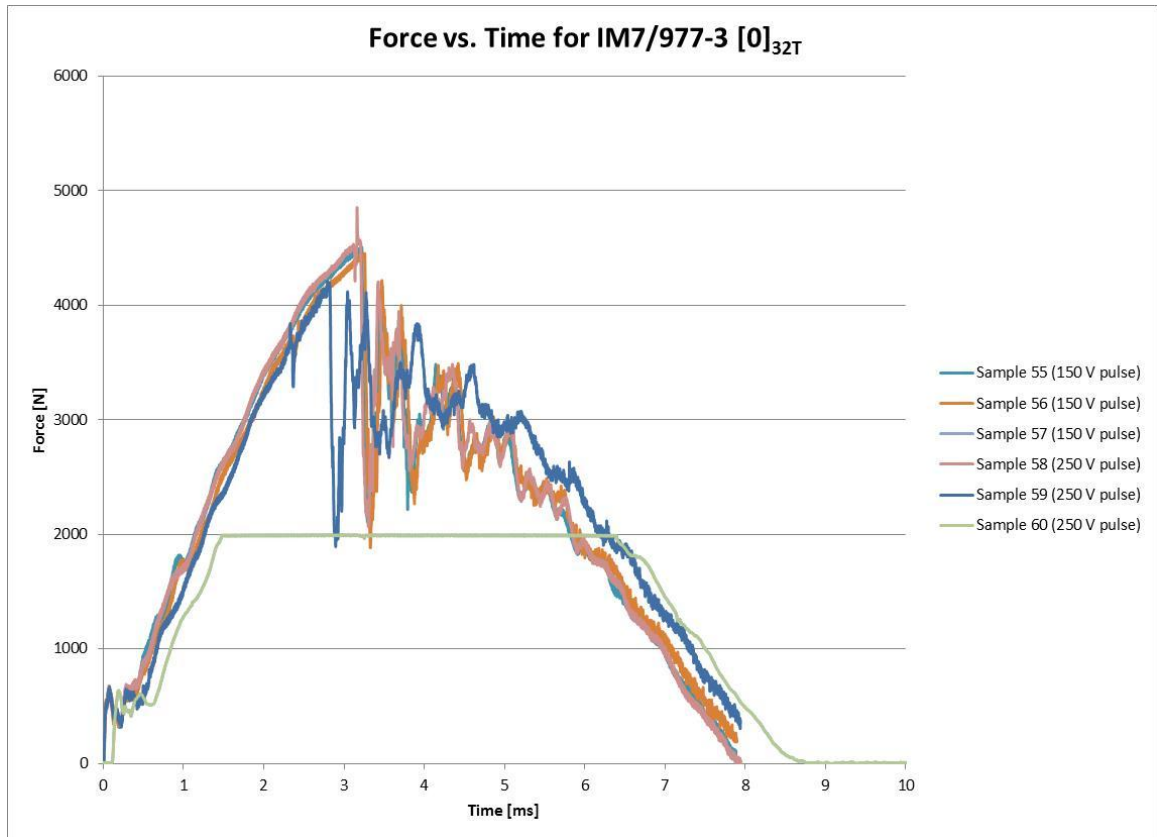
Figure 3.26: Force versus Time for 32 ply Unidirectional Coordinated Impact
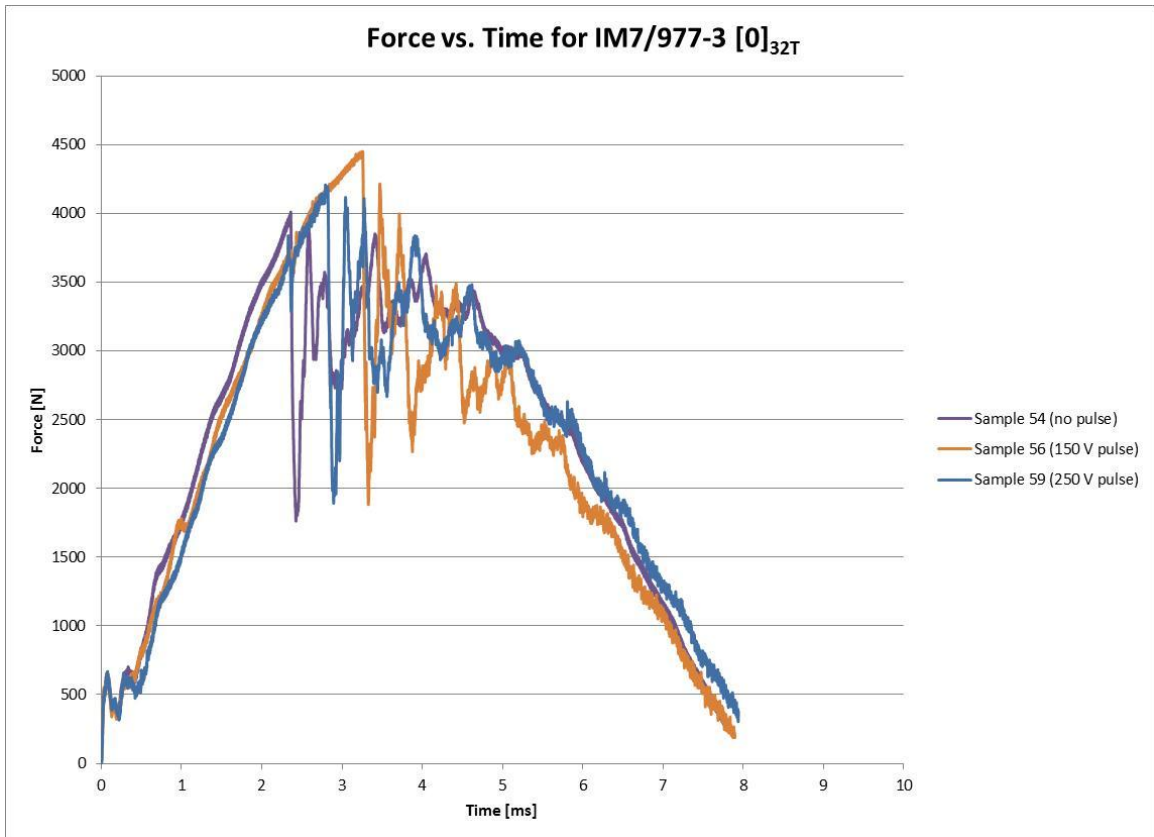
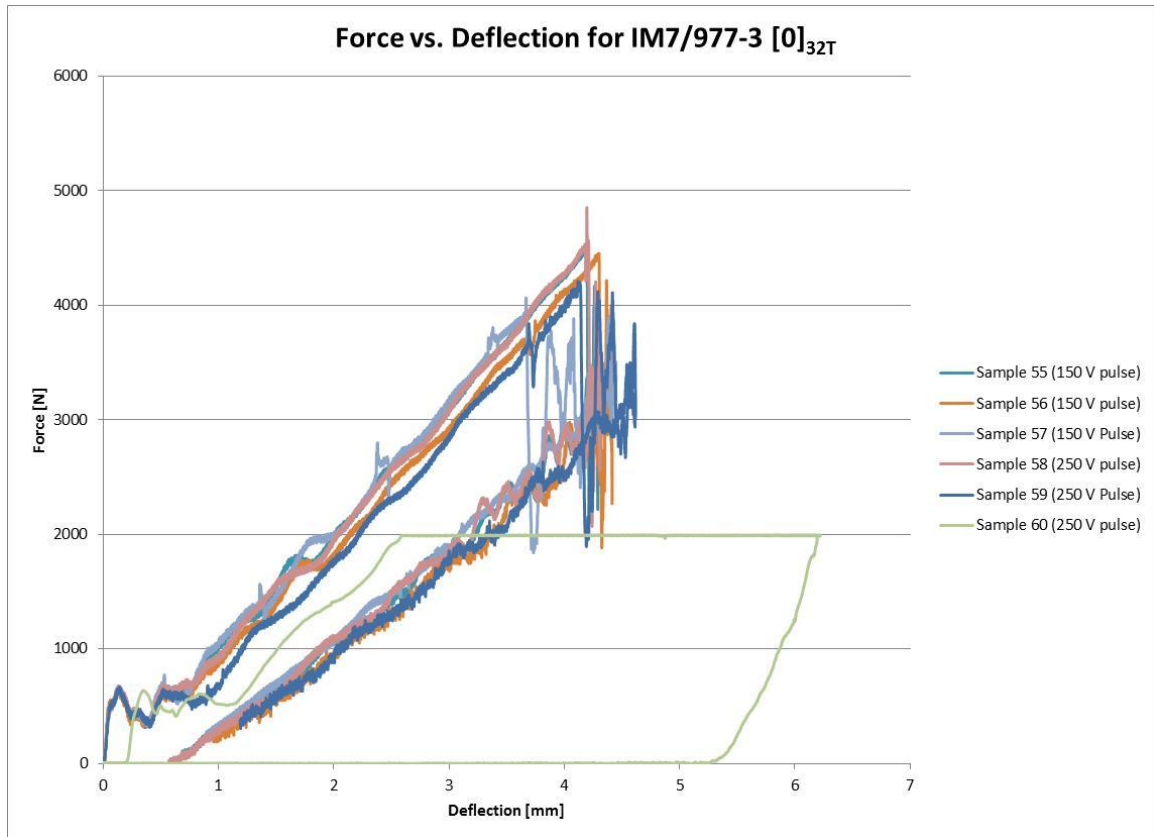Figure 3.27: Force versus Time for 32 ply Unidirectional Coordinated Impact

Figure 3.28: Force versus Deflection for 32 ply Unidirectional Coordinated Impact
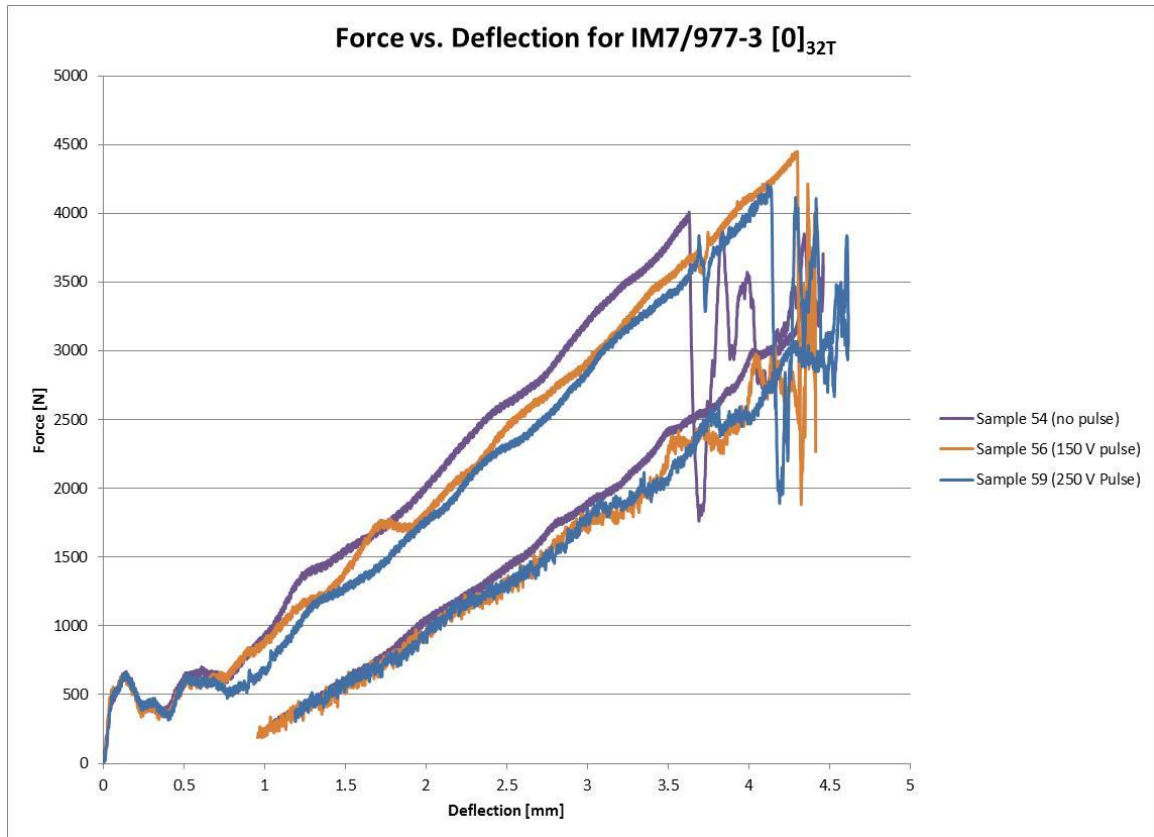
Figure 3.29: Force versus Deflection for 32 ply Unidirectional Coordinated Impact

All six electrified specimens sustained damage in the form of a line crack. It is very obvious from the force versus time and force versus deflection curves that sample 60 was an outlier compared to the other specimens. The force on sample 60 reached 1995.5 N and flattened out for approximately 5 milliseconds before decreasing. This result suggests that the data acquisition system malfunctioned when conditioning the signal from the tup. The visible damage on specimen 60 and electrical results appeared to be similar to other specimens, however, the impact data was quite different. It was

determined that the data from specimen 60 was not reliable. Therefore, sample 60 was neglected for comparison purposes. In order to compare the specimens, the results were tabulated in Table 3.10, and the average values for each of the three test types were calculated.

Table 3.10: Coordinated Impact Characterization Data for 32 ply Unidirectional Specimens

Specimen #	Electrical	Mass [kg]	Height [m]	Velocity [m/s]	Impact Energy [J]	Absorbed Energy [J]	Peak Load [N]	Peak Current [A]	Visible Damage
Sample 52	no pulse	5.054	0.160	1.769	8.6103	9.1890	4496.9	---	Line Crack
Sample 53	no pulse	5.054	0.160	1.767	8.5915	9.3200	3730.6	---	Line Crack
Sample 54	no pulse	5.054	0.160	1.768	8.5998	6.9678	4009.2	---	Line Crack
Average	no pulse	5.054	0.160	1.768	8.6005	8.4923	4078.9		
Sample 55	150 V pulse	5.054	0.160	1.765	8.5759	9.2078	4503.7	964	Line Crack
Sample 56	150 V pulse	5.054	0.160	1.766	8.5869	9.1437	4449.3	906	Line Crack
Sample 57	150 V pulse	5.054	0.160	1.768	8.5973	7.1281	4063.9	957	Line Crack
Average	150 V pulse	5.054	0.160	1.766	8.5867	8.4932	4339.0	942	
Sample 58	250 V pulse	5.054	0.160	1.771	8.6282	9.1642	4850.9	1631	Line Crack
Sample 59	250 V pulse	5.054	0.160	1.770	8.6232	7.9666	4208.3	1516	Line Crack
Sample 60	250 V pulse	5.054	0.160	1.763	8.5497	8.8040	1995.5	1636	Line Crack
Average	250 V pulse	5.054	0.160	1.768	8.6257	8.5654	4529.6	1594	

It should be noted that for the 250 V pulse coordinated tests, sample 60 was excluded from the calculations of average impact energy, absorbed energy, and impact load, since the data acquisition system malfunctioned. From Table 3.10, it can be easily seen that the impact energies of each of the tests were very similar. It can also been seen that on average, as the analog voltage of the current pulse was increased, the maximum

load endured by the plate also increased. The maximum load was 6.4% greater for the 150 V tests and 11.0% greater for the 250 V tests as compared to the non-electrified tests. The results for the absorbed energy were similar. The non-electrified specimens had the lowest absorbed energy, the 150 V electrified specimens had the next lowest, and the 250 V electrified specimens had the highest absorbed energies on average. The 150 V electrified specimens absorbed 0.01% more energy than the non-electrified specimens, and the 250 V electrified specimens absorbed 0.8% more energy than the non-electrified specimens. This result indicates that the non-electrified tests resulted in the most damage and the electrified specimens had less damage, even though the differences in absorbed energy were small. Since the sample size of these tests was small, additional coordinated tests were performed.

3.4.3 IM7/977-2 $[0]_{16T}$ Coordinated Impact

Three 16 ply unidirectional IM7/977-2 specimens were prepared for coordinated impact testing, however, only one sample was tested. Before coordinated impact tests were performed, electrified pulse tests were performed without an impact event. This was to insure that the specimens could withstand the current pulse without arcing. The current pulse generator was set at 100 V, but the initial test resulted in arcing at the composite/electrode interface. Since the first sample arced, it was decided not to perform coordinated tests, since there was a limited supply of samples and coordination with an impact event would only increase the likelihood of arcing. The failed sample 64 is shown in Figure 3.30 with burning at the composite/electrode interface. The burned area extended up to 4 mm from the left edge and 2 mm from the right edge of the specimen. Since the 16 ply unidirectional specimens were not available for coordinated impact, it was determined to move on to testing 16 ply cross-ply specimens.
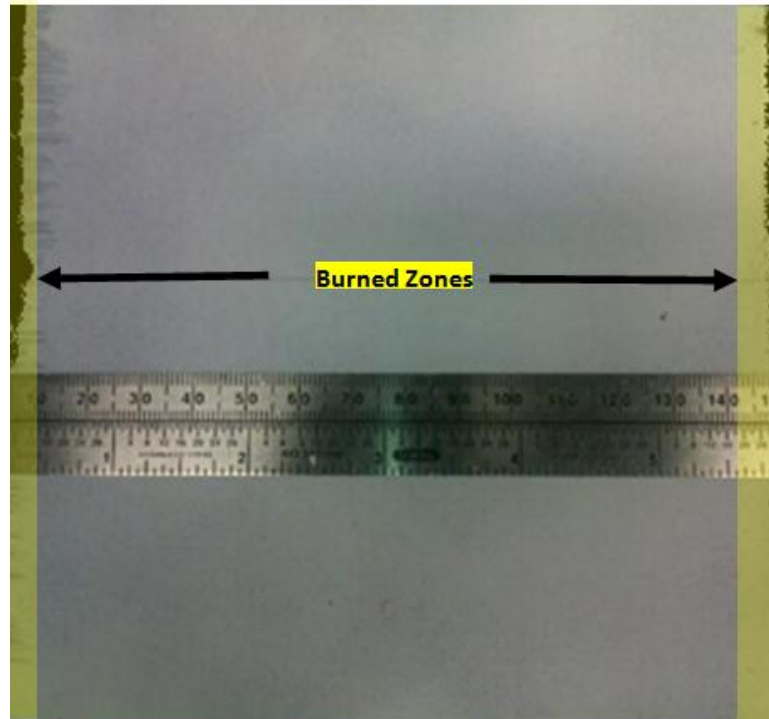
Figure 3.30: 16 Ply Unidirectional Sample 64 with Burned Zones Highlighted

3.4.4 IM7/977-2 [0/90]$_{4S}$ Coordinated Impact

Three 16 ply cross-ply IM7/977-2 samples were used for coordinated impact testing. The specimens were impacted under the same conditions as samples 48, 49, and 50. The drop mass and height were 12.97 kg and 0.30 m, respectively. In addition to the impact conditions, three samples were impacted with the addition of a 100 V current pulse. The results from the impacts of both the non-electrified and electrified specimens

46, 47, 48, 49, 50 , and 51 are shown in Figures 3.31 to 3.34. Figures 3.32 and 3.34 compare one non electrified specimen with an electrified specimen.
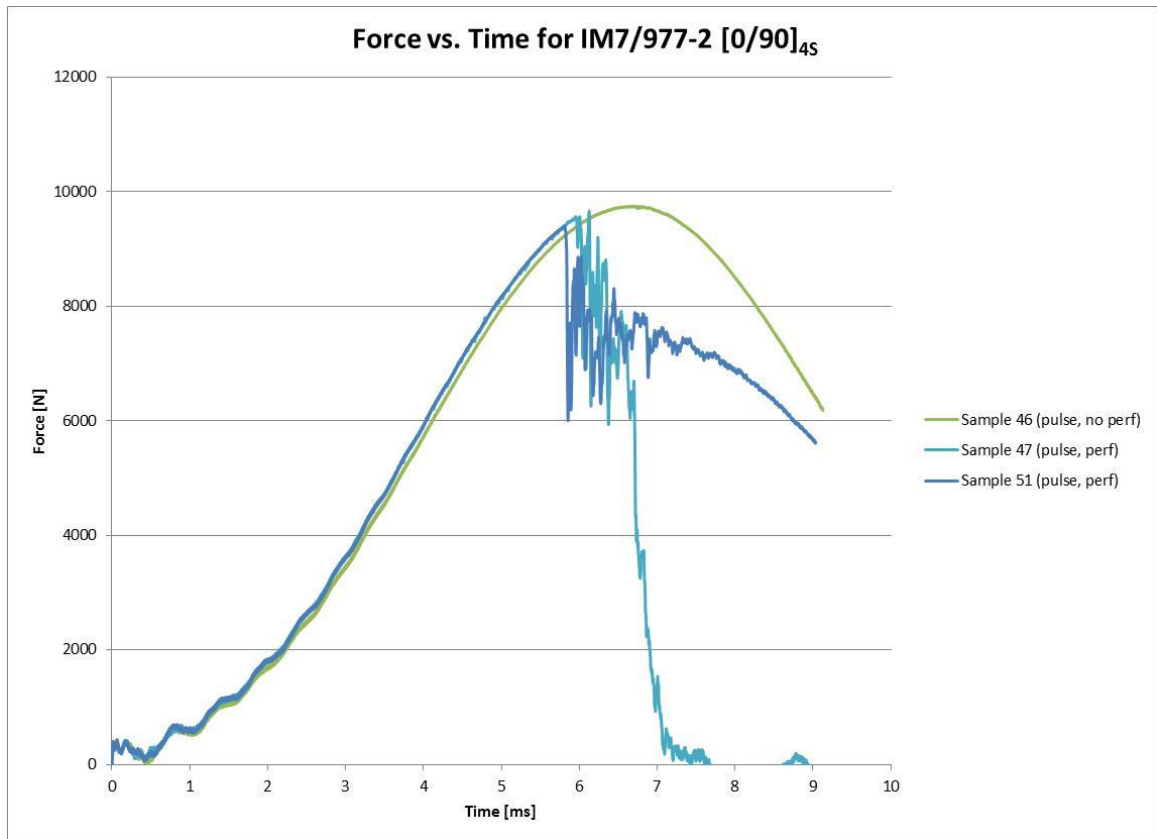

Figure 3.31: Force versus Time for 16 ply Cross-Ply Coordinated Impact
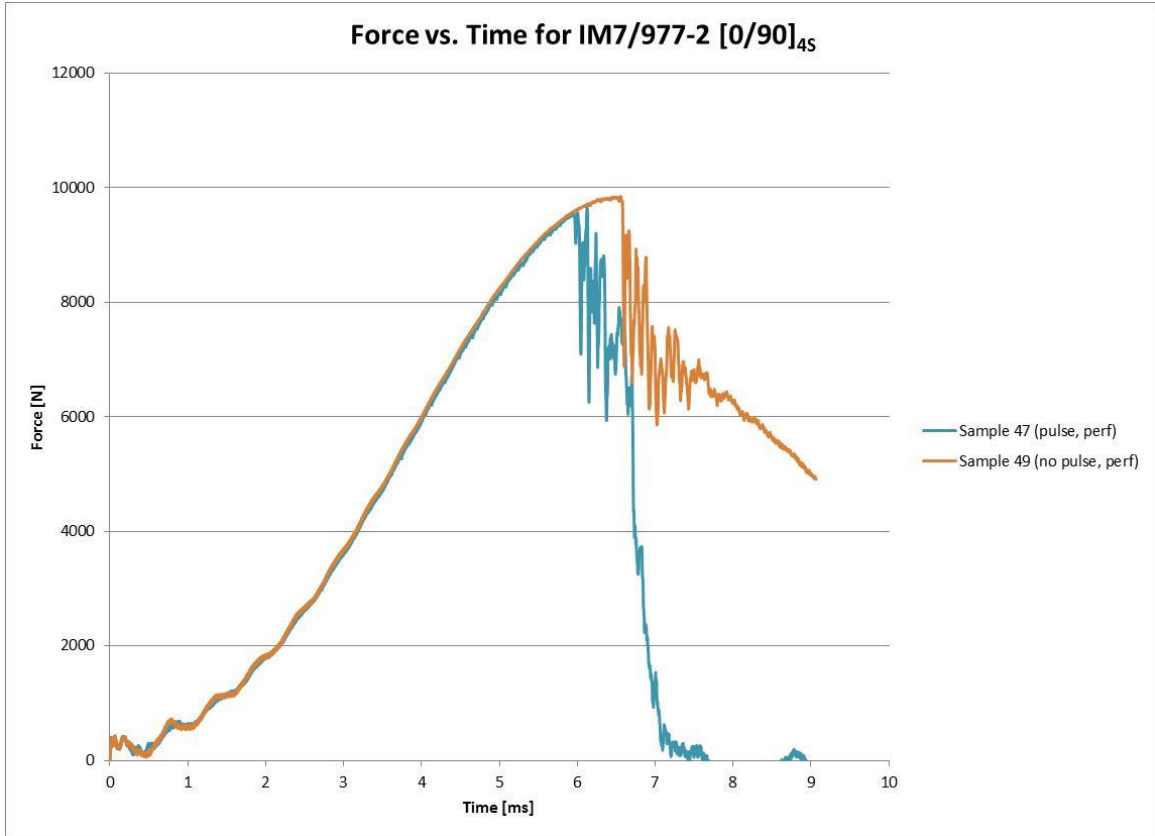
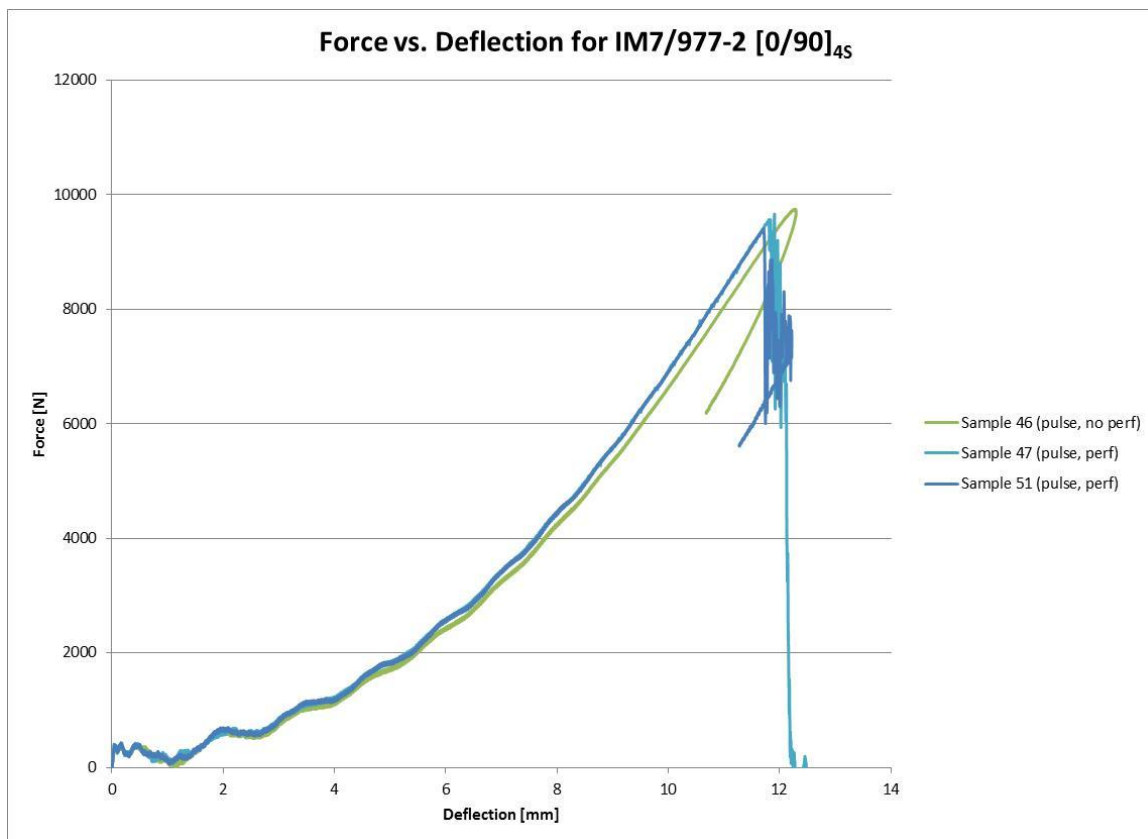Figure 3.32: Force versus Deflection for 16 ply Cross-Ply Coordinated Impact

Figure 3.33: Force versus Deflection for 16 ply Cross-Ply Coordinated Impact
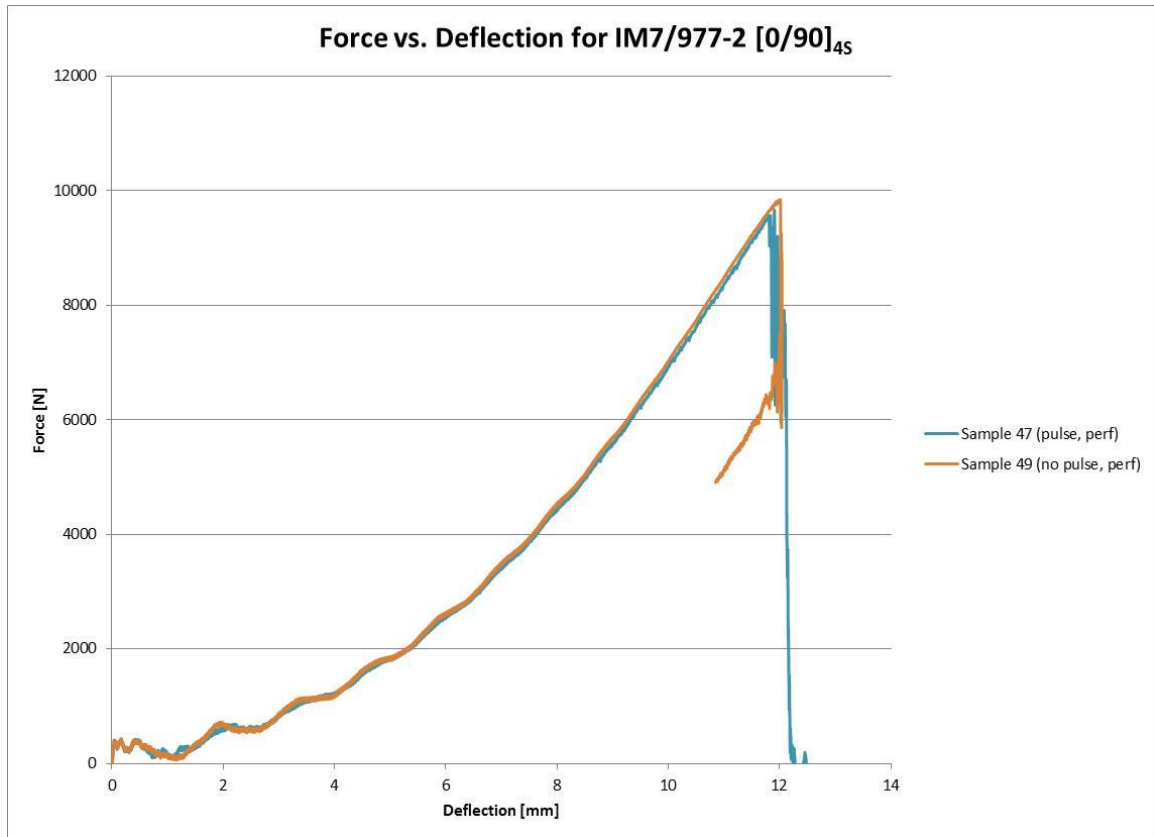
Figure 3.34: Force versus Deflection for 16 ply Cross-Ply Coordinated Impact

Non-electrified samples 47 and 51 were visibly damaged due to the impact, however, sample 46 did not show any visible damage. The electrified samples 47 and 51 had very similar results to the non-electrified samples 48 and 49. These four samples all sustained visible damage due to impact. The electrified sample 46 was very similar to the non-electrified sample 50, both of which showed no visible damage. In order to compare the specimens, the results were tabulated in Table 3.11.

Table 3.11: Coordinated Impact Characterization Data for 16 ply Cross-Ply Specimens

Specimen #	Electrical	Mass [kg]	Height [m]	Velocity [m/s]	Impact Energy [J]	Absorbed Energy [J]	Peak Load [N]	Peak Current [A]	Visible Damage
Sample 48	no pulse	12.97	0.300	2.434	38.4266	40.9138	9863.3	---	yes
Sample 49	no pulse	12.97	0.300	2.432	38.3706	41.5141	9844.8	---	yes
Sample 50	no pulse	12.97	0.300	2.433	38.4042	41.4866	9785.8	---	none
Sample 46	100 V pulse	12.97	0.300	2.433	38.3996	41.5354	9744.1	578	none
Sample 47	100 V pulse	12.97	0.300	2.432	38.3611	39.8389	9659.6	577	yes
Sample 51	100 V pulse	12.97	0.300	2.433	38.3970	37.9707	9404.8	605	yes

From Table 3.11, it can be easily seen that the impact energies of each of the tests were very similar. It can also been seen that on average, the application of the current pulse led to a lower maximum force. The maximum force was 2.3% less for the electrified samples as compared to the non-electrified samples. The samples subjected to a current pulse also absorbed 3.9% less energy than the non-electrified samples. This result indicates that the non-electrified tests resulted in less damage than the electrified tests. This result does not support the premise that the current application improves impact resistance. It should be noted that for 16 ply coordinated impact tests, all electrified specimens showed signs of arcing and burning on the edges of the specimen similar to Figure 3.30. Since burning of the epoxy matrix is detrimental to the strength of the composites, the decrease in peak load and absorbed energy could have been due to arcing of the specimen. In order to verify this suggestion, the experimental setup must be improved so that the contact between the copper electrodes and composite specimen improves.

3.4.5 Coordinated Impact Summary

There were no common trends from the coordinated impact tests of the 32 ply unidirectional specimens and 16 ply cross-ply. The absorbed energy was slightly greater in the electrified specimens compared to the non-electrified specimens for unidirectional 32 ply specimens, where as the opposite was true for 16 ply cross-ply specimens. The trends for peak load were also different. For the 32 ply unidirectional specimens, the peak load increased significantly as analog voltage on the current pulse generator increased. In particular, there was an 11% increase in peak load for electrified specimens at an analog voltage of 250 V compared to non-electrified specimens. The 16 ply cross-ply plates, on the other hand, had a slightly lower peak load for the electrified samples as compared with the non-electrified samples, but the decrease in peak load was insignificant. It should be noted that for 16 ply coordinated impact tests, the specimens showed signs of arcing and burning on the edges. Burning of the epoxy matrix is detrimental to the strength of the composites, so the decrease in peak load and absorbed energy could have been due to arcing of the specimen. In order to verify this suggestion, the experimental setup must be improved so that the contact between the copper electrodes and composite specimen improves, especially for thinner specimens. In addition, further testing is required in order to better see the effect of thickness and layup on the results of coordinated impact tests.

CHAPTER 4

SUMMARY AND RECOMMENDATIONS

4.1 Summary

In this work, a fully automated experimental setup was developed that allows for real time measurements of pulsed electric current, voltage, load, and velocity during coordinated application of a current pulse with an impact load on a carbon fiber polymer matrix composite laminates. The experimental setup included a new custom-built current pulse generator that utilizes a bank of capacitor modules capable of producing a 30 millisecond current pulse with an amplitude of up to 2500 A. The application of the peak of the current pulse was coordinated with the peak of the impact load by specifying the delay between the trigger to release the drop mass and the trigger to initiate the current pulse. The entire setup was designed to be controlled through a single Agilent VEE Pro 8.5 program via a computer and USB connections.

A series of electrical, impact, and coordinated electrical-impact characterization tests were performed on 16 ply IM7/977-2 and 32 ply IM7/977-3 unidirectional and symmetric cross-ply carbon fiber polymer matrix composites. Electrical characterization tests were performed over a vast range of large magnitude current pulses. Impact tests were completed in order to determine the energy at which visible damage was first present. Finally, coordinated electrical-impact tests were performed in order to determine the influence of a current pulse on the impact resistance of the specimens.

Electrical characterization tests were performed at several current levels on 3 specimens each of 16 and 32 ply unidirectional and cross-ply. From these tests, it was determined that the current pulse magnitude varied linearly with the analog voltage on the current pulse generator. By determining the linear approximation equation for the current versus analog voltage, the necessary analog voltage was accurately predicted for a

desired arbitrary current. Next, impact characterization tests were performed on 16 and 32 ply unidirectional and 16 ply cross-ply plates. The impact energy was selected such that slight visible damage was induced but without complete specimen perforation. Next, impact tests were performed at the same energy as before, except with the addition of a current pulse. From the coordinated impact tests, it was determined that the impact load and absorbed energy increased with the application of a current pulse on 32 ply unidirectional specimens. In addition, it was determined that as the magnitude of the current pulse increased, the peak load and absorbed energy increased as well. For 16 ply cross-ply specimens, the peak load and absorbed energy decreased slightly with the application of a current pulse. It was noteworthy that arcing and burning was evident on the edges of the 16 ply cross-ply specimens. This negatively affected the impact resistance of the specimens, so a better method of clamping the copper electrodes to the composite specimens is necessary. Additional recommendations should be considered in order to further the findings of this work.

<div align="center">4.2 Recommendations</div>

The first recommendation to improve the experimental setup is that the method of clamping the copper electrodes to the specimens must be improved. During an impact event, the contact between the composite and electrode decreases and causes contact resistance to increase. This increase in resistance is magnified larger in thinner plates, so it makes it difficult to coordinate an impact event with a current pulse without arcing. The arcing and burning of the epoxy matrix affects the impact resistance of the composites. For this reason, it is necessary to remedy the arcing and burning situation in 16 ply specimens in order to evaluate the effect of a current pulse on impact resistance. Next, the trigger for releasing the drop weight should be addressed. The delay time in the air

actuated trigger varied based on the mass of the drop weight. This variability in the system required frequent recalibration which was very time consuming. Alternative triggers should be considered that won't require recalibration when the drop weight is changed. Once the necessary experimental setup modifications are complete, coordinated impact testing should be performed on 16 ply unidirectional and cross-ply specimens. Upon completion of these recommendations, the effect of current pulse on impact resistance of carbon fiber composite will be further understood.

APPENDIX A

VOLTAGE VERSUS TIME PLOTS

The electrical characterization tests of section 3.2 were performed using the Tektronix TDS 2014B oscilloscope as the data acquisition unit. The voltage across the composite specimens was measured using a probe and a 10x attenuation, however, noise spikes were present in every pulse test. Samples of voltage versus time curves collected by the oscilloscope are shown in Figures A.1 to A.3.
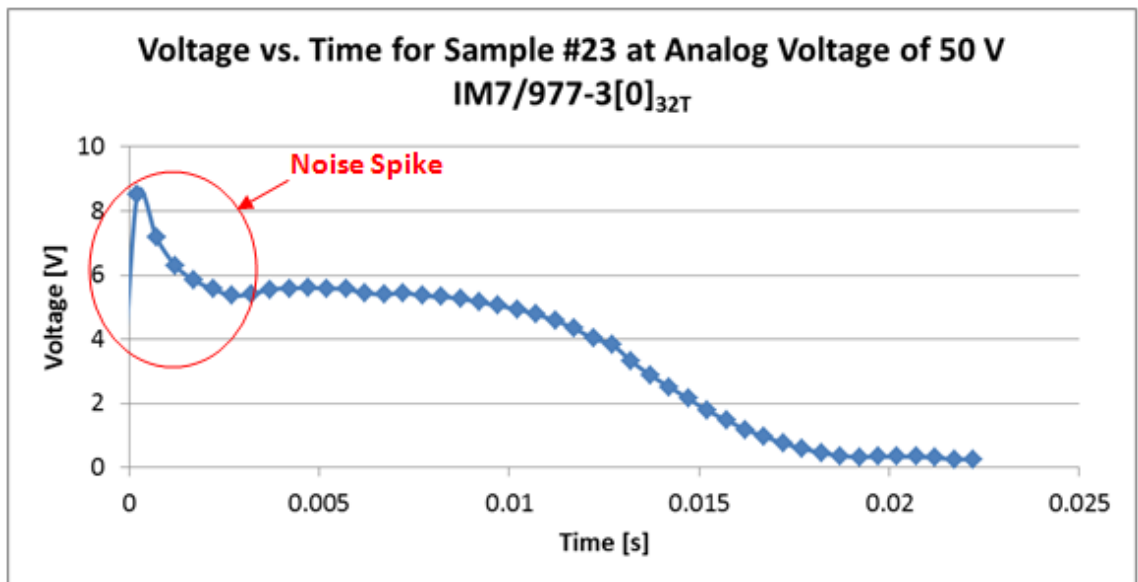

Figure A.1: Voltage versus Time for Sample 23 at 50 V Using Oscilloscope for DAQ
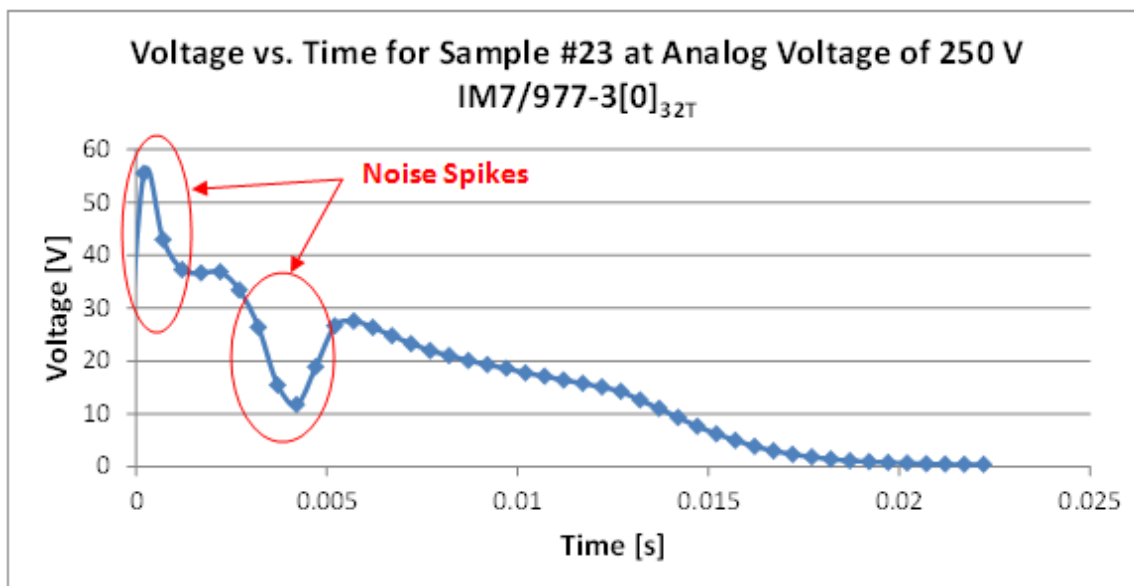
Figure A.2: Voltage versus Time for Sample 23 at 250 V Using Oscilloscope for DAQ
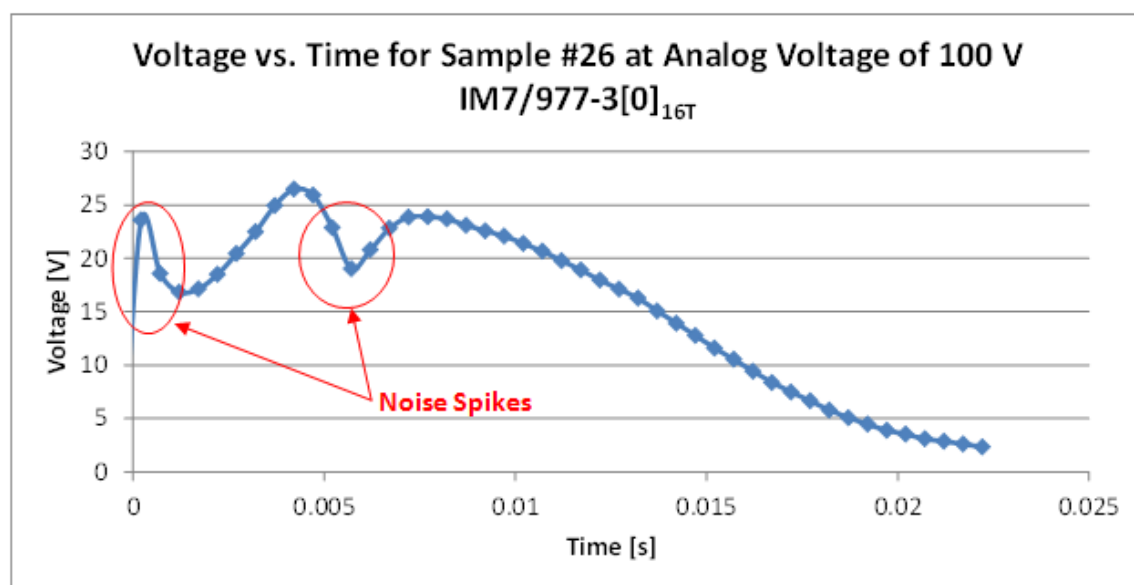

Figure A.3: Voltage versus Time for Sample 26 at 100 V Using Oscilloscope for DAQ

All three of the above voltage versus time curves had significant spikes in voltage at the start of data acquisition. Figures A.2 and A.3 also showed voltage dips after a few milliseconds. These voltage spikes could not be smoothed out or removed, because each contained hundreds of data points. The Agilent U2531A was selected as the new data acquisition unit. After the new system was developed, the coordinated impact tests were completed using the new system. Figures A.4 and A.5 show voltage versus time curves for samples 58 and 64, which were tested with coordinated impact tests.
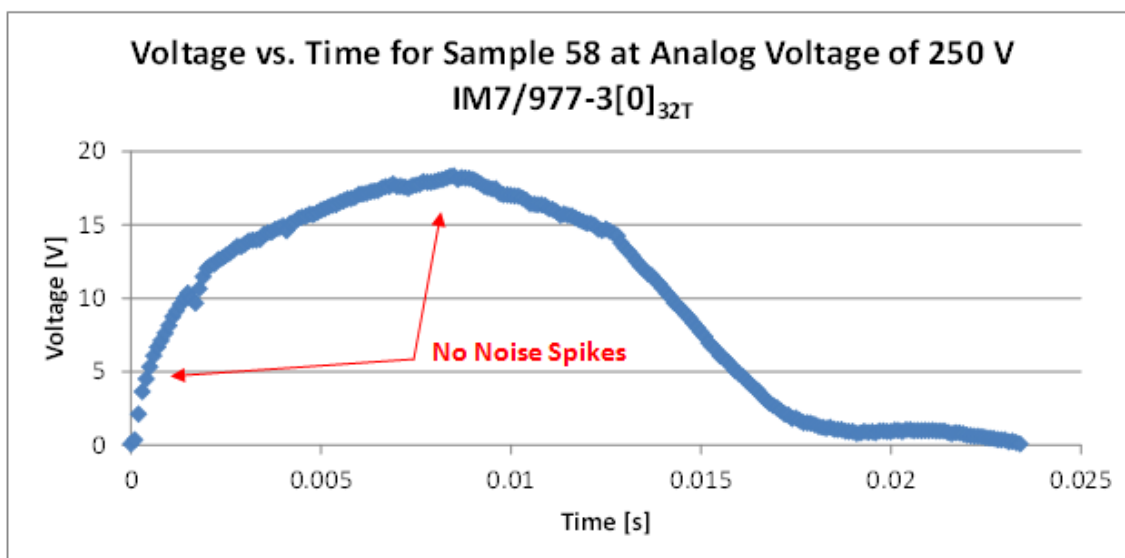

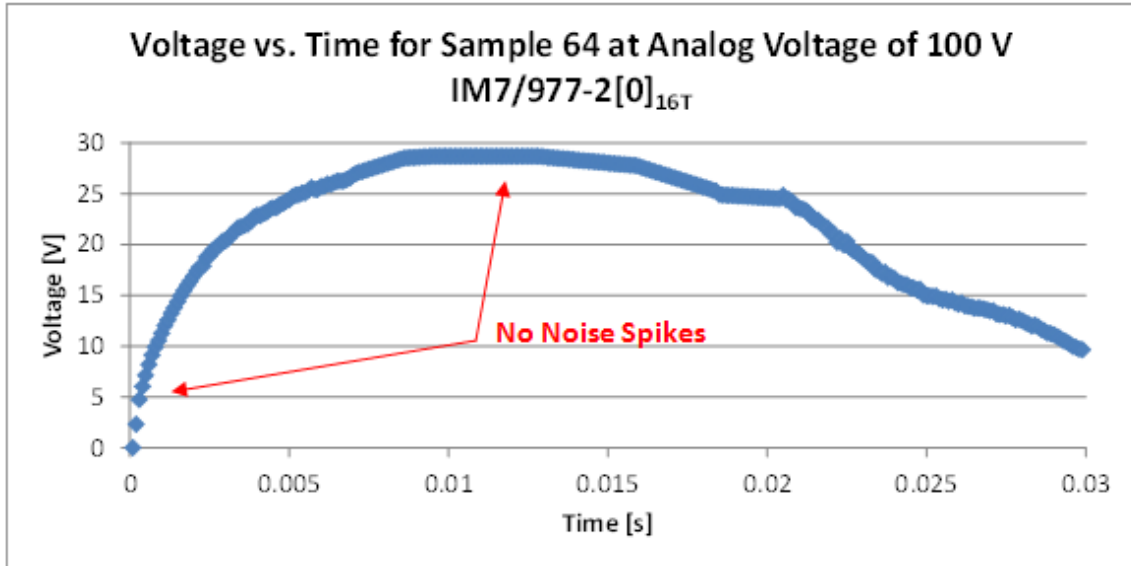Figure A.4: Voltage versus Time for Sample 58 at 250 V Using Agilent 2531A for DAQ

Figure A.5: Voltage versus Time for Sample 64 at 100 V Using Agilent 2531A for DAQ

The voltage versus time curves collected by the Agilent U2531A data acquisition system had none of the voltage spikes present in the previous pulse tests. In both Figures A.2 and A.4, 32 ply unidirectional specimens were tested at analog voltages of 250 V, and the curve from the Agilent U2531A had no spikes. The curve from the oscilloscope had significant spikes. In Figures A.3 and A.5, 16 ply unidirectional specimens were tested at an analog voltage of 100 V. The curve from the oscilloscope had noise spikes, where as the curve from the Agilent U2531A had no noise spikes. From this evidence, it was determined that the new data acquisition system solved the noise issues present in the previous system.

APPENDIX B

CURRENT AND VOLTAGE CURVES FOR COORDINATED IMPACT

TESTS

The current and voltage curves associated with the respective coordinated impact tests of section 3.4 are shown in Figures B.1 to B.4. Figure B.1 shows the current versus time for 32 ply unidirectional specimens at analog voltages of 150 V and 250 V. Samples 55, 56, and 57 were all tested at 150 V. Samples 55 and 57 had similar current curves, where as sample 56 had a strange current curve. For 250 V tests, samples 58 and 60 had similar current curves and sample 59 was abnormal. This phenomenon could be attributed to excessive arcing in the samples resulting in irregular current curves. The voltage curves in Figure B.2 show spikes in voltage with significant noise. These spikes were not arbitrary. The spikes in voltage were caused by the onset of the impact event. The contact resistance between the copper electrodes and composite increased due to the impact load and induced vibrations. The deformation of the specimens, vibrations, and damage propagation caused the voltage spikes present in the specimens. The current and voltage versus time curves in Figures B.3 and B.4 were nearly identical for each of the three specimens. This result followed intuition, since the cross-ply specimens suffered less detrimental damage compared to the unidirectional specimens.
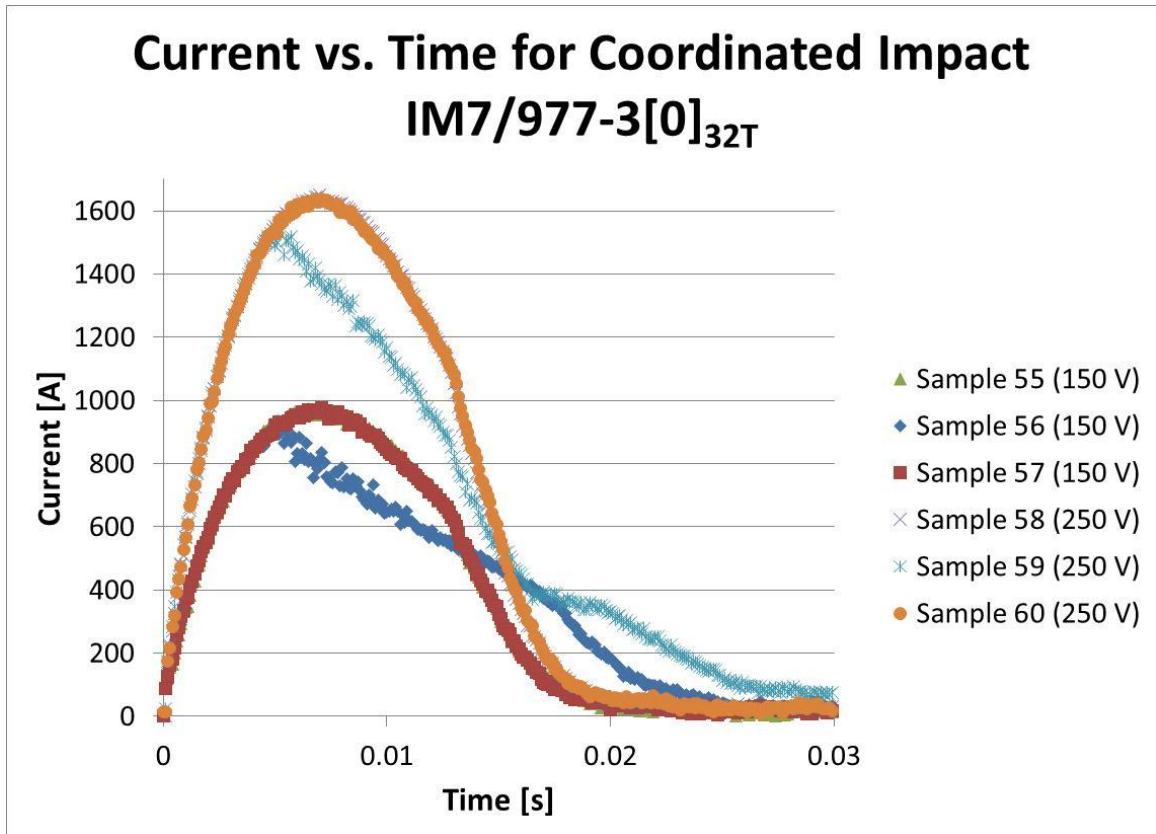
Figure B.1: Current versus Time for 32 Ply Unidirectional Coordinated Impact Tests
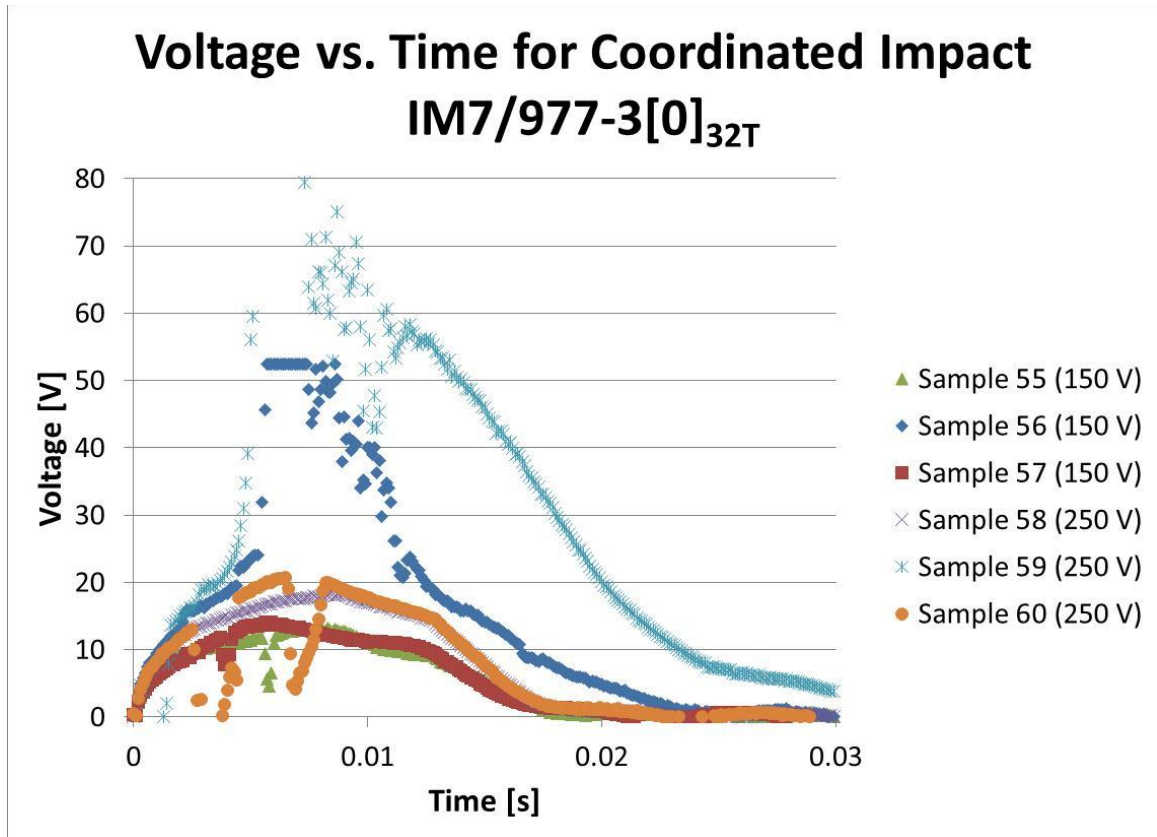
Figure B.2: Voltage versus Time for 32 Ply Unidirectional Coordinated Impact Tests
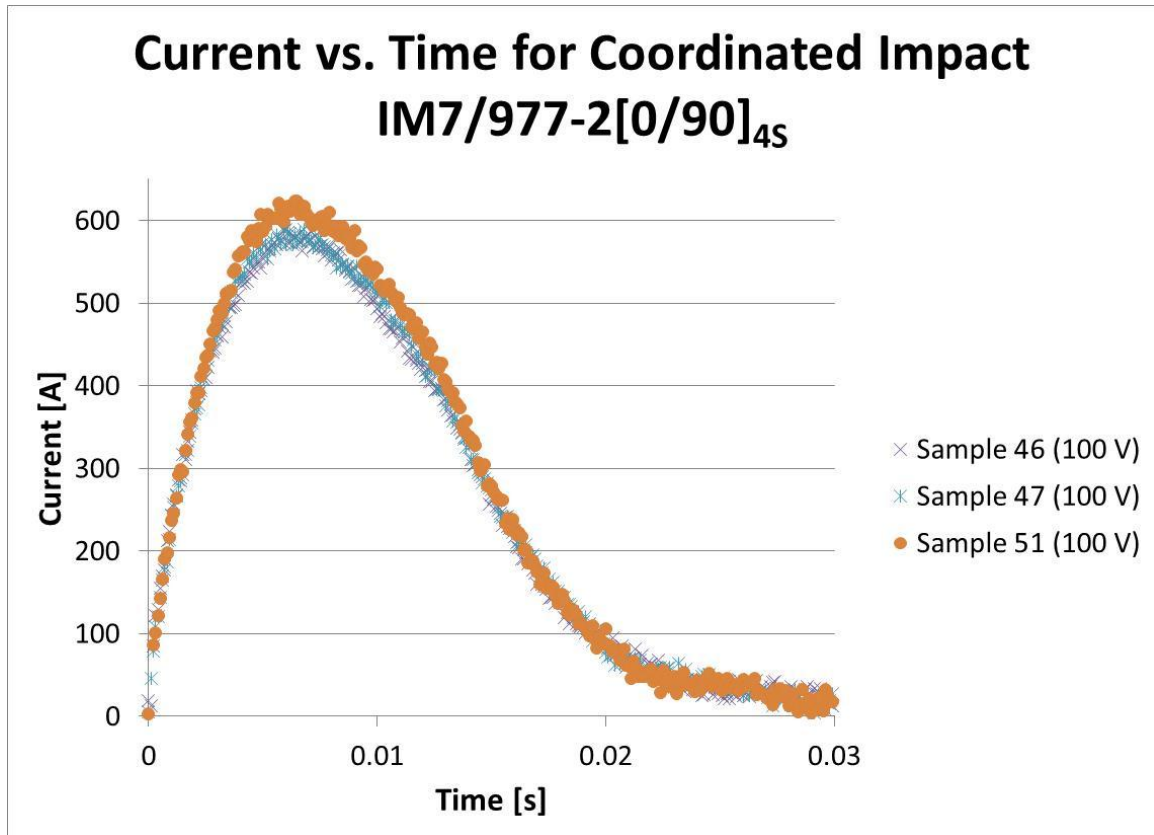
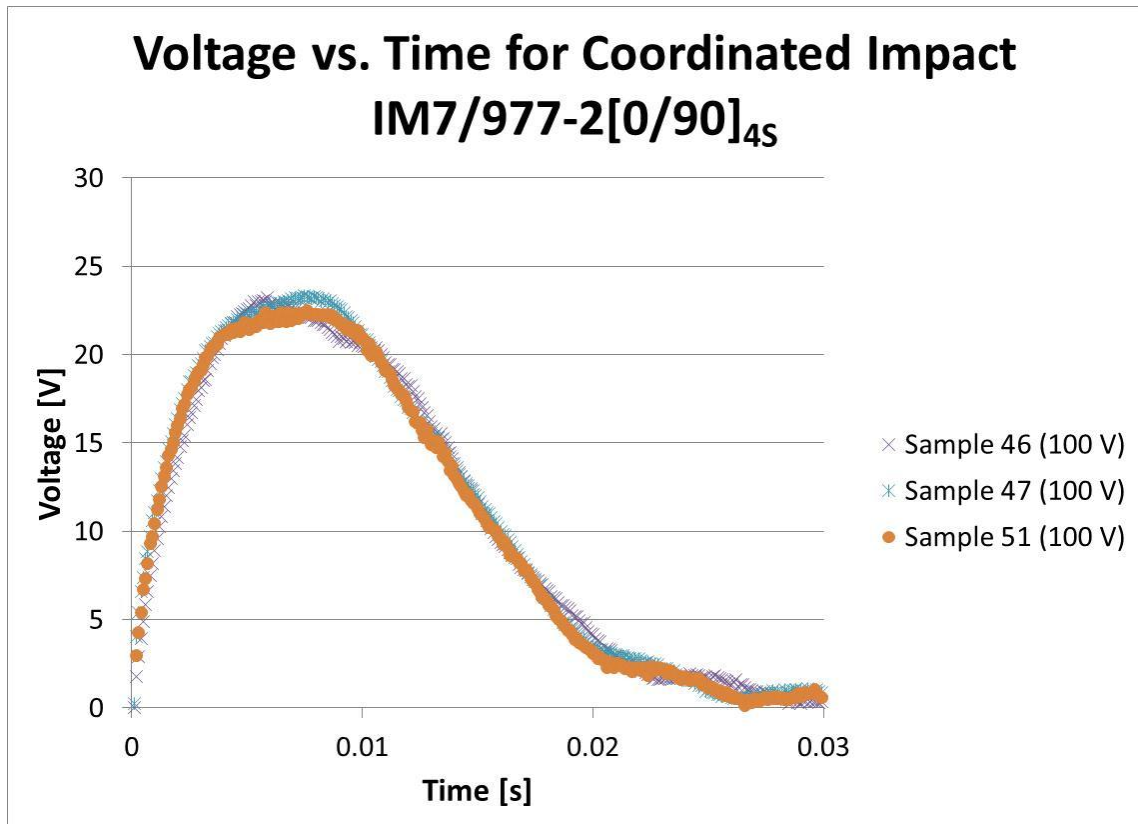Figure B.3: Current versus Time for 16 Ply Cross-Ply Coordinated Impact Tests

Figure B.4: Voltage versus Time for 16 Ply Cross-Ply Coordinated Impact Tests

APPENDIX C

RESISTANCE CURVES FOR ELECTRIC CURRENT PULSE TESTS

The resistance versus time curves associated with select electric current pulse tests are shown in Figures C.1 to C.4. Figure C.1 shows the resistance versus time for sample 55, which is a 32 ply unidirectional specimens at an analog voltage of 150 V. The resistance curve is representative of a normal curve for a pulse test. At the start of the test, the resistance was high, and as current magnitude increased, the resistance decreased and approached a steady value. Towards the end of the current pulse, the resistance began to fluctuate significantly due to the decrease in current magnitude. The resistance curve in Figure C.2 for a 32 ply cross-ply specimen shows a slightly different result. It should be noted, however, that the results in Figure C.2 were obtained from the old DAQ, so further testing would be required to better characterize the resistance of these samples. Figure C.3 shows a representative resistance versus time curve for a 16 ply unidirectional specimen. The increase in resistance was strange, however, was likely due to the poor contact between the electrodes and specimen. Finally, Figure C.4 shows the resistance versus time for a 16 ply cross-ply specimen.
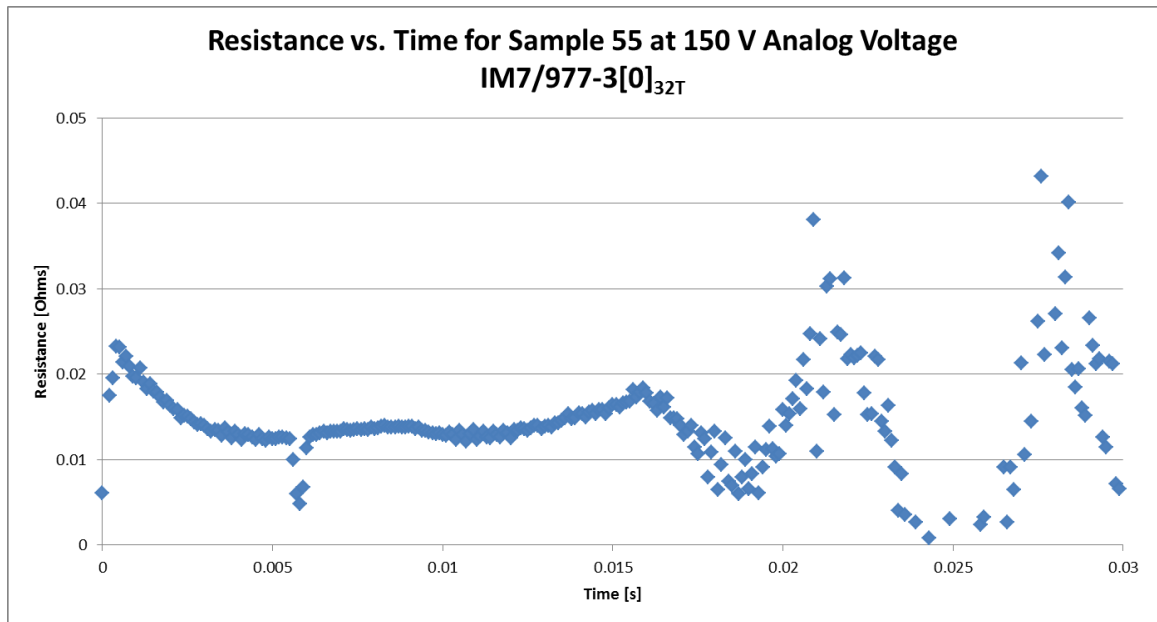
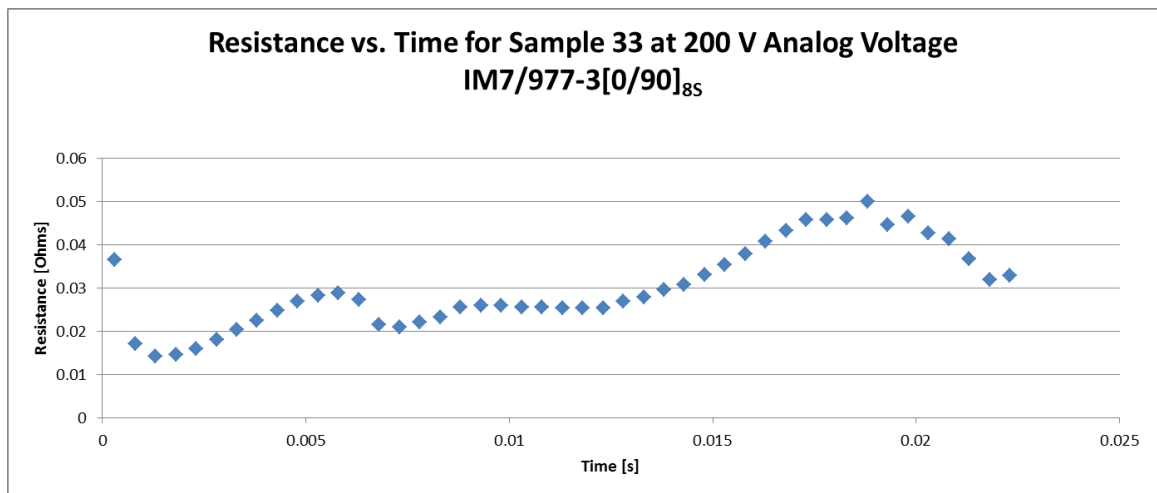Figure C.1: Resistance versus Time for 32 Ply Unidirectional Specimen

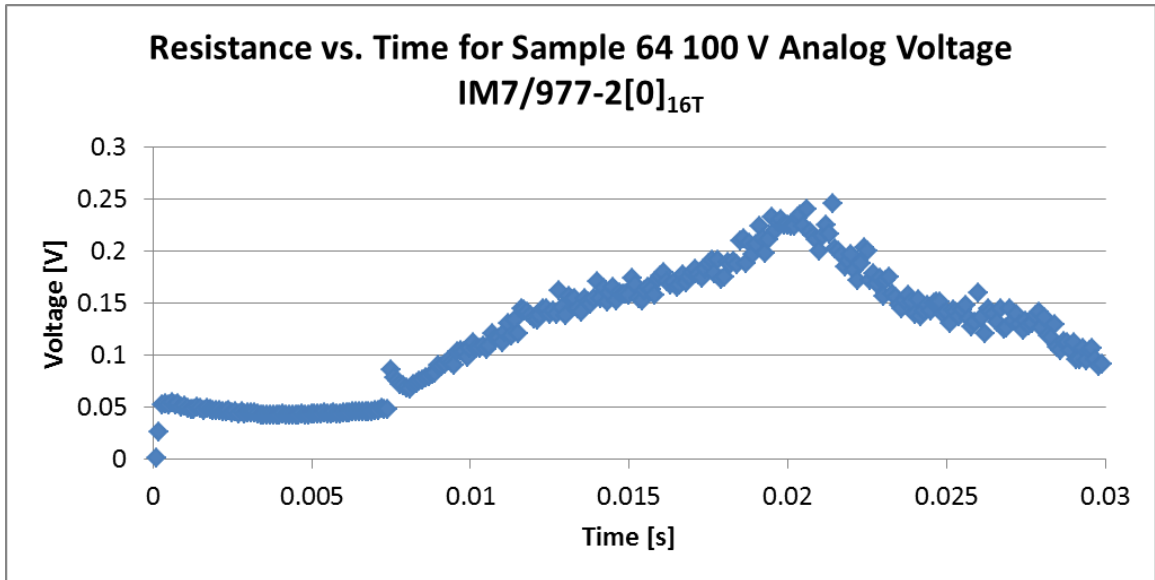Figure C.2: Resistance versus Time for 32 Ply Cross-Ply Specimen

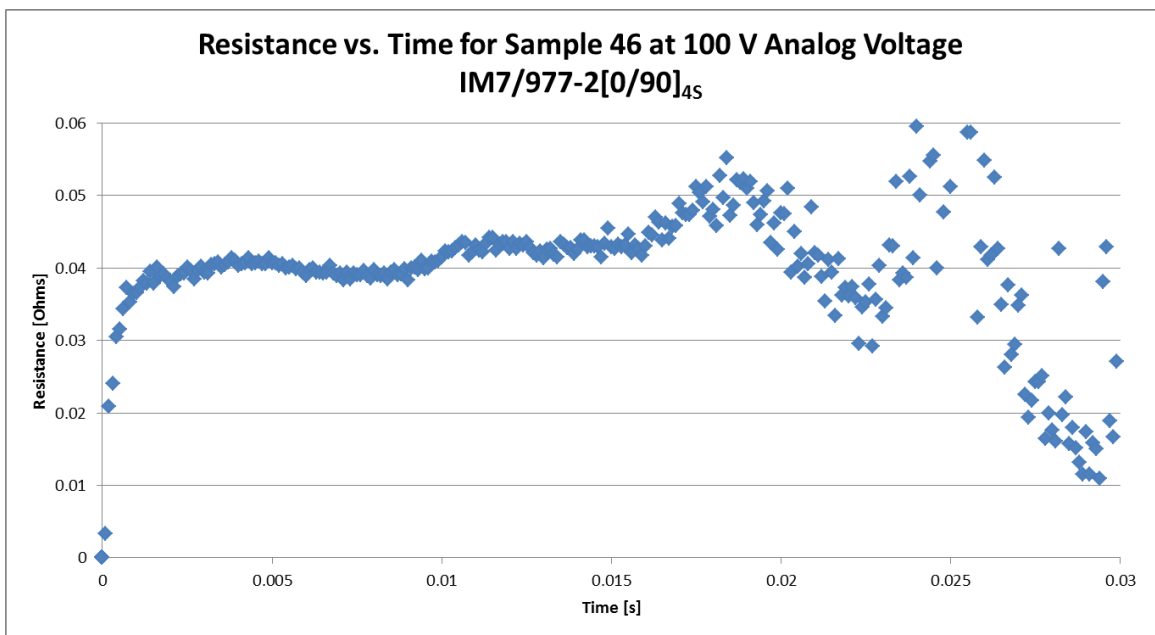Figure C.3: Resistance versus Time for 16 Ply Unidirectional Specimen

Figure C.4: Resistance versus Time for 16 Ply Cross-Ply Specimen

REFERENCES

Abrate, S., 1998. Impact on Composite Structures. Cambridge University Press, Cambridge.

Agilent Technologies. 14 Mar. 2011 <http://www.agilent.com>.

Amaro, A.M., Reis, P.N.B., & de Moura, M.F.S.F. (2008). Delamination effect on bending behaviour in carbon–epoxy composites. *Strain*,

Angelidis N, Khemiri N, Irving PE. Experimental and finite element study of the electrical potential technique for damage detection in CFRP laminates. Smart Materials and Structures 2005; 14: 147-154

Bader, M. G., Bailey, J. E., and Bell, I. "The effect of fibre-matrix strength on the impact and fracture properties of carbon-fibre-reinforced epoxy resin composites." Appl. Phys, 6 (1973): 573-593.

Bernard, M.L., Lagace, P.A., 1989. Impact resistance of composite sandwich plates. Journal of Reinforced Plastics and Composites 8 (5) 432-445.

Braunovic, Milenko, V. V. Konchits, and Nikolai Konstantinovich. Myshkin. Electrical Contacts: Fundamentals, Applications and Technology. Boca Raton: CRC, 2007. Print.

Cherington, M, & Mathys, K. (1995). *Pubmed.gov*. Retrieved from <http://www.ncbi.nlm.nih.gov/pubmed/7575320>

Chung DDL. Damage detection using self-sensing concepts. Proceedings of IMechE, Part G: Journal of Aerospace Engineering 2007; 221: 509-520.

Committee on Materials Research for Defense After Next, Materials Research to Meet 21st Century Defense Needs, National Research Council, The National Academies Press, Washington, DC (2003).

"Cycom 977-3 Toughened Epoxy Resin." Cytec Engineered Materials. 13 Aug. 2010 <http://www.cytec.com>.

de Moura M.S.F.S., & Marques, A. T. (2002) Prediction of low velocity impact damage in carbon-epoxy laminates. Compos. Part A-Appl. S. 33, 361–368.

Deierling, Phillip E., and Olesya I. Zhupanska. Electrical and Thermal Behavior of IM7/977-3 Carbon Fiber Polymer Matrix Composites Subjected to Time-Varying and Steady Electric Currents. Thesis. University of Iowa. Dept. of Mechanical Engineering, 2010. Print.

"Dynatup Drop Weight Impact Test Machine Model 8200." Instron. 16 Mar. 2011
http://www.instron.us/wa/library/default.aspx

Gou, Jihua, Tang, Yong, & Fei, Liang. (2009). Carbon nanofiber paper for lightning
strike protection of composite materials. *Elsevier*,

"Hexcel" Hexcel.com - Carbon Fiber and Composites for Aerospace, Wind Energy and
Industrial. Web. 09 Aug. 2010. <http://www.hexcel.com/>.

Jones, R.M. (1999) *Mechanics of Composite Materials*. Philadelphia: Taylor & Francis,
Inc.

McMaster-Carr. Web. 14 Mar. 2011. <http://www.mcmaster.com>

Oguibe, C.N., Webb, D.C., 1999. Finite-element modelling of the impact response of a
laminated composite plate. Composites Science and Technology 59 (12) 1913-
1922.

Parrish, Alton. (2010, June 3). *Before it's news*. Retrieved from
http://beforeitsnews.com/story/72/098/Carbon_Nanotubes_Used_To_Form_ImprI
Imp_Lightning_Strike_Protection_for_Wind_Turbines.html

Ply Angle. (2011). Retrieved from
<http://help.solidworks.com/2010/english/SolidWorks/cworks/LegacyHelp/Simul
ation/CompositeShells/Ply_Angle.htm>

Post, R.F., Fowler, T.K., & Post, S.F. (1993). A high-efficiency electromechanical
battery. IEEE Post,481(3), 462-475.

Prasse T, Michel F, Mook G, Schulte K, Bauhofer W. A Comparative investigation of
electrical resistance and acoustic emission during cyclic loading of CFRP
laminates. Composites Science and Technology 2007; 61: 831-835.

Shen, Lianxi, Jackie Li, Benjamin M. Liaw, Feridun Delale, and Jaycee H.
Chung."Modeling and analysis of the electrical resistance measurment of carbon
fiber polymer-matrix composites." Composites Science and Technology 67
(2007): 2513-520.

Schulte K, Baron C. Load and failure analysis of CFRP laminates by means of electrical
resistivity measurements. Composites Science and Technology 1989; 36(1): 63-
76.

Sierakowski, R.L., Newaz, G.M., 1995. Damage Tolerance in Advanced Composites.
Technomic, Lancaster.

Sierakowski, R.L., Telitchev, I.Y., & Zhupanska, O.I. (2007). Low velocity impact of electrified carbon fiber polymer matrix composites. Proceedings of the 16th international conference on composite materials (pp. 1-8). Kyoto, Japan:

Sierakowski, Robert L., Telitchev, I. Y., and Olesya I. Zhupanska. "On the Impact Response of Electrified Carbon Fiber Polymer Matrix Composites: Effects of Electric Current Intensity Duration." Composites Science and Technology 6 (2008): 639-649.

Stefanescu, E.A., Xiaoli, T., Zhiqun, L., Bowler, N., & Kessler, M.R. (2011). Multifunctional fiberglass-reinforced pmma-batio3 structural/dielectric composites. *Polymer*, *52*(9), 216-225.

Tektronix. (2011). Retrieved from <http://www.testmart.com/sp.cfm/DIGOSC/TEK/TDS2014B.html>

Telitchev, I. Y., R. L. Sierakowski, and O. I. Zhupanska. "Low-Velocity Impact Testing of Electrified Composites: Part II-Experimental Setup and Preliminary Results." Experimental Techniques (2008): 53-57. Print.

Tita, Volnei, Jonas De Carvalho, and Dirk Vandepitte. "Failure Analysis of Low Velocity Impact on Thin Composite Laminates: Experimental and Numerical Approaches." Composite Structures 83 (2008): 413-428. ScienceDirect. 15 July 2008.

Tudela, Mark A., Paul A. Lagace, and Brian L. Wardel. "Buckling Response of Transversely Loaded Composite Shells, Part 1: Experiments." AIAA Journal 42 (2004): 1457-1465.

United States National Committee on Theoretical and Applied Mechanics (2007) *Research Directionsin Computational and Composite Mechanics*, http://www.usnctam.org.

Wang D, Chung DDL. Comparative evaluation of the electrical configurations for the two-dimensional electric potential method of damage monitoring in carbon fiber polymer-matrix composite. Smart Materials and Structures 2006; 15: 1332-1344.

Zantout, Alan E., and Olesya I. Zhupanska. Electrical and Impact Characterization of Carbon Fiber Polymer Matrix Composites. Thesis. University of Iowa. Dept. of Mechanical Engineering, 2009. Print.

Zhu, et al. (2011). Surfactant-free synthesized magnetic polypropylene nanocomposites: rheological, electrical, magnetic, and thermal properties. Macromolecules, 44(11), 4382.

Zhupanska O. I., Sierakowski R. L. "Effects of an Electromagnetic Field on the
Mechanical Response of Composites", Journal of Composite Materials, Vol. 41
No. 5, pp 633-652, 2007.